

# Printing technologies for silicon solar cell metallization: A comprehensive review

Sebastian Tepner | Andreas Lorenz

Fraunhofer Institute for Solar Energy Systems,  
 Heidenhofstraße 2, Freiburg, 79110, Germany

**Correspondence**

Sebastian Tepner, Fraunhofer Institute for  
 Solar Energy Systems, Heidenhofstraße  
 2, Freiburg 79110, Germany.

Email: [sebastian.tepner@ise.fraunhofer.de](mailto:sebastian.tepner@ise.fraunhofer.de)

## Abstract

This paper presents a comprehensive overview on printing technologies for metallization of solar cells. Throughout the last 30 years, flatbed screen printing has established itself as the predominant metallization process for the mass production of silicon solar cells. For this reason, we will provide a detailed review on its history, its evolution over time, and how the continuous efforts of the scientific and industrial community for further improvements revolutionized the entire PV industry. Furthermore, we will guide the reader through the physics on silicon solar cell metallization, the fundamentals on contact formation, and what type of challenges and requirements these topics create for printing technologies. The main topic of this review addresses the flatbed screen-printing process mechanics, its different process sequences, corresponding screen technology, and the very important impact of paste rheology on the printing result. Finally, we will compare alternative upcoming printing approaches to flatbed screen printing and discuss how they might solve upcoming challenges in metallization in terms of increasing the throughput rates at an ever-decreasing grid line width and reduced silver consumption.

## KEY WORDS

contact formation, metallization, parallel dispensing, rotary printing, screen printing, silicon solar cells, stencil printing

## 1 | INTRODUCTION

Throughout this review, we will attempt to present the reader a comprehensive overview on the unique road printing approaches for PV taken since the beginning of commercial solar cell production in the 1960s. As flatbed screen printing has evolved to become the predominant process when it comes to metallization, we will start by summarizing the history of screen and stencil printing. We will elaborate on the success story and show how this printing technology was able to overcome limitation and challenges over the years and then follow it

up by presenting a comprehensive technological background on metallization of Si-solar cells. Further, we will guide the reader through the physical requirements for metallization from a solar cell physics point of view and then discuss those requirements in terms of the technical challenges they create for printing process. In Section 3, we are going to present a summary on the research around the physics and chemistry of the contact formation mechanism and how its understanding helped to push fine line metallization towards printing Ag-electrode widths below 50 µm. In Section 4, we will describe the screen-printing process mechanics and its variations. This is accompanied by an overview on the important aspects of the screen technology and the efforts of the scientific community to further improve its

Sebastian Tepner and Andreas Lorenz contributed equally to this work.

This is an open access article under the terms of the [Creative Commons Attribution](#) License, which permits use, distribution and reproduction in any medium, provided the original work is properly cited.

© 2023 The Authors. Progress in Photovoltaics: Research and Applications published by John Wiley & Sons Ltd.

design by simulations on screen architectures. In the following section, we present a comprehensive summary on metal pastes and its rheological behavior. The flow characteristics of the printing paste is one of the major aspects when it comes further advancing screen-printed metallization. Finally, we will present the reader an overview on promising alternative printing methods that show great potential to challenge flatbed screen printing in terms of throughput, achievable finger width, and Ag consumption.

## 1.1 | A short history of screen printing for solar cell metallization

The idea to use printing methods for the transfer of conductive circuits on electronic components dates back to the first half of the 20th century and to Paul Eisler, who is commonly—and sometimes controversially—known as the inventor of the printed circuit board (PCB).<sup>1–3</sup> In the early years of photovoltaics (PV) since the development of the first silicon solar cell at Bell Laboratories in 1954,<sup>4</sup> the metal contacts were realized in a cost-intensive and time-consuming process by electroplating, evaporation, or sputtering of various metal layers (i.e., Ti-Pd-Ag) through a photolithographic mask.<sup>5–7</sup> Until the mid-1970s, fabrication of silicon solar cells was a highly specialized, non-automated sequence of processes primarily for space applications with a very low annual production volume. The gradually increasing production volume in the 1970s and a growing terrestrial application of PV triggered a growing demand to automate and accelerate the production process.<sup>8</sup> A logical consequence was the transfer of well-established technologies from other fields of the electronic industry to the PV production process. The development of the screen printed aluminum back surface field (Al BSF) solar cell in the mid 1970s<sup>9</sup> was the starting point to apply the solar cell metallization by printing methods. It was in 1975, when early PV pioneer Spectrolab successfully realized and published first results about screen-printed metal contacts with a sufficiently low contact resistance and minority carrier recombination on high-resistivity p-type silicon.<sup>9</sup> This challenge was solved by forming an aluminum p+-doped BSF using high-temperature in-diffusion of aluminum (Al) from a screen-printed Al paste. On the front side, the contacts were screen printed using a metal paste consisting of silver powder, glass frit, and organic binders.<sup>9</sup> A major challenge of these early research activities was screen-printed metal contacts on the front side of high-ohmic n-type emitters with sufficiently low contact resistance and without shorting the p-n-junction.<sup>8</sup> During the 1980s, Al BSF solar cells rapidly evolved to the predominant industrially fabricated solar cell concept, which eventually lasted for more than 30 years.<sup>10</sup> In the late 1970s and early 1980s, a series of independent research activities quickly achieved progress by optimizing the paste formulation (glass frit, metal particles, and binders),<sup>8,11,12</sup> rapid-thermal processing (RTP) conditions,<sup>8,11,12</sup> and emitter profile.<sup>11,12</sup> Screen-printed front-side electrodes (also referred to as *contact fingers* in the following) typically had a width around 150 µm at that time.<sup>11</sup> To improve the lateral conductivity of the contacts and provide a well-solderable surface particularly on the rear side, it was common to apply a subsequent solder dip—in some cases

on a previously electroplated Cu layer—after screen printing of the metal pastes.<sup>11–13</sup> This complicated process could be overcome by developing fire-through silver (Ag) pastes, which were able to obtain a sufficiently low contact and line resistance as well as a good adhesion strength after RTP without penetrating through shallow pn-junctions.<sup>14</sup> This could be realized by newly developed rapid thermal co-firing processes using high-energy infrared (IR) lamps to efficiently form the front side contact and the BSF on the rear side.<sup>15</sup>

By the early 1980s, screen printing had already become a well-established method to apply the metal contacts on industrial scale.<sup>16</sup> Research activities at this time focused on replacement of cost-intensive silver by non-noble metals and the applicability of screen printing for other production steps like junction formation using dopant pastes<sup>13,16</sup> as well as anti-reflection and protective coating layers.<sup>16</sup> Furthermore, the impact of the metal-semiconductor contact on series resistance of the solar cell and the optimization of paste formulation and RTP process attracted increasing attention.<sup>17–19</sup> An early approach to overcome the limitations of the screen printing process with respect to the printed finger width (and thus shading losses) were so-called “buried contact solar cells.”<sup>20,21</sup> This approach proposed mechanically or laser grooved trenches that were filled with Ag paste in a subsequent fine line screen printing process<sup>22,23</sup> and was investigated until the beginning of the early 2000s<sup>24</sup> until it has completely vanished. Further research activities in the 1990s focused on optimizing the screen printing process in order to achieve finer lines, that is, in combination with selective emitters.<sup>25</sup> Furthermore, first studies regarding the impact of paste rheology<sup>26</sup> and texture roughness<sup>27</sup> on the screen-printing results were carried out.

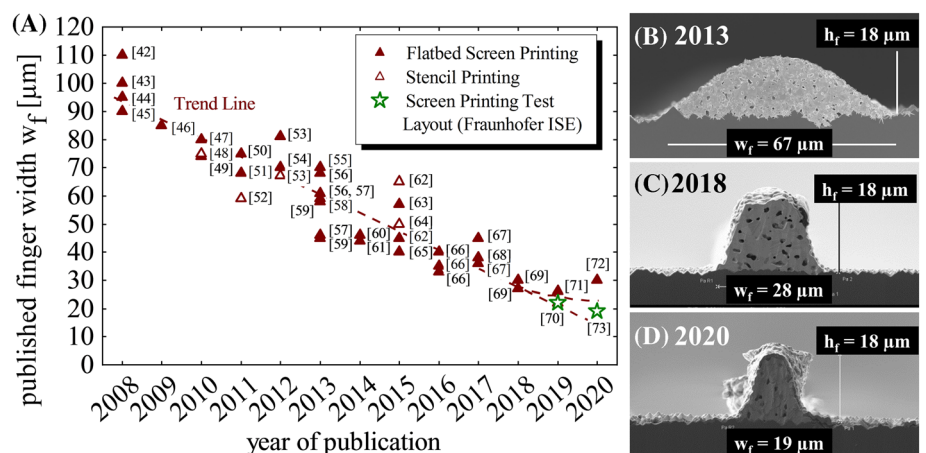
The development of the *passivated emitter and rear contact* (PERC) solar cell concept in the late 1980s based on the work of Blakers et al.<sup>28</sup> and previous conceptual considerations<sup>29</sup> was a further important milestone in the history of industrial PV mass production. The introduction of an additional dielectric passivation layer on the rear side between silicon and Al metallization effectively decreased recombination losses and improved the optical mirroring properties on the rear side.<sup>30–33</sup> A comprehensive overview of the working principle and current status of the PERC technology and related PERx cell concepts is provided by Preu et al.,<sup>31</sup> Dullweber and Schmidt,<sup>33</sup> and Green.<sup>34</sup>

In the early 2000s, the physical and chemical contact formation mechanisms of fire-through Ag pastes on n-type emitters as well as the microstructure of the metal-semiconductor contact interface attracted strong attention in the research community.<sup>35,36</sup> Schubert et al.<sup>37–39</sup> proposed a comprehensive model to explain the chemical and physical formation as well as the current transport mechanisms between the screen printed silver contacts and the n-type emitter. Multiple research studies in the following years formed the basis for today's understanding of the contact formation mechanisms and the development of high-performance fire-through pastes, which are today able to even contact extremely lowly doped emitters with low contact resistance.<sup>38</sup>

The Al BSF solar cell was the unchallenged and predominant industrially fabricated cell concept until 2012/2013. Around this time, the technical possibilities for further optimization of this cell concept had been exhausted, and the cell efficiency stagnated at a level of

~20 % on Cz-Si.<sup>30</sup> From this time on, the PERC solar cell gradually superseded the Al BSF solar cell as the predominant technology. The PERC cell concept enabled a further substantial increase of conversion efficiency beyond this level with an impressive average yearly improvement of approximately  $\Delta\eta \approx 0.6\%_{\text{abs}}$  throughout the last years.<sup>30,33</sup> Starting in 2002, new approaches to replace the originally applied evaporation process<sup>40</sup> for the rear side metallization of PERC cells with cost-effective and industrially feasible methods were investigated. A promising approach that finally did not reach the state of a broad industrial application was the so-called laser-fired contact (LFC) process.<sup>41</sup> Another approach focusing on the development of a firing-stable SiN<sub>x</sub> passivation and diffusion barrier layer with local laser-contact opening (LCO), subsequent screen printing of Al paste, and high-temperature co-firing<sup>42–45</sup> has established itself as the standard technology for industrially fabricated PERC solar cells until today.<sup>31</sup> In the 2010 years, the alloying process of Al and Si as well as the formation of the local BSF has been intensely investigated<sup>41–43</sup>; a comprehensive overview is provided by Dullweber and Schmidt,<sup>33</sup> Riegel et al.,<sup>46</sup> and Rauer et al.<sup>47</sup> The ongoing efforts to further raise conversion efficiency of PERC solar cells demanded for fine line screen printing processes, which enable minimal shading and metal-related recombination losses as well as lower silver consumption by reducing the metallized fraction on the front side. However, such fine line metallization processes had to maintain a sufficient lateral conductivity of the grid as well as a sufficiently low contact resistance even on lowly doped emitters to keep series resistance losses at a minimum. Various approaches like screen printing of hotmelt Ag pastes,<sup>48</sup> double printing,<sup>49,50</sup> usage of fine meshes with optimized emulsion,<sup>51</sup> and the application of single and double layer stencils<sup>52</sup> were evaluated and optimized. Intense industrial and academic research and a consequent optimization of machinery, screens, and pastes as well as newly emerging trends in the field of cell interconnection using narrow ribbons or multiple wires enabled an impressive progress towards fine line metallization within the last decade. Published results of screen and stencil printed finger widths on silicon solar cells underline the progress that has been done in the last decade culminating in extremely narrow finger widths down to less than 20  $\mu\text{m}$  today (Figure 1).

**FIGURE 1** (A) Evolution of screen and stencil printed finger width from 2008 to 2020 based on published results<sup>32,53–83</sup> on silicon solar cells as well as actual results using a test layout with advanced screen technology. The graph is modified and updated based on previously published versions.<sup>31,79,84</sup> (B–D) Comparison of SEM cross-sectional images of typical screen printed fingers using fire-through Ag paste from 2013 to 2020.



## 1.2 | Screen printing meets carrier-selective contacts

While the impact of the bulk and rear surface as recombination channels has been effectively decreased in modern PERC solar cells, recombination losses related to the front side emitter and the metal contacts remain as important limitation factors for the electric performance of modern high-efficiency PERC cells.<sup>85</sup> Exceeding the efficiency of PERC cells towards the theoretical limit of 29.4 %<sup>86</sup> for silicon-based solar cells thus requires an effective suppression of surface recombination related to the metal contacts (expressed as dark saturation current density  $j_{0,\text{met}}$ ).<sup>87</sup> A promising path towards this goal are solar cell concepts with carrier-selective contacts (often also denoted as “passivating contacts”), which provide a good transport of majority carriers to the metal contacts on the one hand and effectively block the minority carriers on the other hand.<sup>85</sup> A comprehensive overview regarding carrier-selective contacts is provided by Hermle et al.<sup>30</sup> and Schmidt et al.<sup>85</sup>

Until today, two particularly promising approaches for carrier-selective contacts have found their way to an industrial large-scale production. The silicon heterojunction (SHJ) solar cell concept<sup>88</sup> using intrinsic and p-/n-type hydrogenated amorphous silicon (a-Si:H) layers for surface passivation has been originally developed<sup>89</sup> in 1983 based on previous work of Fuhs et al.<sup>90</sup> on a-Si:H/c-Si heterostructures. SHJ solar cells enable high conversion efficiencies by an excellent surface passivation and a very high minority-carrier lifetime due to the intrinsic a-Si:H-layers.<sup>91</sup> Thus, modules based on SHJ solar cells have successfully entered the global PV production landscape with an expected strongly increasing market share throughout the coming years.<sup>92</sup> Screen printing will again be the method of choice for metallization of SHJ solar cells on industrial scale. However, the temperature sensitivity of the a-Si:H layers limits the maximum processing temperature to ~200–230 °C.<sup>93</sup> Applying screen printing for the front and rear side metallization thus requires an application of specific low-temperature (LT) curing pastes, which have been intensely investigated and optimized on academic and industrial level throughout the last decade.<sup>94–96</sup>

The second industrially relevant approach for carrier-selective contacts is based on a passivation stack consisting of an ultra-thin

$\text{SiO}_x$  tunneling layer, a heavily doped, partially crystallized polysilicon layer (poly-Si) and a  $\text{SiN}_x$  capping layer.<sup>85,87</sup> This approach—in the following denoted as  $\text{SiO}_x/\text{poly-Si}$  contact—was originally developed in the 1970s as passivation layer for silicon devices<sup>97</sup> and first applied for the so-called *semi-insulating polysilicon solar cell* (SIPOS) by Yablonowitch et al.<sup>98</sup> Further solar cell concepts based on  $\text{SiO}_x/\text{poly-Si}$  contacts were evaluated in the following.<sup>99–101</sup> A milestone towards an industrial implementation was the development of the so-called *tunnel oxide passivated contact* (TOPCon) solar cell by Fraunhofer ISE, which was first presented in 2013.<sup>102,103</sup> Further related cell concepts like Poly-Si on Oxide (POLO),<sup>104</sup> monoPoly<sup>TM</sup>,<sup>105</sup> and PERPoly<sup>106</sup> are based on the same idea. The outstanding surface passivation quality, the compatibility with established high-temperature processes, and the comparatively easy integration of this cell concept into existing PERC production lines are particularly attractive for the mass-production on industrial level. Industrially fabricated i-TOPCon solar cells and modules have demonstrated impressive efficiency results and currently gain a rapidly growing market share within the PV landscape.<sup>107,108</sup> Once more, screen printing has proven to be the method of choice as a highly productive, reliable, and easy-to-handle metallization method for this solar cell concept.

### 1.3 | Screen printing for tomorrow's high-efficiency solar cell concepts

Boosting the conversion efficiency beyond the theoretical limit of silicon-based solar cells requires more than one absorber material. These so-called tandem or multi-junction (MJ) solar cells are built up of at least two cell stacks with a different bandgap. A cell based on a high bandgap material, that is, III-V semiconductors like Gallium Arsenide (GaAs) or Cadmium Tellurite (CdTe), is located on top of cell(s) based on low-bandgap material like silicon or Copper-Indium-Gallium-Selenide (CIGS). The high bandgap of the top cell efficiently reduces thermalization losses, while the low-bandgap cell(s) underneath collect the remaining non-absorbed photons and thus minimize sub-bandgap losses.<sup>109</sup> To date, particular attention is spent on tandem solar cells using lead halide Perovskites on top of a c-Si bottom cell. Perovskites, which have been first described by Kojima et al.,<sup>110</sup> are inorganic-organic hybrid compounds with excellent light absorbing properties and a tunable bandgap over a wide spectral range.<sup>109</sup> Tandem solar cells on laboratory scale based on a Perovskite/c-Si architecture with a conversion efficiency of  $\eta = 29.2\%$  have been demonstrated recently<sup>111</sup> and are already fabricated on industrial scale.<sup>112</sup> While the metallization of tandem solar cells is currently mainly realized by evaporation,<sup>113</sup> the scale-up of tandem solar cells for industrial mass production requires efficient and productive methods for the metallization. Not surprisingly, the “old bull” screen printing once again recommends itself as the method of choice due to its longstanding and captivating benefits. However, new challenges arise due to the sensitivity of Perovskites to environmental factors like oxygen, moisture, UV light, chemicals (i.e., solvents), and temperature, which lead to substantial degradation.<sup>114,115</sup> Applying screen printing for the large-scale metallization of this type of cells thus requires sufficient metallization

pastes and drying/curing methods to guarantee a sufficiently low lateral resistance at curing temperatures as low as 100–150°C.<sup>113</sup> Research and development for this field of application are just at the beginning, and very few studies addressing this topic have been published so far.<sup>113</sup> However, it is very likely that screen printing will prove its powerful ability to cope even with highly sophisticated challenges and still prevail its unrivaled benefits for industrial high-volume metallization of tandem cells once again.

## 2 | SOLAR CELL METALLIZATION: FUNDAMENTAL ASPECTS AND REQUIREMENTS

### 2.1 | Fundamental requirements of solar cell electrodes

Solar cells require metallic electrodes to extract the photo-generated charge carriers from the semiconductor. The electrodes are—except from specific cell concepts like the interdigitated back contact (IBC) solar cell<sup>116,117</sup>—usually applied on the front and rear side using various metallization technologies like printing, electroplating, or evaporation. The metallization has to fulfill several requirements with respect to electric performance and liability on module level:

- Minimal shading of the active cell area by the metal grid on the front side and in case of bifacial solar cells additionally on the rear side.<sup>118</sup>
- Sufficiently low lateral resistance (grid resistance) of the front/rear grid to maintain a low series resistance contribution depending on the selected interconnection scheme.<sup>118</sup>
- Sufficiently low contact resistance of the metal-semiconductor contacts.<sup>118</sup>
- Low recombination velocity (metal-related saturation current density) underneath the metal contacts.<sup>118,119</sup>
- Sufficient adhesion of the interconnection ribbons or wires using soldering or conductive adhesive.<sup>120</sup>

The optimal design and electrical performance of the metallic electrodes are closely connected to the selected interconnection scheme, the solar cell concept, and the material parameters of the semiconductor. All these factors as well as the technical limitations of the metallization process have to be considered when optimizing the metallization layout for a certain solar cell design.

### 2.2 | Interconnection concepts

Within the last decades, a multitude of different cell and interconnection concepts has been developed. To date, solar cell interconnection using 6 ribbons or 9–12 wires with lead-containing solder is the predominant method for cell interconnection in the PV industry with a cumulated market share of more than 90% in 2019.<sup>89</sup> The traditional front side H-pattern grid consists of 3–6 busbars with up to 150 fine

narrow contact fingers. Using modern tabbing/stringing machines, solar cells with up to 6 ribbons down to a width of 0.6 mm can be interconnected. Throughout the last years, interconnection of solar cells by soldering 9–12 solder-coated wires onto regular pads on the front/rear side has gained a strongly increasing market share particularly in the Asian PV production. Modern high-efficiency solar cells with a full size format of 156 mm × 156 mm or more usually have a comparatively high current, which induces substantial resistive power losses on module level.<sup>121</sup> An effective way to prevent these power losses is the reduction of the cell current by separating the cells on half instead of full size.<sup>122,123</sup> Using this approach, the cells with a suitable metallization layout are separated to half cells by scribing and mechanical cleaving or thermal laser separation (TLS).<sup>124</sup> Modules based on half cells have gained a strongly increasing market share within the last years.<sup>92</sup> A further concept with strongly increasing market share is based on bifacial cells/modules, which collect the incoming light from both sides<sup>125</sup> (see Section 2.4). Connecting solar cells by multiple copper-based wires instead of soldered ribbons is a further successful concept that has been established using two different approaches: The Multi Busbar interconnection technology developed in 2012 by the German company Schmid GmbH<sup>126</sup> and MeyerBurger's SmartWire Connection Technology (SWCT),<sup>127</sup> which was originally developed in 2006 by the Canadian company Day4Energy.<sup>128</sup> While the Multi Busbar approach interconnects the cells via 12 copper (Cu) wires coated with solder alloy by an IR soldering process,<sup>129</sup> the SWCT approach interconnects the cells by using a pre-fabricated compound of foil and up to 38 Cu wires coated with a LT melting alloy, which is laminated on busbarless solar cells.<sup>130</sup> Increasing attention is further given to the so-called shingled cell interconnection. The idea of the shingeling concept goes back to the late 1950s<sup>131</sup> and gained increasing attention since the mid-1990s.<sup>132,133</sup> A shingle module consists of several strings of rectangular cell stripes, which are interconnected similar to the tiles on a rooftop. The stripes are cut out from a metallized and fired standard 6 in. host cell with a special, screen-printed metallization layout on the front and rear side. Each cell stripe has a printed solder pad/busbar along the edge, a full-area aluminum (Al) rear side metallization, and a grid of contact fingers on the front side. The cutting process of the strips from the host cell can be realized, that is, by laser scribing mechanical cleaving (LSCM) or TLS.<sup>134</sup> The separation process is critical for the cell performance with respect to micro-cracks and recombination losses of the cutting edge to obtain a high efficiency of the shingle cells. An additional post-metallization passivation of the cutting edges is thus important.<sup>134</sup> For module interconnection, the cell stripes are interconnected to shingled strings by overlapping and connecting the rear busbar of one stripe with the front busbar of the next stripe. Due to the constrained movement possibility of the interconnected shingle cells, thermo-mechanical stress on the joint interconnections within the module is much more critical compared to standard cell interconnection via soldered ribbons.<sup>135</sup> Electrically conductive adhesives (ECAs)—possibly in hybrid combination with non-conductive adhesive—are assumed to fulfill the mechanical and electrical requirements best.<sup>135</sup>

## 2.3 | Optimization of the front side metallization: A narrow ridge

With focus on the screen printing process, realizing fine line grids on the front—and in case of bifacial solar cells on the rear—side is particularly challenging. The front side metallization of a solar cell has to combine an optimal trade-off between shading of the metal grid (finger shape and width, and number of contact fingers), series resistance contribution (lateral grid resistance and contact resistance), and silver consumption (uniformity of fingers). It is thus essential to optimize the grid layout individually depending on the selected interconnection concept, the material parameters of the semiconductor, and the performance of the selected metallization technology. To minimize optical losses due to shading, the grid should reflect as less of the incoming light as possible from the active area of the (encapsulated) solar cell in the module. The optical quality of the contact fingers (considering the actual reflection losses in the module) is referred to as *effective or shading-relevant finger width*  $w_{f,\text{eff}}$ . Models for the calculation of  $w_{f,\text{eff}}$  have been proposed, that is, by Blakers<sup>136</sup> and Woehl et al.<sup>137</sup> The ideal case would be a nearly or totally transparent grid, which could theoretically be realized by a triangular shape of the contact fingers.<sup>138</sup> Yet realizing such a finger geometry using state-of-the-art printing technologies seems to be extremely challenging or even impossible. In reality, the cross-section of typical screen-printed contact fingers is Gaussian-shaped or parabolic (Figure 2A). The electric quality—namely, a sufficiently low series resistance contribution  $r_{s,\text{grid}}$  of the grid—is of great importance to achieve a high fill factor (FF) of the cell. The optimal trade-off between shading and series resistance contribution is strongly affected by the number of busbars/wires and contact fingers<sup>140</sup> and can be optimized using appropriate simulation tools.<sup>141</sup> The maximal tolerable lateral finger resistance  $R_L$  for a defined series resistance contribution limit  $r_{s,f}$  of the fingers can be calculated for a given interconnection scheme and grid layout according to Mette,<sup>139</sup> Fellmeth,<sup>142</sup> and Lorenz.<sup>143</sup> Table 1 and Figure 2B provide an impression of the maximal acceptable mean lateral finger resistance  $R_{L,\text{max}}$  for a given finger series resistance contribution limit of  $r_{s,f} = 0.1 \Omega\text{cm}^2$  calculated for various common interconnection concepts. The results underline the strong relation of the tolerable lateral finger resistance and thus the required electrical quality of the contacts with the selected interconnection concept. Consequently, interconnection concepts with an increasing number of busbars/wires are particularly attractive for solar cells with a higher lateral resistance of the front side contacts, which is the case, that is, for screen printed ultra-fine line grids and metallization concepts using LT pastes like SHJ and tandem cells.

## 2.4 | Rear side metallization

The rear side of a solar cell fulfills several functions, namely, minority carrier transport, passivation, photon mirroring, mechanical adhesion, and—in case of bifacial solar cells—photon collection. Design, properties, and resulting processing parameters of the rear side metallization strongly depend on the selected cell and interconnection concept.

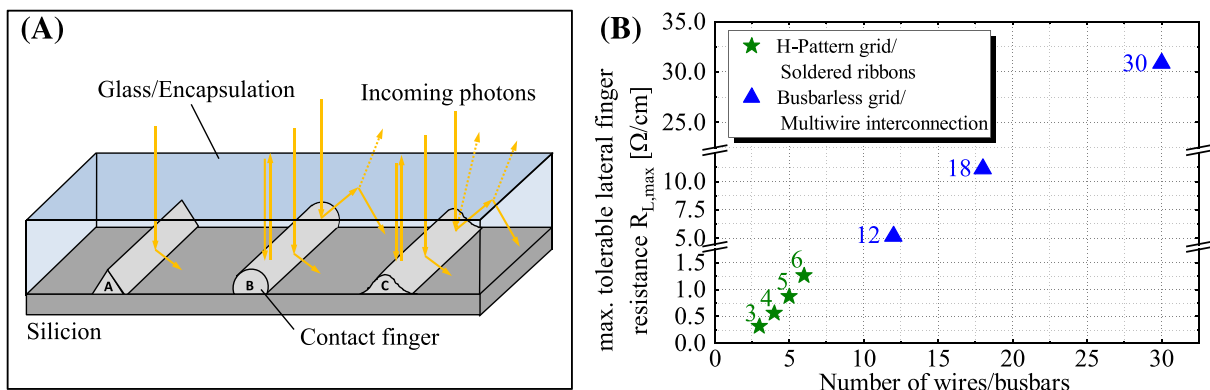


**FIGURE 2** (A) Reflection of incoming light on different finger shapes under EVA/glass encapsulation: (theoretical) triangular finger profile (A); circular finger profile, that is, for dispensed contacts (B); and parabolic or Gaussian-shaped finger profile, that is, for screen printed contacts (B), adapted from Mette.<sup>139</sup> (B) Dependency of the maximal tolerable lateral finger resistance  $R_{L,\max}$  [ $\Omega/\text{cm}$ ] from the number of busbars/wires for interconnection (assuming a target series resistance contribution of  $r_{s,f} \leq 0.1 \Omega\text{cm}^2$ )

**TABLE 1** Maximal tolerable lateral finger resistance  $R_{L,\max}$  [ $\Omega/\text{cm}$ ] to obtain a series resistance contribution of  $r_{s,f} \leq 0.1 \Omega\text{cm}^2$  to the total series resistance of a typical PERC solar cell

Interconnectionconcept	$n_b/n_w$	$R_{L,\max}$ [ $\Omega/\text{cm}$ ]
Busbarless grid/multiwire	30	30.9
	18	11.1
	12	4.9
H-pattern grid/soldered ribbons	6	1.3
	5	0.9
	4	0.6
	3	0.3

Note: The values are calculated for different interconnection concepts and underline the strong dependency of  $R_{L,\max}$  from the number of busbars  $n_b$ /wires  $n_w$ , which is applied for interconnection.

With an estimated market share of over 98% in 2020,<sup>92</sup> flatbed screen printing is the predominant method to apply the rear side metallization for most industrially fabricated silicon solar cells. Depending on the cell concept, the rear side metallization can be generally distinguished in full-area and structured designs. Monofacial cell concepts that collect the incoming light only from the front side currently dominate the market with a production share of 80% in 2020.<sup>92</sup> The rear side metallization of a typical monofacial p-type PERC solar cell consists of separately printed Ag pads and surrounding full-area Al metallization. In the first step, a layout of regularly arranged solder pads is printed using non-fire-through Ag paste. The dimension and number of the Ag pads are optimized with respect to the soldering process and the long-term stability of the interconnection. The impact on the electric performance of the solar cells can be neglected.<sup>144</sup> In the second step, the surrounding area of the backside with exception of a narrow edge region is coated by screen printing of Al paste, which is particularly unsophisticated from a printer's point of view. However, both printing steps require a stable and well-controlled application of a defined wet paste layer thickness within a defined production tolerance, which is determined by the selection of the screen mesh (see Section 3.5), the paste rheology (see Section 4), and—to a small extend—by the selected

printing parameters (see Section 3.2).<sup>145</sup> During production, the layer thickness is usually controlled indirectly by monitoring the applied mass of wet paste on each cell using precision inline scales.

While the rear side metallization of monofacial cell concepts is technically unsophisticated, this is not the case if fine grid-like structures have to be printed on the rear side, which is the case for bifacial solar cell concepts or IBC solar cells. Bifacial solar cells—a concept originally developed in the 1960<sup>146</sup> and later applied for bifacial concentrator cells by Luque et al.<sup>147</sup>—collect the incoming light not only on the front side but also from the albedo, which significantly increases the output power density compared to monofacial cells/modules.<sup>125</sup> Bifaciality can be applied for various cell concepts like PERC,<sup>148,149</sup> Heterojunction,<sup>150</sup> and TOPCon.<sup>151</sup> With respect to the rear side metallization, a grid is applied on the rear side instead of a full-area metallization. In an ideal case, the rear side grid should cover a small fraction of the cell area to minimize shading losses and maintain a sufficiently low lateral grid resistance and metal-semiconductor contact resistance to reduce series resistance losses. Applying a rear side grid on solar cells with rear side passivation requires a precise local opening of the passivation layer(s) or a fire-through approach to contact the semiconductor. Using screen printing, a precise alignment of the printed metal grid on the previously opened structures in the passivation is required. An alternative approach that avoids the previous local opening of structures has been demonstrated by screen printing of Al fire-through pastes, which etches through the rear side passivation and forms a local BSF on the p<sup>+</sup>-doped silicon surface within the subsequent co-firing process.<sup>152</sup> Using this approach, promising results have been demonstrated recently by applying multi-layer screen printing or multi-nozzle dispensing for the rear side metallization of bifacial PERC solar cells.<sup>153,154</sup>

## 2.5 | Metal-semiconductor contact and metal-induced recombination

Realizing a low-ohmic contact between the (screen-printed) metal electrodes and the silicon semiconductor has been a major challenge

since the beginnings screen-printed solar cell metallization.<sup>19,145,155</sup> Starting in the early 2,000 years, the chemical-physical nature of fire-through Ag contacts on n-type silicon gained strong attention<sup>35–37,156</sup> with Schubert et al.<sup>37–39</sup> being the first to present a comprehensive model of the contact formation process. The gradual establishment of the PERC technology as the dominating cell concept additionally required a deep understanding of contact formation and alloying processes using Al paste on p-type silicon surfaces, which was intensely investigated in the 2010s.<sup>46,47,157–160</sup> The introduction of new cell concepts based on n-type material shifted an additional focus on contact formation of Ag/Al and Ag pastes on p<sup>+</sup>-emitter surfaces.<sup>161–172</sup> Realizing screen-printed contacts on passivation layers with carrier-selective properties, that is, for TOPCon solar cells, represents the latest challenge regarding contact formation.<sup>30,85,103,104,106</sup>

Beside the long-lasting challenge of forming a low-ohmic metal-semiconductor contact on various silicon surfaces, the impact of fire-through metal pastes on surface recombination has gained strong attention throughout the last decade.<sup>119,173–180</sup> Focusing on the highly doped surface regions, three dominating recombination sources must be considered: Auger recombination in highly doped regions, Shockley-Read-Hall (SRH) recombination, and defect recombination related to the metal-semiconductor interface. This metal-related recombination source originates from parasitic impurities, which are induced by diffusion processes during the high-temperature contact formation process of the printed metal contacts, leading to a highly recombination-active surface.<sup>119,173,181</sup> The metal-related recombination losses are commonly expressed as dark saturation current density  $j_{0,met}$ . A common method is the determination of  $j_{0,met}$  based on an area-weighted model, which assumes a linear relationship of  $j_0$  with the metallized fraction.<sup>119</sup> New approaches determine  $j_{0e,met}$  with a simulative approach using PL imaging data combined with numerical PL simulations,<sup>179,182</sup> which has proven to be significantly more precise as they consider the non-uniformity of the excess carrier density  $\Delta n$ . The negative effect of metal-related recombination losses on the  $V_{oc}$  of the solar cell can be reduced by various approaches<sup>119</sup>: the consequent reduction of the (fire-through) metallized fraction on the surface of the solar cell, that is, using non-contacting paste for the busbars,<sup>183</sup> applying metallization methods that induce a lower  $j_{0e,met}$ , effectively shielding the minority carriers from the surface by a field-effect passivation (i.e., selective emitter), or introducing an effective surface passivation with carrier-selective properties (“passivating contacts”). Due to the complexity of this topic with respect to various specific metal-silicon interfaces and contact scenarios, this work can only provide a brief overview regarding the current state of science and technology.

Based on manifold studies, the contact formation process and the properties of the metal-semiconductor interface of fire-through silver paste on n-type silicon emitters have been deeply investigated. Today, it is mostly accepted that several current paths contribute to the current flow between the silicon semiconductor and the printed and fired silver grid,<sup>38,184–189</sup> namely, local direct contacts between silver bulk and the silicon surface,<sup>16,145</sup> silver crystallites formed on the silicon surface during the contact formation process,<sup>36</sup> and tunneling of

charge carriers through glass layers enriched with dissolved silver and silver colloids<sup>190–195</sup> as shown in Figure 3. A further important finding discovered the crucial role of electrons during the firing process.<sup>196,197</sup> Depending on the emitter type and the polarity of current injection, electron injection during firing enhances or suppresses the formation of silver crystallites on the emitter and silver colloids/nano-crystallites in the glass and thus strongly affects the resulting macroscopic contact resistance.<sup>196–198</sup> The presence of busbars in the grid layout significantly increases the probability and propagation of such local “short-circuit spots” and thus negatively affects the macroscopic contact resistance.<sup>199</sup> Constant optimization of the silver paste composition for n-type emitters throughout the last two decades enabled an impressive decline of specific constant resistance  $\rho_c$  from values in the range<sup>39,200</sup> of  $10^3$  to  $10^4$   $\text{m}\Omega\text{m}^2$  to values in the lower one-digit range.<sup>201–203</sup> Actual silver fire-through silver pastes reliably obtain very low specific contact resistances below  $1 \text{ m}\Omega\text{cm}^2$  on industry-relevant emitters (Table 2). Intense effort to optimize the emitter, passivation, and paste properties enables a dark saturation current density of the passivated, non-metallized region ( $j_{0e,pass}$ ) in the range of  $20 \text{ fA/cm}^2 \leq j_{0e,pass} \leq 60 \text{ fA/cm}^2$  for typical industrially fabricated p-type PERC solar cells. The metal-induced dark saturation current density can be estimated in the range of  $\sim 500 \text{ fA/cm}^2 \leq j_{0,met\_front} \leq 800 \text{ fA/cm}^2$  (see Table 2).<sup>31,82,202</sup>

Beside the commonly established n-type emitter, p-type emitters with boron doping (p<sup>+</sup>-B-emitter) have gained strongly increasing attention throughout the last decade. Such p<sup>+</sup>-B-emitter is applied for various high-efficiency cell concepts, that is, n-type bifacial PERC solar cells.<sup>233</sup> A further highly relevant application is the front side emitter of solar cells with n-type carrier-selective SiOx/poly-Si rear side passivation (i.e., n-TOPCon cells<sup>102,103</sup>). Most commonly, fire-through screen printing pastes containing silver (Ag) with a certain amount of added aluminum (Ag/Al) are used to contact p<sup>+</sup>-B-

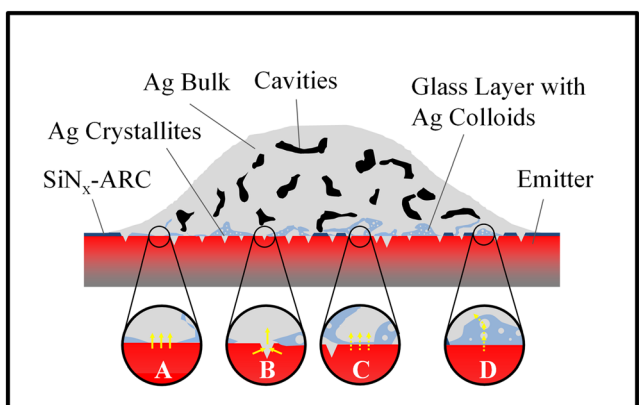


**FIGURE 3** Schematic of a typical sintered silver thick-film contact on an n-type silicon surface. The following current paths are proposed: (A) direct contacts between silver bulk and emitter, (B) current flow via silver crystallites, (C) tunneling through thin glass layers, and (D) multi-step tunneling through glass layer enriched with silver colloids/nano-crystallites (schematic modified based on Lorenz<sup>143</sup>).

**TABLE 2** Overview of the typical passivation/metallization architecture and the typical currently obtained parameter range for screen-printed metallization on selected surfaces based on recently published results and empirical data

Type of surface/ metal contact	Typical architecture of passivation/ metallization <sup>a</sup>		Typical range of selected parameters			References
	Surfacepassivation	Metallization (Paste type)	$j_{0,\text{pass}}$ [fA/cm <sup>2</sup> ]	$j_{0,\text{met}}$ [fA/cm <sup>2</sup> ]	$\rho_c$ [mΩcm <sup>2</sup> ]	
Homogeneous front n <sup>+</sup> -emitter (fire-through contact)	SiO <sub>2</sub> /SiN <sub>x</sub>	Ag	20-60	500-1,000	0.5-1.5	78,82,119,202,204-212
Homogeneous front p <sup>+</sup> -emitter (fire-through contact)	Al <sub>2</sub> O <sub>3</sub> /SiN <sub>x</sub>	Ag/Al or Ag	10-30	650-2,000	1.0-4.0	171,203,211,213-218
Rear side p-type silicon(laser-opened local contacts)	Al <sub>2</sub> O <sub>3</sub> /SiN <sub>x</sub>	Al	5-15	350-800	3.0-5.0	204-206,208-211,219-222
Rear n-type SiO <sub>x</sub> /poly-Si carrier-selective contact	SiO <sub>x</sub> /poly-Si/SiN <sub>x</sub>	Ag	3-10	20-200	1.0-2.0	105,106,108,214,216,223-227
Rear p-type SiO <sub>x</sub> /poly-Si carrier-selective contact	SiO <sub>x</sub> /poly-Si/SiN <sub>x</sub>	Ag/Al or Ag	5-20	60-250	2.0-5.0	223,228-232

<sup>a</sup>Most commonly used surface passivation/metallization architecture.

emitter.<sup>162,165,234</sup> Actual Ag/Al pastes obtain a specific contact resistance in the range of a few mΩcm on typical p<sup>+</sup>-B-emitters (see Table 2). However, fire-through Ag paste without additional Al content has also been successfully applied to contact p<sup>+</sup>-B-emitters<sup>235-238</sup> even with low contact resistance around  $\rho_c \approx 1$  mΩcm<sup>2</sup>, which seriously questions the compelling necessity of Ag/Al pastes to contact p<sup>+</sup>-B-emitters.<sup>40</sup> The contact formation process of Ag/Al pastes on p<sup>+</sup>-B-emitters<sup>172,239</sup> exhibits fundamental differences compared to Ag pastes on n-type emitters. A major challenge is the mitigation of deep Ag/Al spikes during the contact formation process,<sup>165,170,172</sup> which can lead to significant FF losses due to local shunting<sup>165,170</sup> as well as considerable losses due to metal-induced surface recombination.<sup>171</sup> Similar to Ag pastes on n-type emitters, a strong impact of electron availability during the contact formation on p<sup>+</sup>-B-emitters process has been found.<sup>197</sup> While the challenge to realize a low-ohmic contact on p<sup>+</sup>-B-emitters has been largely overcome with actual pastes, further reduction of  $j_{0,\text{met\_front}}$  losses is still an existing challenge. A promising approach is the application of boron emitter profiles with considerably deeper junction depth.<sup>171,240</sup> Recently published results confirm the benefit of such deep emitter profiles with respect to lower  $j_{0,\text{met\_front}}$  losses without deteriorating  $\rho_c$ .<sup>213,214</sup>

Focusing on the rear side of the solar cell, the (screen-printed) electrode can either be applied in form of a full-area pattern (monofacial cell concepts) or a grid-like pattern (bifacial cell concepts). In both cases, the screen printed rear side electrode has to provide a low-ohmic metal-semiconductor contact with preferably minimal  $j_{0,\text{met\_rear}}$  losses after the co-firing process. On a typical industrially fabricated monofacial p-type PERC solar cell, the full area rear side passivation stack (most commonly consisting of an Al<sub>2</sub>O<sub>3</sub> passivation layer covered by a hydrogenated SiN<sub>x</sub> capping layer<sup>31</sup>) is locally removed by local point- or dash-shaped laser ablation (LCO).<sup>241</sup> Subsequently, the rear-side metallization consisting of more or less regularly arranged silver solder pads and a surrounding full area aluminum metallization is applied by a two-step screen printing process.<sup>241</sup> Within the

following co-firing step, a complex Al-Si alloying process takes place, which provides a sufficiently low-ohmic electric contact between the rear side electrode and the p-type silicon bulk and in parallel induces the formation of a local aluminum-doped back surface field (Al-BSF), which effectively prevents surface recombination underneath the metal contacts.<sup>33,47,160</sup> This type or rear-side contact usually exhibits a specific contact resistance in the range of  $3 \text{ m}\Omega\text{cm}^2 \leq \rho_c \leq 5 \text{ m}\Omega\text{cm}^2$ . The metal-induced dark saturation current density can be estimated in the range of  $500 \leq j_{0,\text{met\_rear}} \leq 800 \text{ fA/cm}^2$  (see Table 2).

Solar cell concepts based on carrier-selective SiO<sub>x</sub>/poly-Si contacts (see chapter 1.2) have established themselves as industrially feasible next generation high efficiency solar cells.<sup>30,85</sup> On industrial scale, the metal grid is applied on the front side p<sup>+</sup>-B-emitter and the rear side SiO<sub>2</sub>/poly-Si/SiN<sub>x</sub> passivation layer using screen printing. N-type SiO<sub>x</sub>/poly-Si contacts are metallized with Ag paste,<sup>107,242</sup> p-type SiO<sub>x</sub>/poly-Si contacts either with Ag/Al,<sup>223</sup> or Ag paste.<sup>228</sup> Contact formation of fire-through metal pastes on a carrier-selective SiO<sub>x</sub>/poly-Si passivation is rather demanding. During the high-temperature co-firing process, the metal paste has to locally penetrate through the SiN<sub>x</sub> capping layer to form a low-ohmic contact. However, the penetration and degradation of the SiO<sub>2</sub>/poly-Si passivation layers by the aggressive glass frit must be avoided in order to preserve the outstanding passivation properties of the carrier-selective contact.<sup>30</sup> This challenging task requires specifically optimized metal pastes with adequate glass frit composition<sup>108,224</sup> as well as a careful adaption of the contact firing conditions.<sup>223,229</sup> The majority of current research activities focus on n-type SiO<sub>x</sub>/poly-Si contacts. More questions still arise with respect to screen printed metal contacts on SiO<sub>x</sub>/p<sup>+</sup> poly-Si passivation layers, a field of research that has so far been considered to a much smaller extend.<sup>30,85,228</sup> Table 2 provides an actual overview of the typical range of contact-relevant parameters ( $j_{0,\text{pass}}$ ,  $j_{0,\text{met}}$ ,  $\rho_c$ ) for selected silicon surfaces based on published results and recent achievements on industrial fabrication.

## 2.6 | Characterization of screen printed contacts

Applying the metal contacts using screen printing is a high-precision production step that requires adequate characterization methods to assess the quality and reliability on cell and module level. A comprehensive characterization of the metallization quality has to consider the following aspects:

- Optical quality of the metal grid on the front and—if necessary—on the rear side including the total metallized fraction of the active cell area and the (effective) contact finger width.
- Electric quality of the front and rear side metallization comprising grid resistance, lateral finger resistance, contact resistance, and—in case of full-area rear-side metallization—sheet resistance of the Al layer and the Ag pads.
- Surface-related recombination activity in the non-metallized and metallized areas (dark saturation current density of passivated and metallized areas).

The relevant parameter to assess the optical quality of the screen printed front (and respectively rear) side metallization is the total metallized fraction  $A_{met,tot}$  of the active cell area. On module level, the total shaded area on an individual cell is a combination of the effectively shaded area by the metal grid (fingers, redundancy lines) and the solder ribbons/wires. Thus, the resulting width  $w_f$  and the three-dimensional geometry (see Section 2.3) of the printed and fired/cured contact fingers is of great importance for applying the screen printing step on the front/rear side. It is thus very important to assess the three-dimensional contact finger geometry with sufficient measurement methods and an adequate statistical evaluation. Precisely measuring the three-dimensional finger geometry requires 3D microscopy with a sufficiently high magnification (i.e., 500X). To ensure an adequate statistical evaluation, a certain amount of local measurements of finger segments per cell should be performed, ideally at similar position on each cell using standardized illumination conditions. The exact quantification of the relevant finger geometry parameters should be determined with adequate image analysis algorithms<sup>243,244</sup> to avoid subjective influences and measurement errors of manual measurements and ensure a reproducibility. Recommended three-dimensional geometry parameters are shown in Figure 4A–D. In addition, scanning electron microscopy (SEM) images, that is, of the finger

cross-section, are recommended to analyze the contact microstructure of bulk and interface. To assess the electric quality of the contact fingers related to the finger geometry, Pospischil et al.<sup>245</sup> have introduced the electric aspect ratio  $AR_{el}$ :

$$AR_{el} = \frac{A_{f,0}}{w_{f,0}^2}. \quad (1)$$

In an optimal case, contact fingers should have a large  $AR_{el}$  and minor variations of finger height  $h_f$ , width  $w_f$ , and cross-sectional area  $A_f$  along the length of the finger in order to maximize the optical and electrical performance and efficient use of silver paste.

The front- and rear-side metallization contributes to the total series resistance  $R_s$  and thus the FF of the solar cell (Figure 4E). With respect to electrical characterization, several parameters of the front and rear side metallization are of importance (Table 3). These electrical parameters have to be measured using adequate characterization methods with sufficient statistical certainty. Grid resistance  $R_{Grid}$  and mean lateral finger resistance  $R_f$  should be measured with an automatic measurement device (i.e., an industrial cell tester) under standardized conditions, as manual measurements of individual contact fingers using, that is, the 4-point-probe method, suffer from significant measurement errors and insufficient statistical certainty. Various characterization methods have been established to determine the spatially resolved series resistance of a solar cell. Common methods are the coupled determination of the dark saturation current and the series resistance (C-DCR),<sup>246</sup> series resistance mapping based on electroluminescence ( $R_s$ -EL),<sup>247</sup> and photoluminescence imaging ( $R_s$ -PL).<sup>248,249</sup> Contact resistance is usually measured using characterization tools based on the transmission line model (TLM)<sup>17,250</sup> using manual or semi-automatic measurement devices. To ensure a valid evaluation of contact resistance, it is essential that a statistically significant amount of measurements is carried out and possible errors due to contacting problems of the pins or wrongly chosen sample parameters are avoided. The electric performance of the rear side metallization is usually less critical for the cell performance. However, it can be helpful to assess the series resistance contribution of the rear-side metallization in some cases. This can be done by automatic measurement in an industrial cell tester or by manual measurement of the lateral sheet resistance  $R_{sh,rear}$  of the rear side metal.

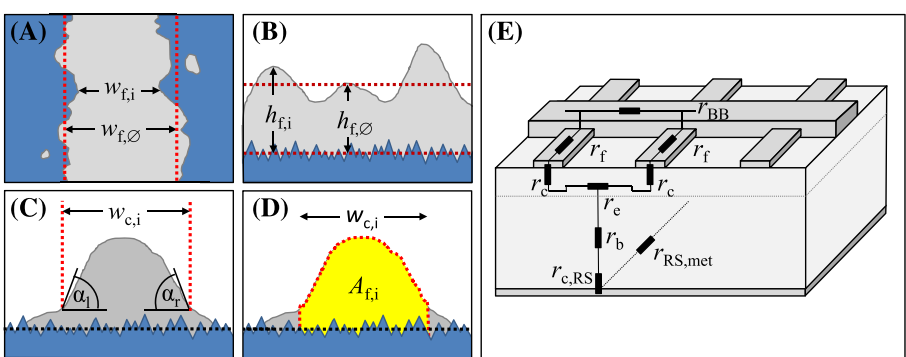


**FIGURE 4** Schematic of selected finger geometry parameters: (A) shading-relevant finger width  $w_f$ , (B) average of maximal finger height  $h_f$  along the ridge line, (C) core finger width  $w_c$ , and (D) cross-section area  $A_f$ . (E) Contribution of different factors on the total series resistance of a typical H-pattern solar cell (adapted from Mette<sup>139</sup>)

**TABLE 3** Recommended electrical parameters related to the front and rear side metallization of solar cells

Parameter	Name	Unit
Grid resistance	$R_{Grid}$	$\Omega/\text{m}$ or $\Omega/\text{cm}$
Lateral busbar resistance	$R_B$	$\Omega/\text{m}$ or $\Omega/\text{cm}$
Lateral finger resistance	$R_f$	$\Omega/\text{m}$ or $\Omega/\text{cm}$
Specific contact resistivity	$\rho_c$	$\text{m}\Omega\text{cm}^2$
Total series resistance contribution of the grid	$r_{s,grid}$	$\Omega\text{cm}^2$
Total series resistance contribution of fingers	$r_{s,f}$	$\Omega\text{cm}^2$
Total series resistance contribution of busbars	$r_{s,b}$	$\Omega\text{cm}^2$
Sheet resistance of rear side metal	$R_{sh,rear}$	$\text{m}\Omega/\text{sq.}$
Front side metal-induced dark saturation current density	$j_0, \text{met\_front}$	$\text{fA}/\text{cm}^2$
Rear side metal-induced dark saturation current density	$j_0, \text{met\_rear}$	$\text{fA}/\text{cm}^2$

### 3 | SCREEN PRINTING FOR SOLAR CELL METALLIZATION: PROCESS MECHANICS AND INFLUENCE FACTORS

#### 3.1 | Configuration and criteria of PV backend production lines

The industrial fabrication of silicon solar cells requires—depending on the solar cell concept—a specific sequence of process steps,<sup>251</sup> which is realized on highly automated production lines. The process chain can be divided in a *frontend* part, which includes process steps like wet-chemical etching, thermal diffusion, and plasma-enhanced chemical vapor deposition (PECVD), and a *backend* part comprising metallization, firing furnace, and testing/sorting units. Beside the processing units, a variety of handling and quality inspection units to detect problems like wafer breakage are required. The individual configuration of a production line strongly depends on the cell concept and the resulting processing scheme. Figure 5 shows the backend part of an exemplary PERC production line.<sup>251</sup>

The selection and configuration of a solar cell production line are complex and have to consider a multitude of aspects. In the following, an exemplary selection of technical criteria with focus on the backend part of a PV production line is provided<sup>252</sup>:

- Number of lanes and throughput of the backend line (up to three parallel lanes).
- Cycle time per wafer and net throughput (cycle time down to ~1.0 s/wafer, throughput up to 4,000 wafers/lane).
- Yield loss and uptime.
- Loading configuration (cassette, stacks, and magazines).
- Transport system (linear belt transport and shuttle system).
- Handling of critical wafer material, particularly very thin wafers.
- Flexibility regarding wafer size (M0 to M12).

- Amount of screen printing units per lane (three units for single printing and four units for double/dual printing).
- Design of printing system (fixed table, moving table, and rotary table).
- Variability regarding screen format.
- Positioning system and alignment accuracy.
- Automation features (i.e., automatic paste supply).
- Inline control systems (i.e., inline inspection of printed front side grid) and possibility for closed loop process control (i.e., for alignment correction).
- Configuration of IV-testing unit (H-pattern, busbarless, and characterization tools).
- Flexibility and configuration of the sorting unit.

#### 3.2 | Screen printing process mechanics

Before we will expand on different screen printing sequences, a short summary of the basic mechanics of flatbed screen printing is illustrated in Figure 6. The main apparatus of the process are the screen (see Section 4.6) and the squeegee. First, a sufficient amount of metallization paste is placed onto the mesh (squeegee side of the screen) in front of the squeegee, which is placed at a certain angle  $\theta$  in respect to the mesh. When the printing sequence is initiated, the squeegee moves over the screen at a given flooding speed  $v_{flooding}$ . This motion induces a circular paste movement before the squeegee tip, causing a downward velocity component for the bulk of the paste into the mesh. This flow behavior is well described in literature and was mathematically modeled by Riemer et al.<sup>253–255</sup> Once the mesh is fully flooded with a sufficient amount of paste, the actual printing step is initiated by moving a second squeegee over the screen with a constant speed  $v_{printing}$ , while at the same time pushing the screen onto the substrate by applying a constant downward squeegee pressure. This motion pushes the paste into the screen opening until contact with the substrate is reached. The screen tension causes the screen to snap-off back to its initial position, leaving behind the printed structure on the wafer.

#### 3.3 | Printing sequence

Reducing the finger width  $w_f$  and in parallel maintaining a low lateral resistance of the grid requires an increasing electric aspect ratio  $AR_{el}$  and in consequence a sufficient finger height  $h_f$  and cross-section area  $A_f$ . An approach to fulfill both goals—reducing  $w_f$  and increasing  $AR_{el}$ —is the application of two subsequent screen printing steps for the front side metallization instead of one. This approach, which is commonly known as double or dual printing, requires modern screen printing machines with a very small alignment tolerance between the two printing steps. A further advantage of two subsequent printing steps is the possibility to use different Ag pastes for the first and second print. The paste used for the first printing process can be optimized with respect to contact formation, while the paste for the

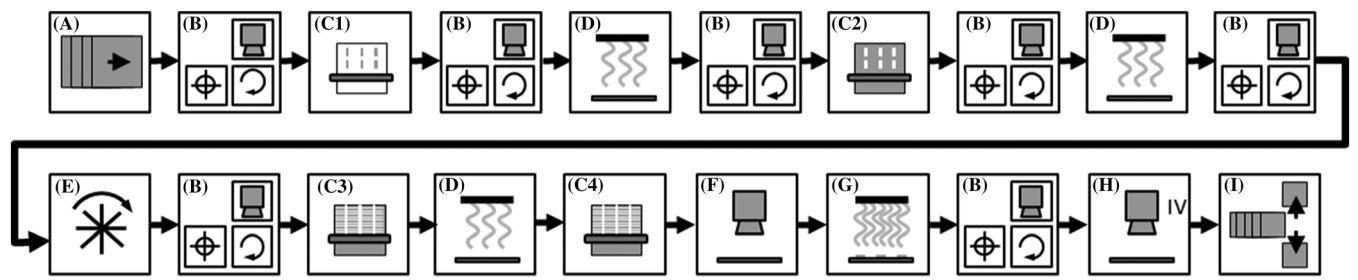
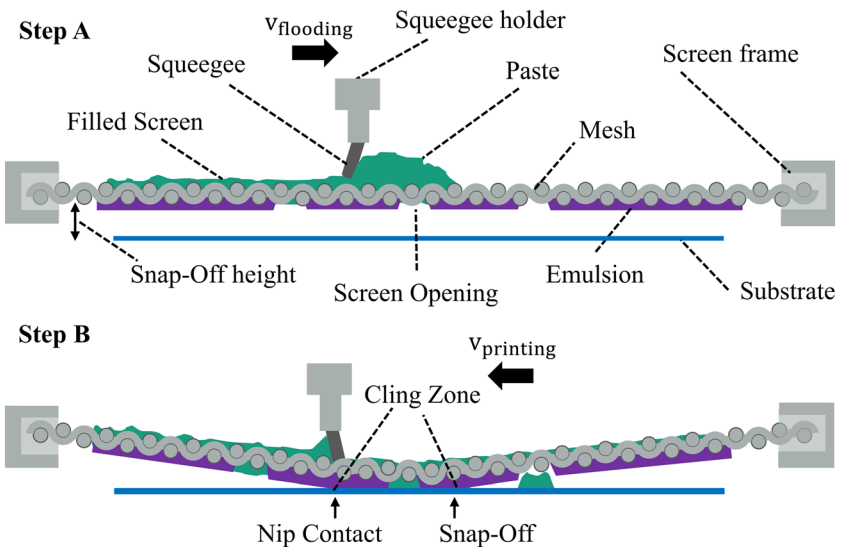


**FIGURE 5** Simplified schematic of the backend part of a production line for PERC solar cells including loading unit (A), alignment and breakage control (B), screen printer for Ag pads (C1), inline dryer (D), screen printer for rear-side Al (C2), flipping unit (E), screen printer for front side Ag grid (C3) with optional printing unit for double order dual printing (C4), optional inspection unit (F), contact firing (G), IV tester (H), and Sorter (I)

**FIGURE 6** Schematic illustration of the screen printing process. In Step A, the squeegee is moving over the screen and fills the mesh with paste. In Step B, a printing squeegee pushes the screen down to the substrate until contact is reached. The mechanics of this movement induce a snap-off behind the squeegee, where the screen moves back to its initial position, while paste remains on the substrate at the defined location.<sup>81</sup>



second printing process can be optimized to increase the aspect ratio and the lateral conduction.<sup>60</sup> From an economic point of view, applying a double or dual printing process requires additional investment for a second front-side screen-printing unit and increased expenses for consumables like screens. On the other hand, the electric performance of the cell performance can be increased with comparatively simple means.

### 3.3.1 | Double printing

Printing the same grid layout in two consecutive printing steps onto the front side of the solar cell is commonly known as *double printing* or *print-on-print* (PoP) process. Usually, the full H-pattern grid (fingers and busbars) is printed in the first step and a finger grid without busbars in the second step to increase the aspect ratio of the contact fingers but reduce the overall silver consumption.<sup>256</sup> Applying double printing enables narrow contact fingers with high aspect ratio due by increasing the finger height.<sup>50</sup> Thus, the lateral grid resistance can be significantly decreased without significant deterioration of optical properties (shading). Double printing processes currently have a relatively constant market share of around 10–12%.<sup>92</sup> From a technical

point of view, several aspects have to be considered for a successful application of double printing on industrial scale:

- Printing a fine line grid in separate, sequentially arranged screen printing units requires very small alignment tolerances of the machinery. Modern screen-printing devices with an alignment tolerance down to  $\pm 12.5 \mu\text{m}$  at  $60^{\circ}\text{C}$ <sup>252</sup> enable such a high-precision alignment for double printing processes.
- Mesh-based screens typically have production tolerances with respect to screen warpage, tension, and the exact position of the layout on the screen. Positioning deviations of the first and second print thus cannot be totally avoided if two separate screens are used.<sup>50</sup> However, these tolerances have to be minimal (see Section 4.6).

During the printing process, the screen mesh is constantly stressed by the transition of the flooding bar and the squeegee within each printing step. During the production lifetime of a screen, thousands of such transitions are applied, which leads to an individual deformation of the screen mesh and in consequence to an increasing distortion of the printed grid on the wafer.<sup>257</sup> Thus, the alignment quality of the two screens is often matched manually, which causes

substantial efforts. During the production process, the alignment quality between the first and second print deteriorates with increasing number of process cycles. The failure of one screen thus requires an exchange of both screens, which is economically unfavorable.

### 3.3.2 | Dual printing

Printing the contact fingers and the busbars in two separate, consecutive steps is commonly known as *dual printing*. Dual printing has been originally applied for stencil printing processes as intersecting elements like busbars and fingers cannot be combined in one stencil layout.<sup>256</sup> However, dual printing is also applied for screen printing processes using two different screens or hybrid processes combining screen and stencil printing.<sup>67</sup> Printing the front side metallization of solar cells with a dual printing sequence means that the busbars are printed in the first step, that is, with non-contacting silver paste. The contact fingers are printed in a second step using, that is, conventional fire-through Ag paste. Dual printing offers several benefits compared to double printing. The possibility to use separate pastes for busbars and fingers has several positive effects on the performance of the solar cell and the Ag consumption, particularly for cell concepts with fire-through contacts on the front side: Using non-contacting Ag paste for the busbars, the total contact area between front side metallization and the emitter surface is substantially reduced. Thus, losses related to  $V_{oc}$  due to metal-induced recombination<sup>119,173</sup> and to FF due to the short-circuit effect are significantly lower.<sup>199</sup> Finally, the requirements regarding alignment precision are less critical compared to double printing. Specific paste compositions for dual printing are commercially available today. Furthermore, it offers the opportunity to use separate, optimal screen configurations for finger and busbar printing, which allows for an individual optimization of the printing result and silver consumption. Fine mesh screens can be used to print the fingers with narrow width, high aspect ratio, and good uniformity. The printing of busbars can be realized using suitable screens to optimize layer thickness, lateral conductivity, adhesion and soldering properties, and low silver consumption. Dual printing processes currently have a market share of around 20%, which is expected to increase throughout the next years.<sup>92</sup>

### 3.4 | Impact of the wafer surface

The front side of a solar cell is typically equipped with a fine texture to decrease the reflection of incoming photons and the path length of photons inside the semiconductor.<sup>258,259</sup> The texture is composed of randomly distributed pyramids (Cz-Si) or round valleys (mc-Si) with a depth of a few micrometers. The industrial standard method to generate the surface texture is wet-chemical etching. While the texture is beneficial for the optical performance of the solar cell, the increased roughness of the surface is disadvantageous with respect to fine-line front side metallization using printing techniques. During the flatbed screen printing process, the emulsion-covered side of the screen is

pressed onto the wafer surface by the transmission of the squeegee. This sealing along the channel edges—also known as “gasket seal effect”—prevents excessive spreading of the paste along the contact finger (Figure 7).<sup>260</sup>

Several parameters affect the effectiveness of the edge sealing and thus the extent of paste spreading along the channel edges. The morphology of the surface (roughness of the texture) obviously has a strong impact on the sealing quality of the channels and thus paste spreading.<sup>260,261</sup> Texturing the wafer surface with small random pyramids or using new approaches like plasma etching<sup>262</sup> can help to increase the quality of the metallization without deteriorating the optical properties. The effectiveness of the edge sealing is further influenced by material properties (softness) and surface roughness (typically specified with the  $R_z$  value) of the emulsion and the printing parameters—predominately the squeegee pressure. Depending on the properties of the emulsion and the printing parameters, the sealing quality deteriorates with increasing lifetime of the screen as the channel edges are gradually damaged on microscopic scale with each printing step. Using single-layer stencils, the channel edges are not sealed during the printing process due to the lack of an emulsion layer. Thus, excessive spreading along the finger channel edges can be observed, which leads to additional shading of the active cell area. This negative effect can be prevented by the use of double-layer stencils with an additional emulsion layer (see Section 5.1).

### 3.5 | Screen technology

The screen is one of the most important components when it comes to fine line screen printing because it serves as the guiding geometry for the entire paste flow. In today's state of the art metallization of Si-

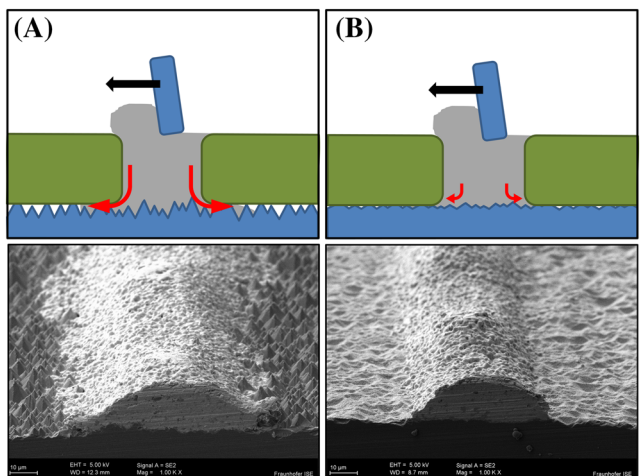


**FIGURE 7** Gasket seal effect of the emulsion on the textured surface of the silicon wafer: On a rough wafer surface/texture, the sealing is less effective, which leads to substantial spreading along the channel edge (A). A smoother surface/texture of the wafer leads to a better sealing of the channel edges and thus decreased paste spreading (B).<sup>260</sup>

Solar cells, the industry uses mainly screens consisting out of a structured emulsion mask layer on top of a quadratic woven metal mesh. Table 4 presents an overview on common screen and mesh parameters which have been investigated in various scientific studies. Figure 8 presents a SEM image of a regular screen opening after the emulsion was first applied onto the mesh and then structured by an etching process. Usually, this mesh and the emulsion are two separate products that are manufactured by different suppliers. The mesh supplier is producing the mesh by weaving a defined number of wires per unit length (usually communicated as mesh count MC per #/inch) into a quadratic mesh. This mesh count combined with the corresponding wire diameter  $d$  and the maximal tensile strength  $\sigma_{uts\_wire\_mat}$  of the wire material defines the maximal possible tension  $\gamma_{screen}$  of the mesh as given in Equation (2).<sup>264,265</sup>

$$\gamma_{screen} = \sigma_{uts\_wire\_mat} \cdot MC \cdot \frac{\pi d^2}{4} \quad (2)$$

This parameter is crucial in screen printing because it dictates the screen life time, which is one of the most important parameters in an industrial production environment.<sup>266</sup> Furthermore, the screen tension influences strongly the snap-off mechanics, resulting in a smooth separation of the screen and printed structure. This correlation was focus on multiple studies in the field of screen printing modeling (see Section 3.7) and rheological investigations of the screen-paste interaction (see section 5). Usually, the mesh is further calendared during a temperature controlled calendaring process, where the thickness of the mesh is compressed. This influences the

theoretical maximal fluid volume  $V_{th}$  a single mesh unit can hold as defined in Equation (3).<sup>264,267</sup>

$$V_{th} = \frac{d \cdot d_0^2}{(d + d_0)^2} \quad (3)$$

The wire-to-wire distance  $d_0$  can be calculated with the known mesh count MC (in 1/inch) by using Equation (4).

$$d_0 = 25,400 / MC - d \quad (4)$$

After the mesh is defined by its mesh count MC, the corresponding wire diameter  $d$ , the wire material with its maximal tensile strength  $\sigma_{uts\_wire\_mat}$ , and the corresponding rate of calendaring, the emulsion layer with a certain thickness EOM (emulsion over mesh), are applied and structured on top.<sup>264</sup> The combination will result in a screen opening with a width  $w_n$  and a certain length  $l$  (usually defined by the dimensions of the substrate or desired pattern). Furthermore, Figure 8A shows that the opening channel is aligned at a certain angle  $\varphi$  in respect to the quadratic mesh (or frame, respectively).

The opening rate OA is the most important parameter in order to describe this geometric apparatus and is defined by Equation (5).<sup>267</sup>

$$OA = \frac{d_0^2}{(d + d_0)^2} \quad (5)$$

State of the art screens are usually made with a screen angle  $\varphi = 22.5^\circ$  for historic reasons. When screen printing was used in the

**TABLE 4** Overview on different screen configurations that were used over a broad range of scientific or technological investigations in the last 20 years

Year	Mesh count	Wire diameter	Wire material	calendaring	Screen tension	Screen opening	Screen angle	EOM	Ref.
1999	325	16	Steel	n/a	n/a	125–250	22.5	7.6	<a href="#">271</a>
2012	325	28	Steel	No	n/a	30–80	22.5	n/a	<a href="#">272</a>
2012	380	14	Steel	No	n/a	30–80	22.5	n/a	<a href="#">272</a>
2015	145	56	Steel	No	n/a	50–1,000	22.5	12	<a href="#">273</a>
2015	200	40	Steel	No	n/a	50–1,000	22.5	12	<a href="#">273</a>
2015	250	36	Steel	No	n/a	50–1,000	22.5	12	<a href="#">273</a>
2015	300	32	Steel	No	n/a	50–1,000	22.5	12	<a href="#">273</a>
2015	325	30	Steel	No	n/a	50–1,000	22.5	12	<a href="#">273</a>
2018	360	16	Steel	No	26	35	30	17	<a href="#">274,275</a>
2018	380	14	Steel	Yes	n/a	30	22.5	n/a	<a href="#">79</a>
2018	380	14	Steel	Yes	n/a	30	0	n/a	<a href="#">79</a>
2019	360	16	Steel	Yes	22	27, 30	22.5	15	<a href="#">80,81</a>
2019	380	14	Steel	Yes	~20	15–24	30, 22.5	15	<a href="#">83,276</a>
2019	440	13	Tungsten	Yes	~20	15–24	30, 0	15	<a href="#">83,276</a>
2019	480	11	Tungsten	Yes	~20	15–24	30, 22.5	15	<a href="#">83,276</a>
2019	380	14	Steel	Yes	n/a	15–24	30	15	<a href="#">80</a>
2019	360	16	Steel	n/a	n/a	37	22.5	16	<a href="#">277</a>
2019	280	20	Steel	n/a	n/a	27	0	15	<a href="#">219</a>

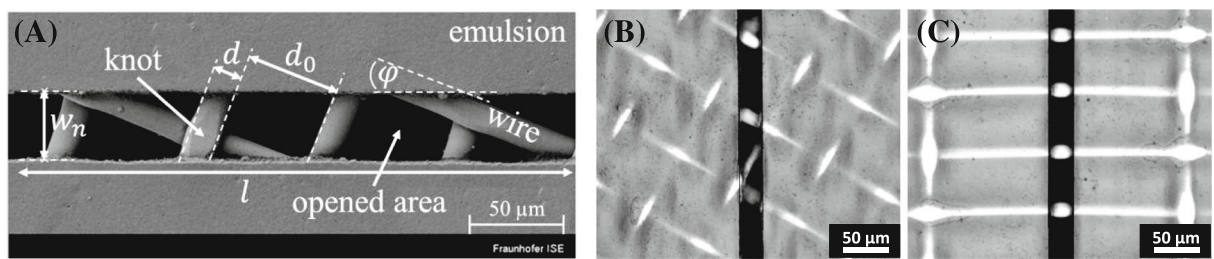


**FIGURE 8** On the left in (A), a SEM image of a regular screen opening with the definition of all relevant parameters is shown.<sup>83,263</sup> On the right in (B) and (C), the comparison of a regular screen with a screen angle of  $\varphi = 22.5^\circ$  (A) versus a so called “knotless”  $0^\circ$  screen is shown.<sup>79</sup>

printed electronics industry, they realized that in order to print orthogonal line paths (e.g., electrodes), they need to use an angle that creates a similar structure of the screen opening channel in both directions in terms of the existence of wire crossings (so called “knots”). Very low or very high angles towards  $45^\circ$  might make it possible to create opening channels with very low or even zero wire crossings in one direction at the expense of having an over proportional amount in the other direction. At the screen angle  $\varphi = 22.5^\circ$ , this trade-off is more or less balanced. It must be noted that to our knowledge there does not exist clear literature on this explanation. Coming now back to the metallization of Si-solar cells, the  $22.5^\circ$  screen angle is the predominantly used standard even though fine lines are only printed in one direction. This is the origin of one major drawback because wire crossings always exist within each screen opening channel  $w_n$ , limiting the printability and therefore reducing the local finger height respectively. In recent years so called “knotless screens” emerged, where the mesh is aligned at a  $0^\circ$  angle in respect to the frame (see Figure 8B,C), avoiding any wire crossings within the screen opening and therefore increasing the potential paste transfer.<sup>79,268,269</sup> However, the approach requires a precise alignment of the screen opening  $w_n$  to avoid a complete blocking of a channel by a parallel wire. Furthermore, this type of screen architecture naturally suffers a lower screen life time because the emulsion edges are stabilized with less wire material. Tepner et al.<sup>270</sup> presented a first modeling attempt of the wire intersection coverage in order to predict the screen life time. Throughout the years, a variety of different screen architectures have been used in a broad range of scientific and technological investigations of the screen printing process. Table 5 presents a summary of different screen architectures, revealing that especially the mesh is not available in arbitrary configurations because changing the wire material or the mesh count MC becomes very expensive in an industrial production environment.

### 3.6 | Screen simulation approach

As discussed above, the opening rate of the screen opening  $w_n$  is one of the most important parameters when it comes to evaluating the expected printing quality of a screen. However, it only describes the average opening rate. As seen in Figure 9, the regularity of the opening rate OA actually depends on the screen parameters (e.g., screen

**TABLE 5** Recommended finger geometry parameters and quality parameters for the characterization of the metallization quality on

Parameter	Name	Unit
Shading-relevant finger width	$w_f$	μm
Finger height along ridge line	$h_f$	μm
Conduction-relevant core finger width	$w_c$	μm
Finger cross-section area	$A_f$	μm <sup>2</sup>
Electric aspect ratio	$AR_{el}$	-

angle  $\varphi$ ). This was studied by Ney et al.<sup>263</sup> and Tepner et al.,<sup>83,270,276</sup> who both developed a mathematical model which is able to calculate the average deviation of the opening rate OA across the length l of the screen opening. They found that increasing the screen angle will reduce the average deviation, suggesting that screen architectures with screen angles above the overall industry standard of  $\varphi = 22.5^\circ$  should be explored in more detail. On the other hand, it should be noted that an increase of the screen angle will also increase the overall production cost of the screen because more mesh will be wasted due to the angled cutting into respective sheets. Tepner et al. presented a full analytical description of the cutting losses based on the screen angle and the dimensions of the weaving machine.

### 3.7 | Process modeling and simulation approaches for screen and stencil printing

In the 1980s, the first significant attempts to provide a theoretical model of the screen printing process were done by Riemer,<sup>253–255,278</sup> who mathematically described how the squeegee orientation creates a pressure distribution within the paste volume in front of the squeegee. Figure 10 presents his famous streamlines of the fluid in front of the squeegee obtained by a hydrodynamic model, which is based on earlier work of Benson<sup>279</sup> and Messerschmitt.<sup>280</sup> This model has led to a few fundamental conclusions, which transformed over the years into something which has come to be known as the “experience of the screen printing operator” in today’s industrial application environment. At about a third of the squeegee angle, the fluid velocity comes to a minimum (center of the stream lines in Figure 10). Following Stokes equations, the pressure of the fluid is at its maximum where its viscous movement becomes minimal. Maintaining this pressure will

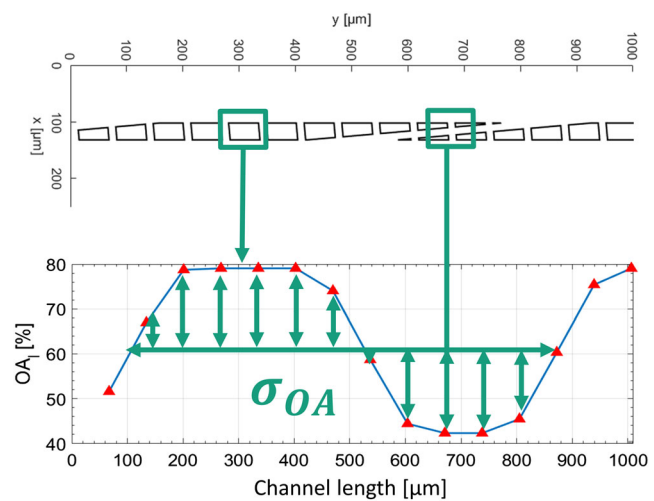


**FIGURE 9** Modeling of the opening rate across the length of the screen channel  $w_n$ . Ney et al.<sup>263</sup> introduced the novel parameter  $\sigma_{OA}$ , which describes the average deviation of OA as a function of the overall screen parameters.

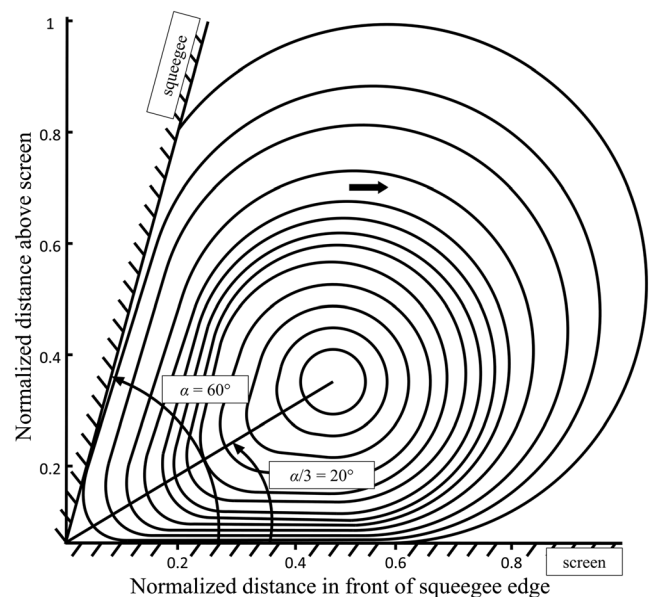


**FIGURE 10** Streamline pattern of a paste volume in front of the squeegee after Riemer.<sup>255</sup> The figure was slightly adapted and simplified from his original publication.

lead to a fragile balance between the distance of this stream line center to the squeegee and screen surface, which are both also influenced by their relative movement to each other. In order to maximize the overall fluid deposition onto the substrate, this hydrostatic pressure should be kept as high as possible during printing. Therefore, the operator finds himself in a situation where he needs to find the optimal process parameters for specific rheological properties of the fluid without knowing them or doing all necessary calculations beforehand. Even though this model was limited to only simplified flow

characteristics of printing inks and pastes, Riemer provided some valuable insights to the optimal process parameters in order to prevent undesired effects like clinging of the screen and sticking of the fluid to the mesh during screen snap off. His work served as fundamental bases for later expansions by Chapman et al.,<sup>281</sup> who expanded the model to shear thinning power law fluids and Hunter et al., who added paste leakage under the squeegee to the model.<sup>282</sup> A continuation of these contributions were done by Owczarek and Howland,<sup>283,284</sup> who studied in their two part series on the modeling of the screen printing process how the flow pattern of a paste volume directly in front of the squeegee is affected by its movement over the screen. They showed how the angle between the squeegee surface and the screen creates a pressure difference on the paste volume, which is causing a circulatory flow pattern in front of the squeegee and therefore a downwards velocity component for the paste, resulting in the desired flooding of the mesh. Further, they fully derived an equation that describes how the shear rate for the paste depends on the squeegee pressure, creating one of the bases for future empirical rheological paste optimizations.<sup>283,284</sup> Later, Mannan et al.<sup>285</sup> added a mathematical description of the squeegee deformation during printing, which was also supported by experimental data. These studies provided analytical models for specific aspects of the screen printing process without a full generalization of the involved geometry because they rely on simple boundary conditions and simplifications of the apparatus. A more recent generalized model for the movement of any Newtonian fluid flow through a screen forced by the squeegee movement was given by White et al. in 2006.<sup>286</sup> They provided a dimensionless set of parameters describing the macroscopic flow situation as well as the inner flow phenomena near the squeegee tip.<sup>286</sup> However, the fact that the model was missing the extension for non-Newtonian shear thinning flow characteristics of industrial relevant suspensions, made an expansion absolutely crucial before its potential use for process optimization. Taroni et al. from the same research group then achieved that by expanding the model for power law fluids in 2012, mathematically describing how the flow ahead of the squeegee depends on where screen deflection takes place, the ratio of paste surface tension to screen tension and the screen permeability.<sup>287,288</sup>

To this date these models are not fully explored in terms of their potential for further process optimization by implementing them into a full process simulation. Only isolated attempts to provide basic simulation tools have been reported by Polfer et al.,<sup>289</sup> who provided a CFD simulation of the movement of a non-Newtonian fluid ahead of a moving blade and its correlation to experimental data. Choi et al.<sup>290</sup> also provided a simple process simulation including the screen snap off mechanic (without the interaction with the mesh). They were able to predict the printed finger geometry without providing any clear correlation to experimental data. Even though their work lacks state of the art rheological modeling of the paste and necessary depth in geometric definition of boundary conditions, it shows that a full process simulation can be done with moderate use of resources.<sup>290</sup>

Glinski et al.<sup>291,292</sup> on the other hand had similar success with simulating the macroscopic flow ahead of the blade in stencil printing, showing how rheological parameters in highly non-Newtonian flow

are affecting the outcome. However, they do lack clear correlation to experimental data. Durairaj et al.<sup>293</sup> later included experimental data for the fluid rheology as additional input parameters, showing that the simulation model is providing reasonable output data for the pressure distribution. They further discussed how the simulation approach could be expanded to include specific rheological phenomena like wall slip effects. Finally, Kapur et al.<sup>294</sup> provided a full CFD simulation of the screen snap-off, which is able to predict the amount of paste deposition depending on the rheological and process parameters. They further provided compelling experimental data to verify the predictability of their simulation approach. Other research groups also published notable contributions to modeling of the screen and stencil printing process with to some extent similar but often more vague results compared to the presented overview.<sup>295–302</sup>

## 4 | RHEOLOGICAL BEHAVIOR OF METAL PASTES

### 4.1 | The state of research on paste rheology for PV

The ongoing development of metal pastes, especially silver fire-through pastes for PERC, low temperature Ag-pastes for SHJ metallization, and aluminum high temperature pastes for fully or structured rear side metallization, played a major role for the success story of flatbed screen printing in the PV industry. Commonly industrial available Ag-pastes for front side metallization of PERC contain a mass share of up to 95% Ag-particles with average particle sizes of 3–4 µm and a more or less spherical shape.<sup>277,303</sup> Additionally, glass frits, based on quartz glass containing lead oxide, are added, which serves on the one hand the purpose of a glue between the substrate and the printed contact line and furthermore enables the contact formation by etching the silicon nitride anti-reflection coating on the wafer surface (see Section 3 for more details).<sup>304,305</sup> The Ag-particles and the glass frit are surrounded by an organic vehicle containing solvents, binder, and rheological additives. This fluid phase is added to control the paste rheology and its stability in order ensure a sufficient structured paste deposition for any of the printing approaches used and researched in the field of solar cell metallization. This correlation of paste rheology and the printing process was focus of several research activities by Hoornstra et al.,<sup>306</sup> Hsu et al.,<sup>307</sup> Thibert et al.,<sup>308,309</sup> Jewell et al.,<sup>273,310</sup> Potts et al.,<sup>311</sup> Pospischil et al.,<sup>312–315</sup> Yüce et al.,<sup>277,316,317</sup> Xu et al.,<sup>274,275</sup> Tepner et al.,<sup>81</sup> and couple others. Throughout this section, we are going to address the key findings and discuss their impact on the future of fine-line metallization of silicon solar cells.

In order to even research the flow behavior of such metal pastes for solar cell metallization, a broad variety of independent studies on highly filled suspension were done over the last couple of centuries, creating the fundamental bases for any rheological investigation of an industrial product utilized in a mass production environment. Starting from the fundamentals of Newtonian fluid mechanics and Hooke's

law,<sup>318</sup> Ostwald-de Waele's introduced its modeling of a power law fluid back in 1929. This model is able to describe the shear thinning nature of pseudo plastic fluids but lacks accuracy for low shear rates. Therefore, Bingham<sup>319</sup> introduced the description of critical onset for shear stress before a fluid shows any plastic deformation. Combining both approaches has led to the famous definition of the Herschel and Bulkley<sup>320</sup> model, which is the state of the art approach for describing the flow characteristics of commonly used metal pastes for PV applications.

Coming back to the printing process, back in 1970, Trease and Dietz<sup>321</sup> introduced a simple model for the different regimes of shear rates during the screen-printing process and therefore the cause for the drastic change in viscosity of a Herschel and Bulkley<sup>320</sup> fluid. In Figure 11 on the left, a schematic of the model is shown, revealing how the fluid experiences a shear stress even before printing by manually applying the paste on the screen by the operator. Usually, the operator stirs the paste in the cub for a significant amount of time to lower the viscosity. For obvious reasons, this is not done in a reproducible manner and shows how the experience of the operator is one of the crucial aspects to a successful printing even in today's production environment. Afterwards, the squeegee pushes the paste over the screen introducing another rate of shear to the paste volume. This movement and its consequences for the paste flow is discussed in more detail in Section 3.7. Within the next phase, the actual printing step occurs, forcing the paste to penetrate all individual openings in the (by the mesh) structured opening of the screen. In this phase, the shear rate rises usually by at least one order of magnitude, resulting in a complete breakdown of the internal structure of the paste and therefore a major drop of its viscosity. Afterwards, the screen snap-off will take place, which leaves the printed contact finger on the substrate at rest (without experiencing further external forces). In this phase, the internal structure recovers depending on the thixotropic characteristics of the paste. This basic model still serves today as one of the first starting points for researchers in the field of paste rheology for screen printing, because it summarizes many critical questions in one single diagram.

- Which values on the right y axes for the shear rate are relevant in today's screen printing process and how are they linked to the process and screen parameters?
- Which values then result on the left y axes for the viscosity of the investigated paste and how to measure it in the relevant shear rate regime?
- How exactly unfolds the presented curve over time during the printing process?
- How to directly test this model by experiment?
- What are the limits of this model and what other phenomena may have to be included in order to predict the flow behavior of the investigated paste during the process steps (e.g., slip effects)?

These five questions summarize the current and recent research activities in this field and the above mentioned researches published over the last ten years significant contributions in answering them.

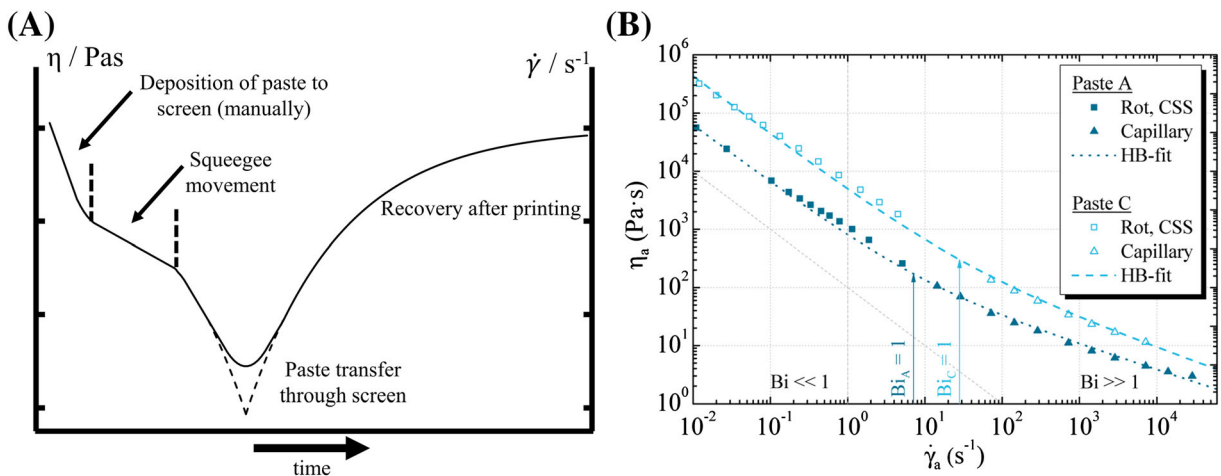


**FIGURE 11** On the left, a schematic diagram for the viscosity and apparent shear rate during the different stages of the screen printing process is presented. The paste experiences a reduction of its viscosity by a few orders of magnitude when being pushed through the screen. Afterwards, depending on the thixotropic behavior of a given paste, the internal structure of the printed paste volume recovers over time. This figure is slightly adapted from the original by Trease and Dietz.<sup>321</sup> Furthermore, it was discussed by Reichl<sup>322</sup> and more recently by Reinhardt.<sup>323</sup> On the right, a flow curve for commercial Ag-paste obtained from rotational and capillary data is shown. Further, the corresponding Bingham number is highlighted, marking the point at which viscous stress starts to dominate and a static flow regime is established. Additionally, Herschel and Bulkley modeling of the experimental data for both pastes is shown.<sup>315</sup>

They examine very similar types of rheological measurements to determine the shear rate depending viscosity in low and high shear regimes, the corresponding yield stress, the thixotropic and viscoelastic behavior, and surface interaction related measurements such as determination of slip phenomena or contact angles. Thibert et al.<sup>308</sup> was focusing on the first two questions by studying how various screen-printing parameters (e.g., typical screen parameters) influences the paste rheology and therefore the shape of printed structures. They found that in order to optimize the interaction between paste and screen during printing, the screen parameters can be chosen in such a way that an optimal compromise between reducing the paste consumption and increasing the homogeneity of the printed structure will emerge. However, in today's mass production environment, the screen parameters are mainly determined by economic choices rather than meeting the given paste rheology for an optimal printing. Furthermore, their attempt to correlate the printed structure back to the screen properties only indirectly answers the first question of what shear rates actually occur during printing. At that time, no detailed information about the spatial resolution of the screen geometry was known, limiting a clear prediction of the rate of shear during screen penetration. Later, Ney et al.<sup>263</sup> and Tepner et al.<sup>270</sup> provided a simulation model which exactly determines the size of all individual openings based the screen parameters (see Section 3.6 for more details). When in the future, this model is utilized to calculate the exact shear rate across the screen opening, a sufficient answer to question 1 will be found.

Hsu et al.<sup>307</sup> and Hoornstra et al.<sup>306</sup> focused more on question 2, analyzing how paste composition will influence the shear rate dependent viscosity and its time dependent thixotropic behavior. Pospischil et al. contributed in a series of publications significant to the overall understanding of how to measure the rheological behavior of

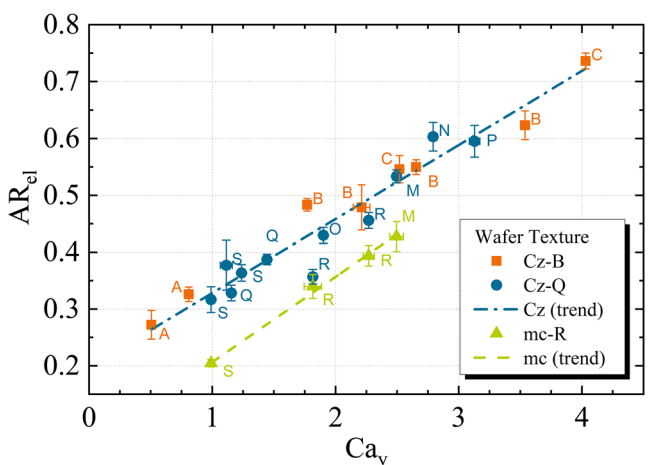


**FIGURE 12** Dependency of the electrical aspect ratio  $AR_{el}$  on the Bingham Capillary number  $Ca_y$  for various combinations of paste and nozzle diameter on three different types of wafer textures<sup>315</sup>

such metal pastes by extending the flow curve from rotational rheometry with experimental data from capillary rheometry. They showed that the transition point from shear to viscous dominated stress (defined by the so-called Bingham number<sup>319</sup>) is crucial when the process relevant relationship between shear rate and the paste viscosity is desired. In Figure 11B, the flow curve for two commercial PERC Ag-pastes for almost seven orders of magnitude is presented.

Furthermore, he worked on generalizing the correlation between finger geometry and paste rheology by deriving a very interesting relationship of the Bingham Capillary number  $Ca_y$  and the electrical aspect ratio  $AR_{el}$  of the contact finger by the dispensing approach as presented in Figure 12.<sup>315</sup> The Bingham capillary number describes the

ratio of yield stress to capillary pressure of a yield stress fluid as described in Equation (6).

$$Ca_y = \frac{\tau_y}{\Delta p_L} = \frac{\tau_y \cdot D}{2\Gamma} \quad (6)$$

Even though this relationship applies for the dispensing process, it reveals a more general guideline for the design of paste rheology. Surface effects cannot be neglected in the micrometer range of today's printing anymore. The presented model that links rheology to printing parameters may need to be expanded by surface effects on the substrate and that of the interacting surfaces of the screen and squeegee.

## 4.2 | The importance of wall slip phenomena

The previous thought addresses directly the fifth of the presented questions on what type of additional phenomena should be included in the presented model of Trease and Dietz.<sup>321</sup> Yuce et al.<sup>277,317</sup> also investigated surface related challenges in determining the correct flow behavior of such paste by studying how wall slip effects during rheological measurements with parallel plate rheometers can be prevented. Kalyon et al. and Barnes contributed significantly to the fundamental understanding on how wall slip effects will influence rheological investigation of highly filled suspensions in a more general sense.<sup>324–331</sup> A highly filled suspension tends to show significant slip behavior when in contact with a smooth rigid surface. This comes due to the fact that at the fluid-wall interface, particles are naturally depleted compared to the bulk of the suspension because they cannot penetrate the wall (they may touch the wall at a specific point when the assumption of spherical particles remains true). Therefore, a small liquid slip layer directly in front of the corresponding wall is created,

which contains a significant reduced volume fraction of particles. If and to what extend this effect may occur depends on various suspension parameters (e.g., particle size, shape, volume fraction, orientation, surface properties, and rheological properties of the vehicle) and wall related parameters such as surface roughness, surface energy, and electrostatic charges. On top of that, the macroscopic shear history of the entire suspension also influences the occurrence of wall slip phenomena.<sup>275,315,316,325,331–335</sup> How this phenomenon is affecting the screen and stencil printing process has been investigated by Durairaj et al.,<sup>336</sup> who demonstrated that finger interruptions during printing processes can be reduced by the existence of slip. That result would directly translate into further reductions of finger width without decreasing the process stability because finger interruptions due mainly occur when the desired printed finger width was too ambitious for the given paste, screen, and process parameters. Further, Xu et al.<sup>275</sup> showed significant differences in the required shear stress for the onset of wall slip between stainless steel and emulsion surfaces for different adaptions of silver pastes. Finally, Tepner et al.<sup>81</sup> discussed how wall slip is influencing the screen printing process by applying functional coatings (optimized for slip) on the emulsion surface in fine line screens and on the rheological measurement equipment respectively (parallel plates of a conventional rheometer). With this approach, they were able to show how much the existence of wall slip reduces the shearing forces experienced by the paste during printing and correlate that to wall slip measurements on a parallel plate rotational rheometer. Results of that study promise a significant reduction of the lateral finger resistance per printed line width when such a coating is applied.<sup>81</sup> Figure 13 presents their explanation for this effect by showing a cross-section of the filled printing channel directly after flooding when the mesh has been fully filled with paste (usually even the opening channel of the underlying emulsion is partially filled during the flooding step). This circumstance is shown in Figure 13A. During the printing phase, the squeegee pushes the paste

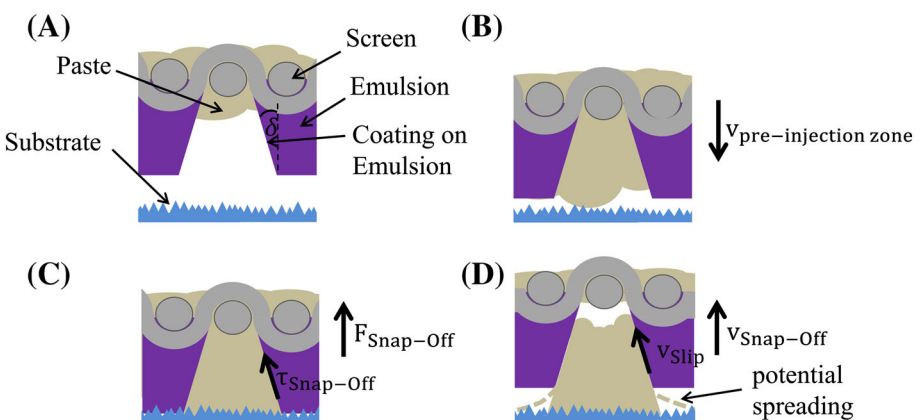


**FIGURE 13** Schematic illustration of the snap-off mechanics in flatbed screen printing. In (A), a cross-section of the filled printing channel after the flooding phase is shown. The mesh is fully and the emulsion channel partially filled with paste. When the printing squeegee returns to create the nip contact, more paste is transferred into the emulsion channel under the mesh. This step is called the pre-injection zone (B). After the nip contact, the snap-off force  $F_{\text{Snap-Off}}$  is acting on the screen. With further movement of the squeegee, this force is increasing and induces an increasing shear stress at the paste-emulsion coated surface (C). When the screen enters the cling zone (after the snap-off), wall slip with the velocity  $v_{\text{Slip}}$  at the interface occurs (D).

into the emulsion channel in Figure 13B. During that motion, the entire screen is pushed onto the substrate until the so called nip contact has been reached in Figure 13C. At this position, the paste wets the surface and creates the substrate-paste interface. As soon as the squeegee moves beyond that position, the screen snap-off is initiated because the screen tension forces the screen back to an equilibrium position. During that motion, wall slip at the emulsion interface (Figure 13D) will be helpful in order avoid additional spreading of the paste after screen snap-off because any additional shearing force at the emulsion-paste interface will cause a reduction of the paste viscosity and further delays the recovery of the internal structure. These results show how wall slip transformed from being an unwanted side effect during rheological measurements to become an extremely beneficial effect at the surface of crucial geometries in the process. We suggest that more studies should be done on such slip phenomena in printing processes as the potential impact is still highly underestimated at this point.

Finally, in order to address questions 3 and 4, Xu et al.<sup>274</sup> and more recently Potts et al.<sup>311</sup> introduced a high speed camera setup up which enables the direct experimental observation of the printing procedure. Xu et al.<sup>274</sup> chose to replace the substrate with a glass plate on top of a high speed camera in order to film the process from below. This allowed him to study mainly the spreading of paste right after printing. They found that the spreading mainly occurs within the first 50 ms after the screen release, further concluding that the internal structure recovered fairly quickly beyond the point where surface interaction with the substrate stops any additional spreading. This shows how thixotropic behavior plays an important role in screen printing even though the actual process speeds are much higher than the timescale of any thixotropic investigation done by conventional rheometers. This result further fits right into the presented overview on the slip phenomena because even the slightest reduction of shearing forces experienced by the paste will have a significant influence in such short time scales. They finally tried to present a more general relationship between printed finger width and rheological parameters (e.g., yield stress and viscosity at a shear rate of 500 1/s) but lack clear experimental correlation at this point.<sup>275</sup> On the other hand, Potts et al.<sup>311</sup> used a different setup with filming the screen snap-off mechanics from the side and correlating it to rheological measurements of the paste viscoelasticity. They could experimentally verify that snap-off distance and printing speed are closely related to the geometry of the printed structure and that parameter settings heavily depend on the viscoelastic behavior of the used paste.

#### 4.3 | Alternative paste systems: Capillary suspensions

At the end of this section about the rheological behavior of common metal pastes, we would like to briefly address the research activities around capillary suspensions, which show great potential in fine line printing for solar cell metallization. Koos et al.<sup>337–342</sup> did fundamental work on the working principle of capillary suspensions in terms of

their theoretical framework, their formulation, and the rheological behavior. These capillary suspensions are solid/fluid/fluid systems without containing any additional non-volatile organic components, which may cause limitations of the paste conductivity after sintering. The secondary fluid in these suspensions is causing the formation of particle network due to the capillary forces. This results in very stable fluids with high yield stresses and promising properties towards a further reduction of Ag-laydown per cell by increasing the grid conductivity significantly. More recently, Yuce et al. investigated the printability of such paste systems in much more detail, finding compositions that almost reach the electrical performance of industrial Ag-pastes with printed finger width of ~45 μm using 37 μm screen openings. They also showed their applicability in pattern transfer printing with printed finger width around 25 μm compared to 20 μm of the reference paste. Further development of such paste systems has the potential of challenging conventional paste compositions in the upcoming years.

### 5 | ALTERNATIVE METALLIZATION APPROACHES

#### 5.1 | Stencil printing

By mid of the 1990s, ECN in Netherlands started intense research activities to apply stencil printing—a technology which had been adopted from PCB manufacturing—for the metallization of silicon solar cells.<sup>343,344</sup> Further promising results on fine line front side metallization using stencil printing were obtained in the 2010 years.<sup>63,68,345</sup> Typical single layer stencils consist of a metal foil, which is partly opened according to the printing layout (Figure 14A). The openings can be realized by electroforming, laser-cutting, or wet-chemical etching. Single-layer stencils do not allow a combined printing of intersecting elements like fingers and busbars. Thus, a dual printing process using two stencils or a screen and a stencil has to be applied. An alternative is the so-called double-layer or hybrid stencil.<sup>343</sup> This type of stencil has been first developed in the mid 1970s<sup>346</sup> but originally not applied for solar cell metallization due to challenges of realizing fine contact openings. Double-layer stencils consist of a partly opened metal foil with regular bridges to stabilize the open areas and an emulsion layer, which defines the printing layout (Figure 14B).

Double-layer stencils allow a combined printing of fingers and busbars using one printing form. Compared to single-layer stencils, a better edge homogeneity of the printed fingers can be achieved due to an optimal sealing between the soft emulsion along the finger channel edges and the textured silicon surface (see Section 3.2). In contrast to screens, the metal foil of a stencil is hardly deformed during the printing process, which leads to a better alignment precision and a significantly longer lifetime when handled adequately. Stencil-printed fingers usually show a significantly better uniformity (no “mesh mark” effect) and a high aspect ratio. Furthermore, the cleaning of stencils is easier compared to screens.<sup>344</sup>

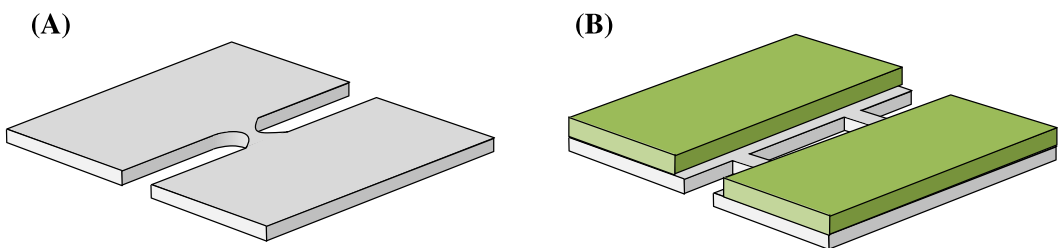


**FIGURE 14** Schematic drawing of (A) single-layer stencil consisting of a partly opened metal foil and (B) a double-layer stencil with a partly opened metal foil with regular stabilizing bridges and an emulsion layer on top, which defines the printing layout

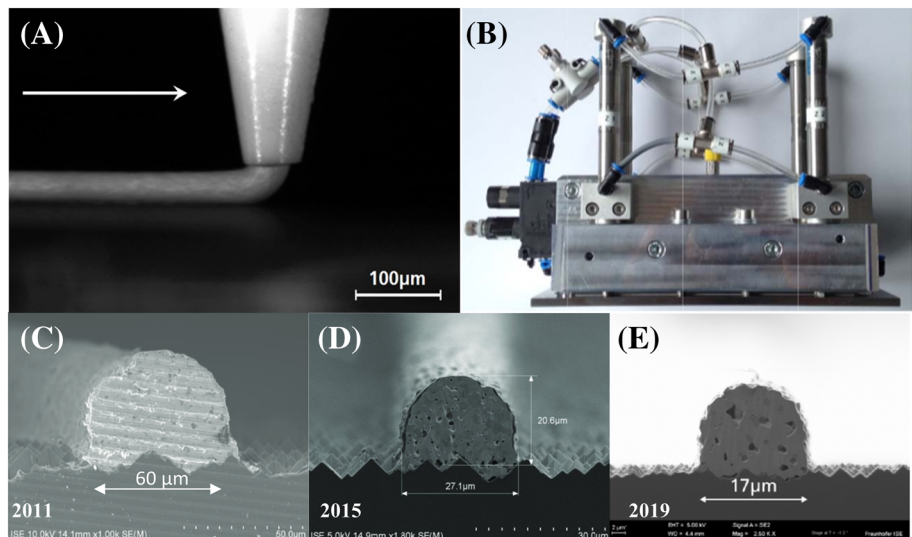


**FIGURE 15** Evolution of the dispensing approach for solar cell metallization. In (A), the single nozzle approach is illustrated, which was used in the early stages of the process development from 2010–2013.<sup>315</sup> In (B), a semi industrial 6" print head with pneumatic clamps for maintenance is shown. With such a device, a large-scale metallization becomes suitable.<sup>349,350</sup> In (C)–(E), SEM images of dispensed finger cross sections from 2011–2019 are shown, revealing the potential of the dispensing approach in terms of cell efficiency and Ag-consumption.<sup>312,351,352</sup>

## 5.2 | Dispensing technology

The beginning of the dispensing technology for solar cell metallization goes back to 1992, when a patent by Hanoka and Danielson was published. Later, this approach was expanded by Schott Solar AG, Germany. They deposited a secondary fluid around the printed finger in order to prevent excessive spreading. One of the main challenges with this approach has been the precise adaptation of the secondary fluid in order to guarantee the desired effect for different generations of Ag-pastes.<sup>347</sup> Later, Solar World Innovations GmbH, Freiberg, applied this approach to an industrial pilot line and demonstrated the technical feasibility of this approach.<sup>315</sup> Since 2010, the parallel dispensing process for metallization of solar cells is mainly being developed at Fraunhofer ISE (Freiburg, Germany). Specht et al.<sup>348</sup> for the first time showed a dispensed Ag front side finger on a silicon solar cell with an average printed finger width of 65 μm. They were able to dispense commercial available Ag-paste (commonly used in screen printing) through a micro nozzle while moving the nozzle over a solar cell using a commercial table robot. Figure 15A presents a microscopic image of the nozzle exit during printing, indicating the working principle of the dispensing approach. Since then, Pospischil et al.<sup>245,312–315,349–351,353–358</sup> were able to demonstrate in a series of publications that the parallel dispensing approach for a fine-line

metallization has an enormous potential for industrial application. They have been constantly improving the finger geometry while at the same time scaling up the process from a single nozzle continuous basic dispensing approach towards a multi nozzle dispensing print head for an intermittent process at very competitive industrial process speeds (Figure 15B). In Figure 15C–E, the evolution of printed finger width using different PERC front side high temperature Ag pastes is presented, revealing an impressive reduction from 65 μm reported in 2012 to only 17 μm in 2019. They showed that this approach led to cell efficiency increases of around 1% rel. compared to screen printing and further reduction of Ag-laydown by over 20% at the same time. This advantage relies on the fact that the approach intrinsically solves a major problem in screen printing: due to mesh marks (further discussed in Section 2.6), it becomes impossible to reach optimal Ag-consumption. The dispensing process provides intrinsically a perfectly homogenous finger geometry across its length removing an entire degree of freedom (deviation of the finger height across its length) from the optimization problem.<sup>315,351</sup>

Besides the front side metallization for PERC, the dispensing approach was further successfully utilized by Erath et al.<sup>359</sup> and Pospischil et al.<sup>351</sup> for metallization of heterojunction solar cells by low temperature curing Ag-pastes. They showed that nozzle diameters down to  $D = 35 \mu\text{m}$  were applicable in a stable process. Due to

spreading of the paste, they ended up with finger width of  $w_f = 46 \mu\text{m}$  with 65 mg Ag-laydown per side. However, a direct comparison to screen printing reference resulted in a +0.3% abs. efficiency gain at a lower paste consumption.<sup>351</sup> Furthermore, they were able to demonstrate an all dispensed bifacial PERC mini module providing a process route without the need of any screen printer. The interconnection was done by the combination of dispensed busbar edges and dispensed ECAs on both sides. On top of that, they utilized the work of Fellmeth et al.<sup>153</sup> by using an Al-fire-through paste, even making the laser process for LCO obsolete. More recently, Ourinson et al.<sup>154</sup> investigated the use of Al-fire-through pastes for the dispensing process in much more detail, showing the potential for an improved contact formation by stacking aligned Al-fire-through fingers with aspect ratios up to 1.76.

### 5.3 | Rotary printing

Rotary printing methods have been used since decades for the large-volume production in many fields of industrial applications. Due to their high precision and throughput capability, these proven technologies can also be applied for a wide range of technical applications or production steps, which require precise and fast coating processes. Among the different rotary printing methods, particularly three technologies are of interest for silicon solar cells: flexography, (indirect) gravure printing, and rotary screen printing. All these technologies are well established and widely used for mass production in other fields of technical printing. Rotary screen printing is primarily applied in niche applications like textile or label printing, usually on roll-to-roll-machines using web-based materials like foil, paper, textile fabrics, and cardboard.<sup>360</sup> Modern roll-to-roll machines can realize fast printing velocities up to 160 m/min. (2.7 m/s)<sup>361</sup> on web-based substrates. Applying such high printing speeds for PV applications would result in

throughput rates for solar cell metallization beyond 10,000 cells per hour. First attempts to use this technology for solar cell metallization date back as far as 1999. However, there are no known published results from these activities.<sup>362</sup> Since 2016, intense research work has been carried out to apply this technology for the metallization of Al BSF and PERC solar cells. Figure 16A shows the working principle of a rotary printing unit for the metallization of silicon solar cells. The printing form is a cylindrical screen with mesh count of up to 400 wires/inch. Alternatively, electroformed, stencil-like cylinders with a hexagonal honeycomb structure made of nickel foil can be used as printing form. During the continuous printing process, the paste is pressed by a fixed squeegee through the openings of the rotating cylinder screen onto the substrate. To ensure a continuous paste flow through the screen openings, a slightly lower viscosity of the paste compared to thick-film pastes for flatbed screen printing is required. The application of rotary screen printing has been successfully demonstrated for the rear side metallization<sup>363</sup> as well as the front side metallization of PERC solar cells.<sup>363</sup> However, further research is necessary to obtain comparable results to flatbed screen printing when realizing fine line grids with contact fingers below 40  $\mu\text{m}$  width.

Flexographic printing is a high-speed letterpress printing method using flexible printing plates or sleeves based on photopolymers or rubber-like material like EPDM (Ethylen-Propylen-Dien rubber). The working principle of a flexo printing unit designed for single item substrates like silicon solar cells is shown in Figure 16B. A medium-viscous fluid containing silver particles, glass frit, and organics is transferred by the so-called anilox roller onto elevated areas of the flexible printing form and directly printed on the silicon wafer. The amount of transferred ink is roughly defined by a regular pattern of finely engraved micro-wells on the surface of the anilox roller, which defines the theoretical ink transfer capability—the so-called dip volume ( $\text{cm}^3/\text{m}^2$ ). Using EPDM printing forms with finely laser-engraved finger elements down to 5  $\mu\text{m}$  width,<sup>364</sup> fine-line front side grid can be printed

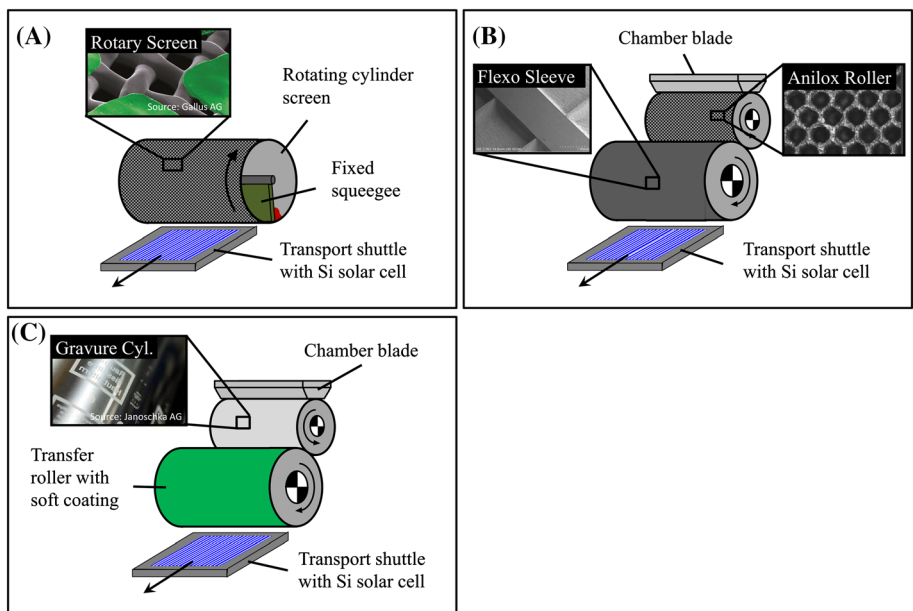


**FIGURE 16** Schematic drawing of three rotary printing methods. (A) Rotary screen printing: The paste is transferred through the open areas of a rotating cylinder screen with an inboard fixed squeegee. (B) Flexographic printing: The anilox roller with a finely engraved surface of microscopic wells transfers a defined volume of ink onto elevated areas of the flexible printing plate or sleeve. The elevated areas of the printing form directly print on the substrate. (C) Rotogravure printing: The printing form the engraved layout is inked by a chamber blade. A transfer roller with soft coating transfers the ink and directly prints on the substrate.

on textured silicon solar cells. Due to a limited layer thickness, flexography is particularly suited for a seed and plate metallization with subsequent reinforcement of a seed layer grid with electroplated Ag or other metal stacks.<sup>365</sup> However, the successful application of flexography for front side metallization without subsequent plating achieving contact finger widths down to around 30 µm has also been demonstrated.<sup>366</sup> Gravure or rotogravure printing is usually applied for large-scale production of packaging and graphic arts products. Gravure printing cylinders consist of a steel core, which is coated with a several millimeter thick, electroplated copper layer. The printing layout is usually engraved into the comparatively soft copper layer by mechanical or laser engraving methods and subsequently covered by a protective, extremely resistive electroplated chromium layer.<sup>367</sup>

The fabrication of the cylinders is cost-intensive and challenging with respect to environmental and safety aspects and is thus only reasonable for large-volume printing products. Gravure printing is able to print very fine structures with high, reproducible quality over millions of print runs. Printing fine patterns on rough and incompressible substrates like textured silicon wafers requires a special variant of gravure printing—the so-called indirect gravure printing or rotary tampon printing process.<sup>368</sup> This rather exotic printing method uses a gravure printing cylinder in combination with a soft-coated transfer printing cylinder (Figure 16C). A successful application of this printing method for the metallization of heterojunction solar cells has been demonstrated.<sup>369</sup>

First attempts to use rotary screen printing for the metallization of silicon solar cells date back to the late 1990s<sup>362</sup> but have not been pursued further. These activities gathered a new momentum in the early 2010 years, when several research groups presented promising results of feasibility studies using flexographic printing,<sup>370–372</sup> rotary screen printing,<sup>373</sup> and gravure printing<sup>369</sup> for solar cell metallization. In the following years, the capability of rotary screen printing and flexographic printing to apply a high-quality front and rear side metallization for Al BSF and PERC silicon solar cells has been demonstrated also on industry-relevant 6" solar cells.<sup>373–376</sup> A first prototype machine for a high-throughput rotary printed metallization of silicon solar cells on industrial level has been recently developed by a German consortium of industry and research institutes.<sup>377</sup>

## 5.4 | Further metallization approaches

Beside screen printing, multi-nozzle dispensing, and rotary printing, further printing and coating technologies to apply the front and/or rear side metallization of silicon solar cells have been investigated in the last decades.

Several studies investigated the application of the front side grid using inkjet technology. Noticeable results were achieved with inkjet-printed seed layer metallization and subsequent reinforcement using electroplating.<sup>365,378</sup> Promising results were also demonstrated using inkjet for the front side metallization of Al BSF<sup>379,380</sup> and heterojunction solar cells<sup>359</sup> without subsequent plating. The main drawback of inkjet-printed front side contacts is a comparatively high lateral

resistance due to the very low layer thickness, respectively, finger height  $h_f$ . Thus, inkjet is particularly interesting in combination with a multi-wire interconnection of the cells, as the impact of the lateral grid resistance on the total series resistance is particularly low (see Section 2.3). Several studies have demonstrated promising results using inkjet for the metallization of multi-wire interconnected monofacial and bifacial heterojunction solar cells.<sup>381,382</sup> A comprehensive overview with regard to inkjet applications for silicon solar cells is provided by Stüwe et al.<sup>383</sup>

A further approach is the so-called Pattern Transfer Printing (PTP™) technology, which has been developed and commercialized by the Israeli company Utilight. PTP™ is a two-step contactless laser deposition process to transfer a fine line grid on the wafer surface<sup>384</sup>: In the first step, a transparent web-based polymer substrate with pre-embossed trenches is filled with high-viscous printing paste using doctor blading. The trenches in the foil substrate can be embossed with a depth and width of 20 µm. In a second step, the foil is placed in a distance of ~100–300 µm to the wafer surface, and the transparent backside of the foil is irradiated with laser light. The laser irradiation instantly evaporates the solvent at the walls of the trenches leading to an overpressure, which accelerates the paste towards the wafer surface.<sup>384</sup> Using the PTP™ approach, finger widths down to ~20 µm with a high aspect ratio of more than 0.5 have been demonstrated.<sup>385,386</sup>

Furthermore, Cu plating is an interesting alternative to printing technologies. A multitude of research groups around the world are working on a scalable plating approach to overcome the challenge of an accelerating Ag consumption in the PV industry. As the use of silver is becoming the critical limitation of Si solar cell metallization, Cu plated metallization may solve this challenge completely if plating technologies becomes feasible for mass production.<sup>120,387–391</sup>

## 6 | CONCLUSION AND OUTLOOK

The economic success story of the past is not a guarantee for a bright future. This platitude is especially true for flatbed screen printing as the predominant metallization process for PV. The technology faces more and more challenging throughput requirements for the upcoming years. A consequent parallelization of various operation steps (i.e., transport, position detection, flooding, and printing) as well as an elevation of the squeegee speed during flooding and printing have enabled cycle times of around 1 s per cell on modern screen printing backend lines. Yet the strong requirement of the market to increase the production capacity and in parallel decrease production costs per device demands a further substantial reduction of cycle time per cell. Increasing the number of parallel production lines is not the most appropriate option as it significantly increases the footprint and investment costs of the required equipment. Following this, the current overall assumption relies on the fact that the screen-printing machine manufacture needs to provide the tools necessary for a high throughput potential. As this is obviously true, the R&D does not end with a fast screen printer, rather than starts with it. The paste-screen

interaction is the crucial physical mechanism that dictates how fast printing at ever decreasing structure sizes becomes possible. Further, the solution needs to be reliable, long living, cheap, and scalable for mass production. This economic pressure dictates paste and screen development in an iterative fashion. For example, the emergence of a robust, cheap, and long living fine-line screen will indirectly force paste manufacturer to adjust their paste rheology to that screen emulsion to ensure sufficient printability of their product. This optimization cycle proved to be very successful over the last 20 years as it creates many opportunities for disruptive events in the market.

When looking into further paste development, the challenge lies in adjusting the paste rheology in such a way that paste penetration of the screen becomes viable and reproducible at a minimal shearing of the paste volume. Presented research studies around wall slip phenomena are a promising candidate to achieve that. Further, the clogging of individual openings within the screen needs to be prevented to guarantee a stable printing process across thousands of wafers. When approaching the 20 µm level for finger widths, this seems to become one of the major problems. Adjusting the particle size distribution of such paste is very sensitive to overall production cost and electrical performance. Therefore, this tool of solving the clogging problem does not seem to be a promising option. Latest research has shown that the screen development has on the other hand the great potential of achieving that by optimizing the screen pattern through simulation. For example, old conventions of keeping a 22.5° angle between the mesh and screen opening were only recently challenged by the introduction of the 0°-knotless screen technology and discussed screen simulation algorithm.

These types of incremental improvements demonstrate how flatbed screen printing has managed to stay on top of the metallization market. Its continuous evolution has manifested itself to revolutionize the PV industry by demonstrating how a mechanical and fairly easy to use process was able to contribute major progression to the development of a global PV market. However, flatbed screen printing might still reach a technical limitation, which does not allow a further substantial reduction of the cycle time per cell because up to this date, there is no solution known to perform the metallization step on a moving cell by flatbed screen printing. Thus, the requirement of a technology leap towards high-throughput metallization methods like rotary printing or parallel dispensing might appear on the horizon.

## AUTHOR CONTRIBUTIONS

S. Tepner and A. Lorenz both contributed equally to all aspects of this work. S. Tepner primarily authored chapter 4 (the role of screen printing in the PV industry) and chapter 5 (paste rheology) and also contributed to the other chapters within this work. A. Lorenz primarily authored chapter 1 (history) and chapter 2 (fundamental aspects) and also contributed to the other chapters within this work.

## ACKNOWLEDGEMENTS

Both authors would like to thank their colleagues at the Fraunhofer Institute for Solar Energy Systems ISE for many valuable discussions over the last years. The open exchange regarding metallization topics contributed significantly to this work. Further, they would like to

specifically thank Dr. Elmar Lohmüller, Dr. Sebastian Mack, Dr. Andreas Wolf, Dr. Florian Clement, and Dr. Maximilian Pospischil for guidance and feedback on the manuscript. Open Access funding enabled and organized by Projekt DEAL.

## DATA AVAILABILITY STATEMENT

The data that support the findings of this study are available from the corresponding author upon reasonable request.

## ORCID

Sebastian Tepner  <https://orcid.org/0000-0001-8611-5295>

## REFERENCES

1. Gillo K. The circuit centennial. 2003. *ET-Trends*. [citeseerx.ist.psu.edu/viewdoc/download?doi=10.1.1.455.5439&rep=rep1&type=pdf](http://citeseerx.ist.psu.edu/viewdoc/download?doi=10.1.1.455.5439&rep=rep1&type=pdf).
2. Petherbridge K, Evans P, Harrison D. The origins and evolution of the PCB: A review. *Circuit World*. 2005;31(1):41-45. doi:[10.1108/03056120510553211](https://doi.org/10.1108/03056120510553211)
3. Eisler P, Eisler, P. Manufacture of electric circuit components. USA Patent No US2441960A.
4. Chapin DM, Fuller CS, Pearson GL. A new silicon p-n junction photocell for converting solar radiation into electrical power. *J Appl Phys*. 1954;25(5):676-677. doi:[10.1063/1.1721711](https://doi.org/10.1063/1.1721711)
5. Lennon A, Yao Y, Wenham S. Evolution of metal plating for silicon solar cell metallisation. *Prog Photovolt: Res Appl*. 2013;21(7):1454-1468. doi:[10.1002/pip.2221](https://doi.org/10.1002/pip.2221)
6. Taylor WE, Mardesich N, Gay CF. The impact of screen printing on the cost of solar cell metallization. *J Sol Energy Eng*. 1980;102(1):55. doi:[10.1115/1.3266122](https://doi.org/10.1115/1.3266122)
7. Taylor WE. Solar cell metallization: historical perspective; 1983; N84 21981. [ntrs.nasa.gov/archive/nasa/casi.ntrs.nasa.gov/19840013913.pdf](https://ntrs.nasa.gov/archive/nasa/casi.ntrs.nasa.gov/19840013913.pdf).
8. Field MB, Scudder LR. Application of thick-film technology to solar cell fabrication. In: IEEE, ed. Conference Records of the 12th IEEE Photovoltaic Specialists Conference; 1976:303-308.
9. Ralph EL. Recent advancements in low cost solar cell processing. In: IEEE, ed. Conference Records of the 11th IEEE Photovoltaic Specialist Conference (PVSC); 1975:315-316.
10. Green MA. Photovoltaic technology and visions for the future. *Jpn J Appl Phys*. 2019;1(1):13001. doi:[10.1088/2516-1083/ab0fa8](https://doi.org/10.1088/2516-1083/ab0fa8)
11. Frisson L, Lauwers P, Mertens R, van Overstraeten R, Govaerts R. Screen printed metallization of silicon solar cells. *ElectroComponent Sci Technol*. 1980;7(1-3):107-111. doi:[10.1155/APEC.7.107](https://doi.org/10.1155/APEC.7.107)
12. Frisson L, Lauwers P, Bulteel P, de Smet L, Mertens R, Govaerts R. Screen printed contacts on silicon solar cells with low series resistance. In: Conference Records of the 13th IEEE Photovoltaic Specialists Conference (PVSC). IEEE; 1978:590-592.
13. Frisson L, Honoré M, Mertens R, Govaerts R, van Overstraeten R. Silicon solar cells with screen printed diffusion and metallization. In: Conference Records of the 14th IEEE Photovoltaic Specialists Conference (PVSC). IEEE; 1980:941-942.
14. Nunoi T, Nishimura N, Nammori T, Sawai H, Suzuki A. High performance BSF silicon solar cell with fire through contacts printed on AR coating. *Jpn J Appl Phys*. 1980;19(S2):67. doi:[10.7567/JJAPS.19S2.67](https://doi.org/10.7567/JJAPS.19S2.67)
15. Okamoto K, Nammori T, Nunoi T, Takemoto T, Tsuji T. Rapid firing of printed pastes for BSF solar cell under high intensity light source. In: Conference Records of the 16th IEEE Photovoltaic Specialists Conference (PVSC). IEEE; 1982:818-823.
16. Firor K, Hogan S. Overview of thick-film technology as applied to solar cells; 1980. Contract No. EG 77 C 01-4042; Task No. 3221.10.

17. Meier D. Contact resistance: its measurement and relative importance to power loss in a solar cell. *IEEE Trans Electron Devices*. 1984; ED-31(5):647-653.
18. Schroder DK, Meier DL. Solar cell contact resistance—a review. *IEEE Trans Electron Devices*. 1984;31(5):637-647. doi:[10.1109/T-ED.1984.21583](https://doi.org/10.1109/T-ED.1984.21583)
19. Prudenzati M, Moro L, Morten B, Sirotti F, Sardi L. AG-based thick-film front metallization of silicon solar cells. *Act Passive Electron Compon*. 1989;13(3):133-150. doi:[10.1155/1989/27954](https://doi.org/10.1155/1989/27954)
20. Hezel R. Solar cell with increased efficiency—has buried metal finger electrode system to reduce charge carrier diffusion path length. Patent No. DE2846097A1.
21. Wenham SR, Green MA. Buried contact solar cell. EP0156366A2. March 26, 1984.
22. Mason NB, Jordan D, Summers JG. A high efficiency silicon solar cell production technology. In: *10th E.C. Photovoltaic Solar Energy Conference*. Dordrecht: Springer; 1991:280-283.
23. Heasman KC, Balbuena MA, Russell R, et al. Large area high efficiency silicon solar cells made by the laser grooved buried grid process. In: *Proc. of the 12th Photovoltaic Solar Energy Conference (EUPVSEC)*. WIP; 1994:761-762.
24. Butturi MA, Stefancich M, Vincenzi D, et al. Contact shadowing losses reduction by fine line screen printing. In: IEEE, ed. *Conference Record of the 29th IEEE Photovoltaic Specialists Conference*. IEEE; 2002:407-409.
25. Nijs J, Demesmaeker E, Szlufcik J, et al. Latest efficiency results with the screenprinting technology and comparison with the buried contact structure. In: IEEE, ed. *Conference Records of the 1st World Conference on Photovoltaic Energy Conversion—WCPEC (A Joint Conference of PVSC, PVSEC and PSEC)*. IEEE; 1994:1242-1249.
26. Hoornstra J, Weeber AW, de Moor, HHC, Sinke WC. The importance of paste rheology in improving fine line, thick film screen printing of front side metallization. In: *Proceedings of the 14th European Photovoltaic Solar Energy Conference (EPSEC)*; 1997:823-826.
27. Reis I, Huljic D, Hahne P, et al. Fine-line screen printing for silicon solar cells. In: *Technical Digest of the International PVSEC-11*; 1999: 335-336.
28. Blakers AW, Wang A, Milne AM, Zhao J, Green MA. 22.8% efficient silicon solar cell. *Appl Phys Lett*. 1989;55(13):1363. doi:[10.1063/1.101596](https://doi.org/10.1063/1.101596)
29. Green MA, Blakers A, Kurianski J, et al. Ultimate performance silicon solar cells: final report NERDDP project 81/1264; 1984.
30. Hermle M, Feldmann F, Bivour M, Goldschmidt JC, Glunz SW. Passivating contacts and tandem concepts: approaches for the highest silicon-based solar cell efficiencies. *Appl Phys Rev*. 2020;7(2):21305. doi:[10.1063/1.5139202](https://doi.org/10.1063/1.5139202)
31. Preu R, Lohmüller E, Lohmüller S, Saint-Cast P, Greulich JM. Passivated emitter and rear cell—devices, technology, and modeling. *Appl Phys Rev*. 2020;7(4):41315. doi:[10.1063/5.0005090](https://doi.org/10.1063/5.0005090)
32. Dullweber T, Gatz S, Hannebauer H, et al. Towards 20% efficient large-area screen-printed rear-passivated silicon solar cells. *Prog Photovolt: Res Appl*. 2012;20(6):630-638. doi:[10.1002/pip.1198](https://doi.org/10.1002/pip.1198)
33. Dullweber T, Schmidt J. Industrial silicon solar cells applying the Passivated Emitter and Rear Cell (PERC) concept—a review. *IEEE J Photovoltaics*. 2016;6(5):1366-1381. doi:[10.1109/JPHOTOV.2016.2571627](https://doi.org/10.1109/JPHOTOV.2016.2571627)
34. Green MA. The Passivated Emitter and Rear Cell (PERC): from conception to mass production. *Solar Energy Mater Solar Cells*. 2015; 143:190-197. doi:[10.1016/j.solmat.2015.06.055](https://doi.org/10.1016/j.solmat.2015.06.055)
35. Ballif C, Huijic DM, Hessler-Wyser A, Willeke G. Nature of the Ag-Si interface in screen-printed contacts: a detailed transmission electron microscopy study of cross-sectional structures. In: IEEE, ed. *Conference Record of the 29th IEEE Photovoltaic Specialists Conference*. IEEE; 2002:360-363.
36. Ballif C, Huljić DM, Willeke G, Hessler-Wyser A. Silver thick-film contacts on highly doped n-type silicon emitters: structural and electronic properties of the interface. *Appl Phys Lett*. 2003;82(12):1878. doi:[10.1063/1.1562338](https://doi.org/10.1063/1.1562338)
37. Schubert G, Huster F, Fath P. Current transport mechanism in printed AG thick film contacts to an n-type emitter of a crystalline silicon. In: *Proc. of the 19th Photovoltaic Solar Energy Conference (EUPVSEC)*. WIP; 2004:813-816.
38. Schubert G, Huster F, Fath P. Physical understanding of printed thick-film front contacts of crystalline Si solar cells—review of existing models and recent developments. *Solar Energy Mater Solar Cells*. 2006;90(18-19):3399-3406. doi:[10.1016/j.solmat.2006.03.040](https://doi.org/10.1016/j.solmat.2006.03.040)
39. Schubert G. Thick film metallisation of crystalline silicon solar cells: mechanisms, models and applications. [PhD Thesis]. Konstanz: Universität Konstanz; 2006.
40. Knobloch J, Aberle A, Voss B. Cost effective processes for silicon solar cells with high performance. In: *WIP*; 777-780.
41. Schneiderlöchner E, Grupp G, Emanuel G, et al. Silicon solar cells with screen printed front contact and dielectrically passivated laser-fired rear electrode. In: *Proc. of the 19th Photovoltaic Solar Energy Conference (EUPVSEC)*. WIP; 2004.
42. Engelhart P, Hermann S, Neubert T, et al. Laser ablation of SiO<sub>2</sub> for locally contacted Si solar cells with ultra-short pulses. *Progr Photovoltaics: Res Appl*. 2007;15(6):521-527. doi:[10.1002/pip.758](https://doi.org/10.1002/pip.758)
43. Engelhart P, Harder N-P, Neubert T, et al. Laser processing of 22% efficient back-contacted silicon solar cells. In: *Proc. of the 21st Photovoltaic Solar Energy Conference (EUPVSEC)*. WIP; 2006: 773-776.
44. Agostinelli G, Szlufcik J, Choulat P, Beaucarne G. Local contact structures for industrial PERC-type solar cells. In: *Proc. of the 20th Photovoltaic Solar Energy Conference (EUPVSEC)*. WIP; 2005: 942-945.
45. de Wolf S, Agostinelli G, Beaucarne G. Surface passivation with SiN<sub>x</sub>:H for rear side locally contacted Si solar cell. In: *Proc. of the 19th Photovoltaic Solar Energy Conference (EUPVSEC)*. WIP; 2004.
46. Riegel S, Mutter F, Lauermann T, Terheiden B, Hahn G. Review on screen printed metallization on p-type silicon. *Energy Procedia*. 2012; 21:14-23. doi:[10.1016/j.egypro.2012.05.003](https://doi.org/10.1016/j.egypro.2012.05.003)
47. Rauer M, Schmiga C, Glatthaar M, Glunz SW. Quantitative theoretical and experimental analysis of alloying from screen-printed aluminum pastes on silicon surfaces. *Solar Energy Mater Solar Cells*. 2018; 176:295-301. doi:[10.1016/j.solmat.2017.10.010](https://doi.org/10.1016/j.solmat.2017.10.010)
48. Olaisen BR, Holt A, Marstein ES, et al. Hot-melt screen-printing of front contacts on crystalline silicon solar cells. In: *Conference Record of the 31st IEEE Photovoltaic Specialists Conference*. Vol.2005. IEEE; 2005:1084-1087.
49. Raabe B, Huster F, McCann M, Fath P. High aspect ratio screen printed fingers. In: *Proc. of the 20th Photovoltaic Solar Energy Conference (EUPVSEC)*. WIP; 2005:930-933.
50. Galiazzo M, Furin V, Cellere G, Baccini A. New technologies for improvement of metallization line. In: *Proc. of the 24th Photovoltaic Solar Energy Conference (EUPVSEC)*. WIP; 2009:1502-1505.
51. Tavares R, Dobie A, Buzby D, Zhang W. Optimal screen mesh, emulsion chemistry, and emulsion thickness for fine-line front metallization pastes on crystalline silicon solar cells. In: *Proc. of the 26th Photovoltaic Solar Energy Conference (EUPVSEC)*. WIP; 2011:2040-2043.
52. Cotter JE, Yao G, Eggleston B. Laser-formed stencils for printed silicon solar cells. In: IEEE, ed. *Conference Record of the 31st IEEE Photovoltaic Specialists Conference*. Vol.2005. IEEE; 2005:1169-1172.
53. Mette A. Potential of both-sides contacted solar cells. Crystal clear—workshop on metallization; Utrecht; 2008.
54. Hörtelis M. Aerosol-printed silicon solar cell exceeding 20% efficiency. Crystal clear—workshop on metallization; Utrecht; 2008.

55. Erath D. Advanced screen printing technique for high definition front side metallization of crystalline silicon solar cells. Crystal clear—workshop on metallization; Utrecht; 2008.
56. Hofmann M, Erath D, Bitnar B, et al. Industrial type Cz Silicon Cells with screen-printed fine line front contacts and passivated rear contacted by laser firing. In: *Proc. of the 23rd Photovoltaic Solar Energy Conference (EUPVSEC)*. WIP; 2008:1704-1707.
57. Clement F, Menkoe M, Erath D, et al. Industrially feasible mc-Si solar cells with fine line printed front contacts on high emitter sheet resistance towards 17% efficiency. In: *Proc. of the 24th Photovoltaic Solar Energy Conference (EUPVSEC)*. WIP; 2009:2172-2176.
58. Falcon T, Hobby A. High accuracy, high aspect ratio metallization on silicon solar cells using a print on print process. In: *Proc. of the 25th Photovoltaic Solar Energy Conference (EUPVSEC)*. WIP; 2010: 1651-1655.
59. Hoornstra J. Thick film printing: towards fine line high aspect ratio. 2nd Metallization Workshop; Constance; 2010.
60. Galiazzo M, Furin V, Tonini D, Cellere G, Baccini A. Double printing of front contact Ag in c-Si solar cells. In: *Proc. of the 25th Photovoltaic Solar Energy Conference (EUPVSEC)*. WIP; 2010:2338-2340.
61. Magnone P, de Rose R, Zanuccoli M, et al. Understanding the impact of double screen-printing on silicon solar cells by 2-D numerical simulations. In: IEEE, ed. *Conference Records of the 37th IEEE Photovoltaic Specialists Conference (PVSC)*. IEEE; 2011:2177-2180.
62. Hannebauer H, Falcon T, Hesse R, Dullweber T, Brendel R. 18,9 %-efficient screen-printed solar cells applying a print-on-print process. In: *Proc. of the 26th Photovoltaic Solar Energy Conference (EUPVSEC)*. WIP; 2011:1607-1610.
63. Falcon T, Clasper S. Ultra fine line print process development for silicon solar cell metallisation. In: *Proc. of the 18th European Microelectronics and Packaging Conference (IMPC)*; 2011.
64. Pesce M, Maugeri M, Marsili M, et al. Technological and economic assessment of two-steps printing processes in a mc-Si solar cells production environment. *Energy Procedia*. 2012;21:24-31. doi:[10.1016/j.egypro.2012.05.004](https://doi.org/10.1016/j.egypro.2012.05.004)
65. Carroll AF. Screen printed metal contacts to Si solar cells—formation and synergistic improvements. In: *2013 IEEE 39th Photovoltaic Specialists Conference (PVSC): 16-21 June 2013, Tampa, Florida*. Piscataway, NJ: IEEE; 2013:3435-3440.
66. Bottosso C, Tao W, Wang X, Ma L, Galiazzo M. Reliable Metallization Process For Ultra Fine Line Printing. *Energy Procedia*. 2013;43: 80-85. doi:[10.1016/j.egypro.2013.11.091](https://doi.org/10.1016/j.egypro.2013.11.091)
67. Hannebauer H, Dullweber T, Falcon T, Chen X, Brendel R. Record low Ag paste consumption of 67.7 mg with dual print. *Energy Procedia*. 2013;43:66-71. doi:[10.1016/j.egypro.2013.11.089](https://doi.org/10.1016/j.egypro.2013.11.089)
68. Hannebauer H, Dullweber T, Falcon T, Brendel R. Fineline printing options for high efficiencies and low Ag paste consumption. *Energy Procedia*. 2013;38:725-731. doi:[10.1016/j.egypro.2013.07.339](https://doi.org/10.1016/j.egypro.2013.07.339)
69. Chang Y-H, Su W-M, Huang P-S, Cheng L-W. Improvement of the solar cell efficiency by fine line print on print technology. In: *2013 IEEE 39th Photovoltaic Specialists Conference (PVSC): 16-21 June 2013, Tampa, Florida*. Piscataway, NJ: IEEE; 2013:2176-2178.
70. Voltan A, Bortoletto E, Zamuner M, Martire M, Bertazzo M, Galiazzo M. Double printing feasibility of 35um printed Ag finger width. In: *Proc. of the 29th Photovoltaic Solar Energy Conference (EUPVSEC)*. WIP; 2014:1387-1391.
71. Hannebauer H, Dullweber T, Baumann U, Falcon T, Brendel R. 21.2%-efficient fineline-printed PERC solar cell with 5 busbar front grid. *Rapid Res Lett*. 2014;8(8):675-679. doi:[10.1002/pssr.201409190](https://doi.org/10.1002/pssr.201409190)
72. Galiazzo M, Voltan A, Bortoletto E, et al. Fine line double printing and advanced process control for cell manufacturing. *Energy Procedia*. 2015;67:116-125. doi:[10.1016/j.egypro.2015.03.295](https://doi.org/10.1016/j.egypro.2015.03.295)
73. Voltan A, Galiazzo M, Oberholzter F, Emsley M, Dubé CE, Graff JG. Cell efficiency improvement of fully implanted nPERT solar cells realized through metallization optimization. In: *Proc. of the 31st Photovoltaic Solar Energy Conference (EUPVSEC)*. WIP; 2015: 779-782.
74. Shanmugam V, Wong J, Peters IM, et al. Analysis of fine-line screen and stencil-printed metal contacts for silicon wafer solar cells. *IEEE J Photovoltaics*. 2015;1:1-9. doi:[10.1109/JPHOTOV.2014.2388073](https://doi.org/10.1109/JPHOTOV.2014.2388073)
75. Voltan A, Bortoletto E, Borsato O, Galiazzo M. Toward 30  $\mu\text{m}$  printed Ag finger width by ultra fine line double printing. In: *Proc. of the 31st Photovoltaic Solar Energy Conference (EUPVSEC)*. WIP; 2015: 704-708.
76. Galiazzo M. Fine line double printing for today and tomorrow cell metallization and module integration; 6th Metallization Workshop; Constance; 2016.
77. Galiazzo M Status and perspectives of metallization technologies for HVM. 7th Metallization Workshop; Konstanz, 2017.
78. Werner S, Lohmüller E, Saint-Cast P, et al. Key aspects for fabrication of p-type Cz-Si PERC solar cells exceeding 22% conversion efficiency. In: *Proc. of the 33rd Photovoltaic Solar Energy Conference (EUPVSEC)*. WIP; 2017.
79. Lorenz A, Linse M, Frintrup H, et al. Screen printed thick film metallization of silicon solar cells—recent developments and future perspectives. 35th European Photovoltaic Solar Energy Conference and Exhibition. 2018:819-824. doi:[10.4229/35THEUPVSEC20182018-2DV.3.65](https://doi.org/10.4229/35THEUPVSEC20182018-2DV.3.65)
80. Clement F, Linse M, Tepner S, et al. “Project FINALE”—screen and screen printing process development for ultra-fine-line contacts below 20  $\mu\text{m}$  finger width. 36th EU PVSEC Conference Proceedings. 2019:259-262. doi:[10.4229/EUPVSEC20192019-2DO.5.1](https://doi.org/10.4229/EUPVSEC20192019-2DO.5.1)
81. Tepner S, Wengenmeyr N, Ney L, Linse M, Pospischil M, Clement F. Improving wall slip behavior of silver pastes on screen emulsions for fine line screen printing. *Solar Energy Mater Solar Cells*. 2019;200: 109969. doi:[10.1016/j.solmat.2019.109969](https://doi.org/10.1016/j.solmat.2019.109969)
82. Lohmüller E, Greulich J, Saint-Cast P, et al. Front side optimization on boron- and gallium-doped Cz-Si PERC solar cells exceeding 22% conversion efficiency. In: *37th European Photovoltaic Solar Cenergy Conference and Exhibition*. WIP; 2020.
83. Tepner S, Ney L, Linse M, et al. Screen pattern simulation for an improved front-side Ag-electrode metallization of Si-solar cells. *Prog Photovolt: Res Appl*. 2020;1054-1062. doi:[10.1002/pip.3313](https://doi.org/10.1002/pip.3313)
84. Beaucarne G, Schubert G, Tous L, Hoornstra J. Summary of the 8th workshop on metallization and interconnection for crystalline silicon solar cells. *AIP Conf Proc*. 2019;2156(1):20001. doi:[10.1063/1.5125866](https://doi.org/10.1063/1.5125866)
85. Schmidt J, Peibst R, Brendel R. Surface passivation of crystalline silicon solar cells: present and future. *Solar Energy Mater Solar Cells*. 2018;187:39-54. doi:[10.1016/j.solmat.2018.06.047](https://doi.org/10.1016/j.solmat.2018.06.047)
86. Richter A, Hermle M, Glunz SW. Reassessment of the limiting efficiency for crystalline silicon solar cells. *IEEE J Photovoltaics*. 2013; 3(4):1184-1191. doi:[10.1109/JPHOTOV.2013.2270351](https://doi.org/10.1109/JPHOTOV.2013.2270351)
87. Glunz SW, Feldmann F. SiO<sub>2</sub> surface passivation layers—a key technology for silicon solar cells. *Solar Energy Mater Solar Cells*. 2018;185:260-269. doi:[10.1016/j.solmat.2018.04.029](https://doi.org/10.1016/j.solmat.2018.04.029)
88. de Wolf S, Descoedres A, Holman ZC, Ballif C. High-efficiency silicon heterojunction solar cells: a review. *GREEN*. 2012;2(1). doi:[10.1515/green-2011-0018](https://doi.org/10.1515/green-2011-0018)
89. Hamakawa Y, Fujimoto K, Okuda K, Kashima Y, Nonomura S, Okamoto H. New types of high efficiency solar cells based on a -Si. *Solar Cells*. 1983;43(7):644-646. doi:[10.1063/1.94462](https://doi.org/10.1063/1.94462)
90. Fuhs W, Niemann K, Stuke J. Heterojunctions of amorphous silicon and silicon single crystals. In: *International Conference on Tetrahedrally bonded amorphous semiconductors*; 1974:345-350.
91. Descoedres A, Allebé C, Badel N, et al. Silicon heterojunction solar cells: towards low-cost high-efficiency industrial devices and application to low-concentration PV. *Energy Procedia*. 2015;77:508-514. doi:[10.1016/j.egypro.2015.07.072](https://doi.org/10.1016/j.egypro.2015.07.072)

92. ITRPV. International Technology Roadmap for Photovoltaic (ITRPV): results 2020. 11th Edition; 2020.
93. Chen D, Zhao L, Diao H, Zhang W, Wang G, Wang W. Low-temperature sintering properties of the screen-printed silver paste for a-Si: H/c-Si heterojunction solar cells. *J Mater Sci Mater Electron.* 2014;25(6):2657-2664. doi:[10.1007/s10854-014-1925-z](https://doi.org/10.1007/s10854-014-1925-z)
94. Haschke J, Dupré O, Boccard M, Ballif C. Silicon heterojunction solar cells: recent technological development and practical aspects—from lab to industry. *Sol Energy Mater Sol Cells.* 2018;187:140-153. doi:[10.1016/j.solmat.2018.07.018](https://doi.org/10.1016/j.solmat.2018.07.018)
95. Haschke J, Lemerle R, Aissa B, et al. Annealing of silicon heterojunction solar cells: interplay of solar cell and indium tin oxide properties. *IEEE J Photovoltaics.* 2019;9(5):1202-1207. doi:[10.1109/JPHOTOV.2019.2924389](https://doi.org/10.1109/JPHOTOV.2019.2924389)
96. Descoedres A, Allebé C, Badel N, et al. Low-temperature processes for passivation and metallization of high-efficiency crystalline silicon solar cells. *Solar Energy.* 2018;175:54-59. doi:[10.1016/j.solener.2018.01.074](https://doi.org/10.1016/j.solener.2018.01.074)
97. Aoki T, Matsushita T, Yamoto H, Hayashi H, Okayama M, Kawana Y. Oxygen-doped polycrystalline silicon films applied to surface passivation. *J Electrochem Soc.* 1975;122(3):C82.
98. Yablonovitch E, Gmitter T, Swanson RM, Kwark YH. A 720 mV open circuit voltage SiO<sub>x</sub>: c -Si:SiO<sub>x</sub> double heterostructure solar cell. *IEEE Electron Device Lett.* 1985;47(11):1211-1213. doi:[10.1063/1.96331](https://doi.org/10.1063/1.96331)
99. Tarr NG. A polysilicon emitter solar cell. *IEEE Electron Device Lett.* 1985;6(12):655-658. doi:[10.1109/EDL.1985.26264](https://doi.org/10.1109/EDL.1985.26264)
100. Lindholm FA, Neugroschel A, Arienzo M, Iles PA. Heavily doped polysilicon-contact solar cells. *IEEE Electron Device Lett.* 1985;6(7):363-365. doi:[10.1109/EDL.1985.26155](https://doi.org/10.1109/EDL.1985.26155)
101. Kwark YH, Swanson RM. N-type SIPOS and poly-silicon emitters. *Solid-State Electron.* 1987;30(11):1121-1125. doi:[10.1016/0038-1101\(87\)90076-1](https://doi.org/10.1016/0038-1101(87)90076-1)
102. Feldmann F, Bivour M, Reichel C, Hermle M, Glunz SW. A passivated rear contact for high-efficiency n-type silicon solar cells enabling high Voc<sub>s</sub> and FF > 82%. In: *Proc. of the 28th Photovoltaic Solar Energy Conference (EUPVSEC).* WIP; 2013.
103. Feldmann F, Bivour M, Reichel C, Hermle M, Glunz SW. Passivated rear contacts for high-efficiency n-type Si solar cells providing high interface passivation quality and excellent transport characteristics. *Solar Energy Mater Solar Cells.* 2014;120:270-274. doi:[10.1016/j.solmat.2013.09.017](https://doi.org/10.1016/j.solmat.2013.09.017)
104. Peibst R, Römer U, Larionova Y, et al. Working principle of carrier selective poly-Si/c-Si junctions: is tunnelling the whole story? *Sol Energy Mater Sol Cells.* 2016;158:60-67. doi:[10.1016/j.solmat.2016.05.045](https://doi.org/10.1016/j.solmat.2016.05.045)
105. Duttagupta S, Nandakumar N, Padhamnath P, Buatis JK, Stangl R, Aberle AG. monoPoly™ cells: large-area crystalline silicon solar cells with fire-through screen printed contact to doped polysilicon surfaces. *Sol Energy Mater Sol Cells.* 2018;187:76-81. doi:[10.1016/j.solmat.2018.05.059](https://doi.org/10.1016/j.solmat.2018.05.059)
106. Stodolny MK, Lenes M, Wu Y, et al. n-Type polysilicon passivating contact for industrial bifacial n-type solar cells. *Sol Energy Mater Sol Cells.* 2016;158:24-28. doi:[10.1016/j.solmat.2016.06.034](https://doi.org/10.1016/j.solmat.2016.06.034)
107. Chen Y, Chen D, Liu C, et al. Mass production of industrial tunnel oxide passivated contacts (i-TOPCon) silicon solar cells with average efficiency over 23% and modules over 345 W. *Prog Photovolt: Res Appl.* 2019;27(10):827-834. doi:[10.1002/pip.3180](https://doi.org/10.1002/pip.3180)
108. Chen D, Chen Y, Wang Z, et al. 24.58% total area efficiency of screen-printed, large area industrial silicon solar cells with the tunnel oxide passivated contacts (i-TOPCon) design. *Solar Energy Mater Solar Cells.* 2020;206:110258. doi:[10.1016/j.solmat.2019.110258](https://doi.org/10.1016/j.solmat.2019.110258)
109. Werner J, Niesen B, Ballif C. Perovskite/silicon tandem solar cells: marriage of convenience or true love story?—an overview. *Adv Mater Interfaces.* 2018;5(1):1700731. doi:[10.1002/admi.201700731](https://doi.org/10.1002/admi.201700731)
110. Kojima A, Teshima K, Shirai Y, Miyasaka T. Organometal halide perovskites as visible-light sensitizers for photovoltaic cells. *J Am Chem Soc.* 2009;131(17):6050-6051. doi:[10.1021/ja809598r](https://doi.org/10.1021/ja809598r)
111. Helmholtz-Zentrum Berlin. World record: efficiency of perovskite silicon tandem solar cell jumps to 29.15 per cent; 2020. [helmholtz-berlin.de/pubbin/news\\_seite?nid=21020;sprache=en;seitenid=1](http://helmholtz-berlin.de/pubbin/news_seite?nid=21020;sprache=en;seitenid=1).
112. Oxford PV. Oxford PV sets world record for perovskite solar cell; 2018. [oxfordpv.com/news/oxford-pv-sets-world-record-perovskite-solar-cell](http://oxfordpv.com/news/oxford-pv-sets-world-record-perovskite-solar-cell). Accessed March 15, 2020.
113. Kamino BA, Paviet-Salomon B, Moon S-J, et al. Low-temperature screen-printed metallization for the scale-up of two-terminal perovskite-silicon tandems. *ACS Appl Energy Mater.* 2019;2(5):3815-3821. doi:[10.1021/acsaem.9b00502](https://doi.org/10.1021/acsaem.9b00502)
114. Niu G, Guo X, Wang L. Review of recent progress in chemical stability of perovskite solar cells. *J Mater Chem A.* 2015;3(17):8970-8980. doi:[10.1039/C4TA04994B](https://doi.org/10.1039/C4TA04994B)
115. Leijtens T, Eperon GE, Noel NK, Haberreuter SN, Petrozza A, Snaith HJ. Stability of metal halide perovskite solar cells. *Adv Energy Mater.* 2015;5(20):1500963. doi:[10.1002/aenm.201500963](https://doi.org/10.1002/aenm.201500963)
116. Swanson RM, Beckwith SK, Crane RA, et al. Point-contact silicon solar cells. *IEEE Trans Electron Devices.* 1984;31(5):661-664. doi:[10.1109/T-ED.1984.21586](https://doi.org/10.1109/T-ED.1984.21586)
117. van Kerschaver E, Beaucarne G. Back-contact solar cells: a review. *Prog Photovolt: Res Appl.* 2006;14(2):107-123. doi:[10.1002/pip.657](https://doi.org/10.1002/pip.657)
118. Green MA. *Silicon Solar Cells: Advanced Principles & Practice.* Sydney: Centre for Photovoltaic Devices and Systems Univ. of New South Wales; 1995.
119. Fellmeth T, Born A, Kimmerle A, Clement F, Biro D, Preu R. Recombination at metal-emitter interfaces of front contact technologies for highly efficient silicon solar cells. *Energy Procedia.* 2011;8:115-121. doi:[10.1016/j.egypro.2011.06.111](https://doi.org/10.1016/j.egypro.2011.06.111)
120. Kraft A. Plated copper front-side metallization on printed seed-layers for silicon solar cells. [Dissertation]. Freiburg: Albert-Ludwigs-Universität; 2015.
121. Muller J, Hinken D, Blankemeyer S, et al. Resistive power loss analysis of PV modules made from halved 15.6 × 15.6 cm<sup>2</sup> silicon PERC solar cells with efficiencies up to 20.0%. *IEEE J Photovoltaics.* 2015;5(1):189-194. doi:[10.1109/JPHOTOV.2014.2367868](https://doi.org/10.1109/JPHOTOV.2014.2367868)
122. Schneider J, Schönfelder S, Dietrich S, Turek M. Solar module with half size solar cells. [5 pages/29th European Photovoltaic Solar Energy Conference and Exhibition]. In: *Proc. of the 29th Photovoltaic Solar Energy Conference (EUPVSEC).* WIP; 2014:185-189.
123. Guo S, Schneider J, Lu F, et al. Investigation of the short-circuit current increase for PV modules using halved silicon wafer solar cells. *Sol Energy Mater Sol Cells.* 2015;133:240-247. doi:[10.1016/j.solmat.2014.11.012](https://doi.org/10.1016/j.solmat.2014.11.012)
124. Eiternick S, Kaule F, Zühlke H-U, et al. High quality half-cell processing using thermal laser separation. *Energy Procedia.* 2015;77:340-345. doi:[10.1016/j.egypro.2015.07.048](https://doi.org/10.1016/j.egypro.2015.07.048)
125. Kreinin L, Bordin N, Karsenty A, Drori A, Eisenberg N. Experimental analysis of the increases in energy generation of bifacial over mono-facial PV modules. In: *Proc. of the 26th Photovoltaic Solar Energy Conference (EUPVSEC).* WIP; 2011:3140-3143.
126. Schindler S, Schneider J, Poenisch C, Nissler R, Habermann D. Soldering process and material characterization of miniaturized contact structures of a newly developed multi busbar cell metallization concept. In: *Proc. of the 28th Photovoltaic Solar Energy Conference (EUPVSEC).* WIP; 2013:480-483.
127. Söderström T, Papet P, Ufheil J. Smart wire connection technology. In: *Proc. of the 28th Photovoltaic Solar Energy Conference (EUPVSEC).* WIP; 2013:495-499.
128. Schneider A, Rubin L, Rubin G. Solar cell efficiency improvement by new metallization techniques—the day 4 electrode concept. In: *2006 IEEE 4th WCPEC;* 2006:1095-1098.

129. Walter J, Tranitz M, Volk M, Ebert C, Eitner U. Multi-wire interconnection of busbar-free solar cells. *Energy Procedia*. 2014;380-388.
130. Söderström T, Papet P, Ufheil J. Smart wire connection technology; 2013.
131. Dickson DC, Jr; Hoffmann Electronics Corp. Photovoltaic semiconductor apparatus or the like. US 2938938 A. 07 March.
132. Zhao J, Wang A, Yun F, et al. 20 000 PERL silicon cells for the '1996 World Solar Challenge' solar car race. *Prog Photovolt: Res Appl*. 1997;5(4):269-276. doi:10.1002/(SICI)1099-159X(199707/08)5:4<269::AID-PIP174>3.0.CO;2-1
133. Zhao J, Wang A, Green MA. 24% efficient PERL structure silicon solar cells. In: *Conference Records of 21st IEEE Photovoltaic Specialists Conference (PVSC)*. IEEE; 1990:333-335.
134. Baliozian P, Al-Akash M, Lohmuller E, et al. Postmetallization "passivated edge technology" for separated silicon solar cells. *IEEE J Photovoltaics*. 2020;10(2):390-397. doi:10.1109/JPHOTOV.2019.2959946
135. Beaucarne G. Materials challenge for shingled cells interconnection. *Energy Procedia*. 2016;98:115-124. doi:10.1016/j.egypro.2016.10.087
136. Blakers AW. Shading losses of solar-cell metal grids. *J Appl Phys*. 1992;71(10):5237. doi:10.1063/1.350580
137. Woehl R, Hörteis M, Glunz SW. Analysis of the optical properties of screen-printed and aerosol-printed and plated fingers of silicon solar cells. *Adv Optoelectron*. 2008;2008:1-7. doi:10.1155/2008/759340
138. Saive R, Borsuk AM, Emmer HS, et al. Effectively transparent front contacts for optoelectronic devices. *Adv Opt Mater*. 2016;4(10):1470-1474. doi:10.1002/adom.201600252
139. Mette A. New concepts for front side metallization of industrial silicon solar cells. [PhD Thesis]. Freiburg: Albert-Ludwigs-Universität; 2007.
140. Altermatt PP. Shape and homogeneity of front metal fingers: impact on cell efficiency and its distribution in production lines. 6th Metallization Workshop; Constance, 2016.
141. Fellmeth T, Clement F, Biro D. Analytical modeling of industrial-related silicon solar cells. *IEEE J Photovoltaics*. 2014;4(1):504-513. doi:10.1109/JPHOTOV.2013.2281105
142. Fellmeth T. Silicon solar cells for the application in low concentrator systems-development and characterization. [Dissertation]. Tübingen: Eberhard Karls Universität Tübingen; 2014.
143. Lorenz A. Evaluierung von Rotationsdruckverfahren für die Metallisierung von Silicium-Solarzellen. [Dissertation]. Freiburg: Albert-Ludwigs-Universität; 2017.
144. Kiefer F, Brendemühl T, Berger M, et al. Influence of solder pads to PERC solar cells for module integration. *Energy Procedia*. 2013;38:368-374. doi:10.1016/j.egypro.2013.07.291
145. Cheek GC, Mertens RP, van Overstraeten R, Frisson L. Thick-film metallization for solar cell applications. *IEEE Trans Electron Devices*. 1984;31(5):602-609. doi:10.1109/T-ED.1984.21575
146. Hiroshi M. Radiation energy transducing device. US 3278811 A.
147. Luque A, Cuevas A, Ruiz JM. Double-sided n+-p-n+ solar cell for bifacial concentration. *Solar Cells*. 1980;2(2):151-166. doi:10.1016/0379-6787(80)90007-1
148. Dullweber T, Kranz C, Peibst R, et al. PERC+: industrial PERC solar cells with rear Al grid enabling bifaciality and reduced Al paste consumption. *Prog Photovolt: Res Appl*. 2016;24(12):1487-1498. doi:10.1002/pip.2712
149. Krauß K, Fertig F, Greulich J, Rein S, Preu R. biPERC silicon solar cells enabling bifacial applications for industrial solar cells with passivated rear sides. *Phys Status Solidi (a)*. 2016;213(1):68-71. doi:10.1002/pssa.201532737
150. Goldbach HD, Bink A, Schropp REI. Bifacial silicon heterojunction solar cell with deposited back surface field. *MRS Proc*. 2005;862:2CV.1.41. doi:10.1557/PROC-862-A23.4
151. Wu W, Bao J, Ma L, et al. Development of industrial n-type bifacial TopCon solar cells and modules. In: *Proc. of the 36th Photovoltaic Solar Energy Conference (EUPVSEC)*. WIP; 2019:100-102.
152. Thaidigsmann B, Kick C, Drews A, Clement F, Wolf A, Biro D. Fire-through contacts—a new approach to contact the rear side of passivated silicon solar cells. *Sol Energy Mater Sol Cells*. 2013;108:164-169. doi:10.1016/j.solmat.2012.09.029
153. Fellmeth T, Ourinson D, Riebe T, et al. Al fire through contacts for p-type bifacial PERC devices. *AIP Conference Proceedings*. 2019. doi:10.1063/1.5123878
154. Ourinson D, Fellmeth T, Tepner S, et al. Optimization of Al fire-through contacts for AlOx-SiNx rear passivated bifacial p-PERC. *IEEE J Photovoltaics*. 2020;1-9. doi:10.1109/JPHOTOV.2020.2983006
155. Schroder D, Meider D. Solar cell contact resistance—a review. *IEEE Trans Electron Devices*. 1984;ED-31(5):637-647.
156. Schubert G, Fischer B, Fath P. Formation and nature of Ag thick film front contacts on crystalline silicon solar cells. In: *Proc. of PV in Europe—From PV Technology to Energy Solutions*. WIP; 2002:343-346.
157. Uruena A, John J, Beaucarne G, et al. Local Al-alloyed contacts for next generation Si solar cells. In: *Proc. of the 24th Photovoltaic Solar Energy Conference (EUPVSEC)*. WIP; 2009.
158. Urrejola E, Peter K, Plagwitz H, Schubert G. Al-Si alloy formation in narrow p-type Si contact areas for rear passivated solar cells. *J Appl Phys*. 2010;107(12):124516. doi:10.1063/1.3437070
159. Rauer M, Woehl R, Ruhle K, et al. Aluminum alloying in local contact areas on dielectrically passivated rear surfaces of silicon solar cells. *IEEE Electron Device Lett*. 2011;32(7):916-918. doi:10.1109/LED.2011.2143385
160. Rauer M, Schmiga C, Woehl R, et al. Investigation of aluminum-alloyed local contacts for rear surface-passivated silicon solar cells. *IEEE J Photovoltaics*. 2011;1(1):22-28. doi:10.1109/JPHOTOV.2011.2161864
161. Mikhtaryan V, Kravtchenko A, Garanzha S, et al. Lead free silver aluminum paste for crystalline silicon solar cells. In: *Proc. of the 21st Photovoltaic Solar Energy Conference (EUPVSEC)*. WIP; 2006:2353-2356.
162. Kerp H, Kim S, Lago R, et al. Development of screen printable contacts for p+ emitters in bifacial solar cells. In: *Proc. of the 21st Photovoltaic Solar Energy Conference (EUPVSEC)*. WIP; 2006:892-894.
163. Seyedmohammadi S, Graddy E, Shaikh A. Screen printable Ag-Al metal pastes for p+ silicon application in solar cells. In: *Conference Records of the 35th IEEE Photovoltaic Specialists Conference (PVSC)*. IEEE; 2010:3600-3603.
164. Riegel S, Mutter F, Hahn G, Terheiden B. Contact formation in the silver/aluminium thick film firing process: a phenomenological approach. In: *Proc. of the 25th Photovoltaic Solar Energy Conference (EUPVSEC)*. WIP; 2010.
165. Lago R, Pérez L, Kerp H, et al. Screen printing metallization of boron emitters. *Prog Photovolt: Res Appl*. 2010;18(1):20-27. doi:10.1002/pip.933
166. Riegel S, Mutter F, Hahn G, Terheiden B. Influence of the dopant on the contact formation to p+-type silicon. *Energy Procedia*. 2011;8:533-539. doi:10.1016/j.egypro.2011.06.178
167. Edler A, Mihailescu V, Kopecik R, et al. Improving screen printed metallization for large area industrial solar cells based on n-type material. *Energy Procedia*. 2011;8:493-497. doi:10.1016/j.egypro.2011.06.171
168. Ok Y-W, Upadhyaya AD, Zimbardi F, et al. Effect of Al content on the performance of Ag/Al screen printed N-type Si solar cells. In: *2013 IEEE 39th Photovoltaic Specialists Conference (PVSC)*; 16-21 June 2013, Tampa, Florida. Piscataway, NJ: IEEE; 2013:2247-2249.

169. Fritz S, Riegel S, Gloger S, et al. Influence of emitter properties on contact formation to P+ silicon. *Energy Procedia*. 2013;38:720-724. doi:[10.1016/j.egypro.2013.07.338](https://doi.org/10.1016/j.egypro.2013.07.338)
170. Heinz FD, Breitwieser M, Gundel P, et al. Microscopic origin of the aluminium assisted spiking effects in n-type silicon solar cells. *Solar Energy Mater Solar Cells*. 2014;131:105-109. doi:[10.1016/j.solmat.2014.05.036](https://doi.org/10.1016/j.solmat.2014.05.036)
171. Lohmüller E. Transfer of the metal wrap through solar cell concept to n-type silicon. [PhD Thesis]. Freiburg, Germany: Albert-Ludwigs-Universität; 2015.
172. Fritz S, Konig M, Riegel S, Herguth A, Horteis M, Hahn G. Formation of Ag/Al screen-printing contacts on B emitters. *IEEE J Photovoltaics*. 2015;5(1):145-151. doi:[10.1109/JPHOTOV.2014.2364117](https://doi.org/10.1109/JPHOTOV.2014.2364117)
173. Hoenig R, Glatthaar M, Clement F, Greulich J, Wilde J, Biro D. New measurement method for the investigation of space charge region recombination losses induced by the metallization of silicon solar cells. *Energy Procedia*. 2011;8:694-699. doi:[10.1016/j.egypro.2011.06.203](https://doi.org/10.1016/j.egypro.2011.06.203)
174. Hannebauer H, Sommerfeld M, Müller J, Dullweber T, Brendel R. Analysis of the emitter saturation current density of industrial type silver screen-printed front contacts. In: *Proc. of the 27th Photovoltaic Solar Energy Conference (EUPVSEC)*. WIP; 2012:1360-1363.
175. Deckers J, Loozen X, Posthuma N, et al. Injection dependent emitter saturation current density measurement under metallized areas using photoconductance decay. In: *Proc. of the 28th Photovoltaic Solar Energy Conference (EUPVSEC)*. WIP; 2013:806-810.
176. Hoenig R. Evaluation and microstructure analysis of thick film contacts for industrial silicon solar cells. 2014. [PhD Thesis]. Freiburg: Albert-Ludwigs-Universität; urn:nbn:de:bsz:25-opus-99157.
177. Shanmugam V, Mueller T, Aberle AG, Wong J. Determination of metal contact recombination parameters for silicon wafer solar cells by photoluminescence imaging. *Solar Energy*. 2015;118:20-27. doi:[10.1016/j.solener.2015.05.010](https://doi.org/10.1016/j.solener.2015.05.010)
178. Koduvvelikulathu LJ, Mihailescu VD, Olibet S, Rudolph D, Cabrera E, Kopecek R. Two-dimensional modeling of the metallization-induced recombination losses of screen-printed solar cells. *IEEE J Photovoltaics*. 2015;5(1):159-165. doi:[10.1109/JPHOTOV.2014.2365453](https://doi.org/10.1109/JPHOTOV.2014.2365453)
179. Herrmann D, Lohmuller S, Hoffler H, Fell A, Brand AA, Wolf A. Numerical simulations of photoluminescence for the precise determination of emitter contact recombination parameters. *IEEE J Photovoltaics*. 2019;9(6):1759-1767. doi:[10.1109/JPHOTOV.2019.2938400](https://doi.org/10.1109/JPHOTOV.2019.2938400)
180. Herrmann D, Fell A, Höffler H, Lohmuller S, Wolf A. Impact of non-uniform carrier density on the determination of metal induced recombination losses. In: *15th International Conference on Concentrator Photovoltaic Systems (CPV-15)*. AIP Publishing; 2019. AIP Conference Proceedings
181. Cuevas A, Basore PA, Giroult-Matlakowski G, Dubois C. Surface recombination velocity of highly doped n-type silicon. *IEEE Electron Device Lett*. 1996;80(6):3370-3375. doi:[10.1063/1.363250](https://doi.org/10.1063/1.363250)
182. Fell A, Walter D, Kluska S, Franklin E, Weber K. Determination of injection dependent recombination properties of locally processed surface regions. *Energy Procedia*. 2013;38:22-31. doi:[10.1016/j.egypro.2013.07.245](https://doi.org/10.1016/j.egypro.2013.07.245)
183. Koenig M, Deckelmann M, Henning A, Hoenig R, Clement F, Hörteis M. Dual screen printing featuring novel framed busbar screen layout and non-contacting Ag busbar paste. *Energy Procedia*. 2012;27:510-515. doi:[10.1016/j.egypro.2012.07.102](https://doi.org/10.1016/j.egypro.2012.07.102)
184. Kontermann S, Hörteis M, Kasemann M, et al. Physical understanding of the behavior of silver thick-film contacts on n-type silicon under annealing conditions. *Solar Energy Mater Solar Cells*. 2009; 93(9):1630-1635. doi:[10.1016/j.solmat.2009.04.019](https://doi.org/10.1016/j.solmat.2009.04.019)
185. Cabrera E, Olibet S, Glatz-Reichenbach J, Kopecek R, Reinke D, Schubert G. Current transport in thick film Ag metallization: direct contacts at silicon pyramid tips? *Energy Procedia*. 2011;8:540-545. doi:[10.1016/j.egypro.2011.06.179](https://doi.org/10.1016/j.egypro.2011.06.179)
186. Cooper IB, Tate K, Renshaw JS, et al. Investigation of the mechanism resulting in low resistance Ag thick-film contact to Si solar cells in the context of emitter doping density and contact firing for current-generation Ag paste. *IEEE J Photovoltaics*. 2014;4(1): 134-141. doi:[10.1109/JPHOTOV.2013.2285621](https://doi.org/10.1109/JPHOTOV.2013.2285621)
187. Eberstein M, Schmidt U, Korner S, Reinhardt K, Jurk R, Partsch U. In-situ observations of glass frit related effects during the front side paste contact formation. In: *Conference Records of the 40th IEEE Photovoltaic Specialists Conference (PVSC)*. IEEE; 2014:3463-3469.
188. Ferrada P, Portillo C, del Campo V, et al. Metallization of a lightly doped emitter with different industrial silver pastes: performance and microscopy analysis. *IEEE J Photovoltaics*. 2017;7(3):727-734. doi:[10.1109/JPHOTOV.2017.2673663](https://doi.org/10.1109/JPHOTOV.2017.2673663)
189. Kim Y, Huh J, Kim H. Effect of basicity of glass frits on electrical properties of Si solar cells. *Solar Energy Mater Solar Cells*. 2018;185: 97-103. doi:[10.1016/j.solmat.2018.05.015](https://doi.org/10.1016/j.solmat.2018.05.015)
190. Lin C-H, Tsai S-Y, Hsu S-P, Hsieh M-H. Investigation of Ag-bulk/glassy-phase/Si heterostructures of printed Ag contacts on crystalline Si solar cells. *Solar Energy Mater Solar Cells*. 2008;92(9): 1011-1015. doi:[10.1016/j.solmat.2008.02.032](https://doi.org/10.1016/j.solmat.2008.02.032)
191. Li ZG, Liang L, Cheng LK. Electron microscopy study of front-side Ag contact in crystalline Si solar cells. *J Appl Phys*. 2009;105(6): 66102. doi:[10.1063/1.3086663](https://doi.org/10.1063/1.3086663)
192. Cheng LK, Liang L, Li Z. Nano-Ag colloids assisted tunneling mechanism for current conduction in front contact of crystalline Si solar cells. In: *Conference Records of the 34th IEEE Photovoltaic Specialists Conference (PVSC)*. IEEE; 2009:2344-2348.
193. Li ZG, Liang L, Ionkin AS, et al. Microstructural comparison of silicon solar cells' front-side Ag contact and the evolution of current conduction mechanisms. *J Appl Phys*. 2011;110(7):74304. doi:[10.1063/1.3642956](https://doi.org/10.1063/1.3642956)
194. Ren K, Ye T, Zhang Y, Ebong A. The role of nano-crystallites on conduction mechanisms of current through Ag gridlines of Si solar cells. *MRS Adv*. 2019;4:311-318.
195. Zhang J, Tong H, Sun X, et al. An investigation on determinants of silver paste metallization contact performance on crystalline silicon solar cells. *J Mater Sci Mater Electron*. 2020;31(7):5752-5759. doi:[10.1007/s10854-020-03145-9](https://doi.org/10.1007/s10854-020-03145-9)
196. Kim H-S, Cho S-B, Kim H, et al. Electrochemical nature of contact firing reactions for screen-printed silicon solar cells: origin of "gray finger" phenomenon. *Prog Photovolt: Res Appl*. 2016;24(9):1237-1250. doi:[10.1002/pip.2783](https://doi.org/10.1002/pip.2783)
197. Kim C, Choi J-W, Choi S, et al. Effects of current-injection firing with Ag paste in a boron emitter. *Sci Rep*. 2016;6:21553. doi:[10.1038/srep21553](https://doi.org/10.1038/srep21553)
198. Bae S, Choi J-W, Kim C, et al. Effective contact formation method on high-sheet-resistance boron-doped emitter with current injection. *IEEE J Photovoltaics*. 2019;9(3):615-620. doi:[10.1109/JPHOTOV.2019.2896984](https://doi.org/10.1109/JPHOTOV.2019.2896984)
199. Chu H, Preis P, Lossen J, et al. Impact of the presence of busbars during the fast firing process on contact resistances. *IEEE J Photovoltaics*. 2018;8(4):1-7. doi:[10.1109/JPHOTOV.2018.2828824](https://doi.org/10.1109/JPHOTOV.2018.2828824)
200. Cooper IB, Tate K, Carroll AF, Mikeska KR, Reedy RC, Rohatgi A. Low resistance screen-printed Ag contacts to  $\text{POCl}_3$  emitters with low saturation current density for high efficiency Si solar cells. In: *38th IEEE Photovoltaic Specialists Conference (PVSC)*, 2012: 3-8 June 2012, Austin Convention Center, Austin, Texas. Piscataway, NJ: IEEE; 2012:3359-3364.
201. Werner S, Lohmuller S, Maier S, et al. Process optimization for the front side of p-type silicon solar cell. In: *Proc. of the 29th Photovoltaic Solar Energy Conference (EUPVSEC)*. WIP; 2014.
202. Werner S, Lohmuller E, Maier S, Mourad S, Wolf A. Challenges for lowly-doped phosphorus emitters in silicon solar cells with screen-

- printed silver contacts. *Energy Procedia*. 2017;124:936-946. doi:[10.1016/j.egypro.2017.09.274](https://doi.org/10.1016/j.egypro.2017.09.274)
203. Werner S, Lohmüller E, Wolf A, Clement F. Extending the limits of screen-printed metallization of phosphorus- and boron-doped surfaces. *Solar Energy Mater Solar Cells*. 2016;158:37-42. doi:[10.1016/j.solmat.2016.05.064](https://doi.org/10.1016/j.solmat.2016.05.064)
  204. Zhang Y, Wang L, Chen D, Kim M, Hallam B. Pathway towards 24% efficiency for fully screen-printed passivated emitter and rear contact solar cells. *J Phys D Appl Phys*. 2021;54(21):214003. doi:[10.1088/1361-6463/abe900](https://doi.org/10.1088/1361-6463/abe900)
  205. Wang P, Li G, Wang M, et al. Numerical study of mono-crystalline silicon solar cells with passivated emitter and rear contact configuration for the efficiency beyond 24% based on mass production technology. *J Semicond*. 2020;41(6):62701. doi:[10.1088/1674-4926/41/6/062701](https://doi.org/10.1088/1674-4926/41/6/062701)
  206. Messmer C, Fell A, Feldmann F, Schön J, Hermle M. Upgrade PERC with TOPCon: efficiency potential by taking into account the electrical gains and optical losses. In: *Proc. of the 36th Photovoltaic Solar Energy Conference (EUPVSEC)*. WIP; 2019.
  207. Fell A, Altermatt PP. A detailed full-cell model of a 2018 commercial PERC solar cell in Quokka3. *IEEE J Photovoltaics*. 2018;8(6):1443-1448. doi:[10.1109/JPHOTOV.2018.2863548](https://doi.org/10.1109/JPHOTOV.2018.2863548)
  208. Messmer C, Fell A, Feldmann F, Wohrle N, Schon J, Hermle M. Efficiency roadmap for evolutionary upgrades of PERC solar cells by TOPCon: impact of parasitic absorption. *IEEE J Photovoltaics*. 2020; 10(2):335-342. doi:[10.1109/JPHOTOV.2019.2957642](https://doi.org/10.1109/JPHOTOV.2019.2957642)
  209. Kruse CN, Bothe K, Lim B, Dullweber T, Brendel R. Synergistic efficiency gain analysis for the photovoltaic community: an easy to use SEGA simulation tool for silicon solar cells. In: *Proc. of the 35th Photovoltaic Solar Energy Conference (EUPVSEC)*. WIP; 2018:249-253.
  210. Lohmüller S, Schmidt S, Lohmüller E, et al. Transfer of POCl<sub>3</sub> diffusion processes from atmospheric pressure to high throughput low pressure. *AIP Conf Proc*. 2018;070002. doi:[10.1063/1.5049301](https://doi.org/10.1063/1.5049301)
  211. Fell A, Schon J, Muller M, Wohrle N, Schubert MC, Glunz SW. Modeling edge recombination in silicon solar cells. *IEEE J Photovoltaics*. 2018;8(2):428-434. doi:[10.1109/JPHOTOV.2017.2787020](https://doi.org/10.1109/JPHOTOV.2017.2787020)
  212. Dullweber T, Hannebauer H, Dorn S, et al. Emitter saturation current densities of 22 fA/cm<sup>2</sup> applied to industrial PERC solar cells approaching 22% conversion efficiency. *Prog Photovolt Res Appl*. 2017;25(7):509-514. doi:[10.1002/pip.2806](https://doi.org/10.1002/pip.2806)
  213. Lohmüller E, Glatz M, Lohmüller S, et al. BBr<sub>3</sub> diffusion: process optimization for high-quality emitters with industrial cycle times. In: *Proc. of the 37th European Photovoltaic Conference (EUPVSEC)*. WIP; 2020.
  214. Bao J, Chen C, Huang C, et al. Towards 24% efficiency for industrial n-type bifacial passivating-contact solar cells with homogeneous emitter. In: *Proc. of the 37th European Photovoltaic Conference (EUPVSEC)*. WIP; 2020:160-163.
  215. Huang Y-Y, Ok Y-W, Madani K, et al. Fully screen-printed bifacial large area 22.6% N-type Si solar cell with lightly doped ion-implanted boron emitter and tunnel oxide passivated rear contact. *Solar Energy Mater Solar Cells*. 2020;214:110585. doi:[10.1016/j.solmat.2020.110585](https://doi.org/10.1016/j.solmat.2020.110585)
  216. Huang Y-Y, Ok Y-W, Upadhyaya AD, Upadhyaya VD, Madani K, Rohatgi A. Large area 21.6% efficiency front junction N-type cell with screen printed tunnel oxide passivated poly-Si rear contact. In: *Conference Records of the 46th IEEE Photovoltaic Specialists Conference (PVSC)*. IEEE; 2019:1120-1123.
  217. Lohmüller E, Werner S, Norouzi MH, et al. Low-ohmic contacting of laser-doped p-type silicon surfaces with pure Ag screen-printed and fired contacts. *Phys Status Solidi (a)*. 2017;214(12):1700587. doi:[10.1002/pssa.201700587](https://doi.org/10.1002/pssa.201700587)
  218. Tao Y, Book F, Terheiden B, et al. Large-area n-type TOPCon cells with screen-printed contact on selective boron emitter formed by wet chemical etch-back. In: *Conference Records of the 44th IEEE Photovoltaic Specialist Conference (PVSC)*. IEEE; 2017:1824-1827.
  219. Brendel R, Peibst R. Contact selectivity and efficiency in crystalline silicon photovoltaics. *IEEE J Photovoltaics*. 2016;6(6):1413-1420. doi:[10.1109/JPHOTOV.2016.2598267](https://doi.org/10.1109/JPHOTOV.2016.2598267)
  220. Tomizawa Y, Ikeda Y, Itoh H, et al. Analysis of contact recombination at rear local back surface field via boron laser doping and screen-printed aluminum metallization on p-type PERC solar cells. *Energy Procedia*. 2017;124:384-391. doi:[10.1016/j.egypro.2017.09.256](https://doi.org/10.1016/j.egypro.2017.09.256)
  221. Kruse CN, Bothe K, Brendel R. Comparison of free energy loss analysis and synergistic efficiency gain analysis for PERC solar cells. *IEEE J Photovoltaics*. 2018;1:1-6. doi:[10.1109/JPHOTOV.2018.2802779](https://doi.org/10.1109/JPHOTOV.2018.2802779)
  222. Wu W, Zhang Z, Zheng F, Lin W, Liang Z, Shen H. Efficiency enhancement of bifacial PERC solar cells with laser-doped selective emitter and double-screen-printed Al grid. *Prog Photovolt: Res Appl*. 2018;26(9):752-760. doi:[10.1002/pip.3013](https://doi.org/10.1002/pip.3013)
  223. Çiftpinar HE, Stodolny MK, Wu Y, et al. Study of screen printed metallization for polysilicon based passivating contacts. *Energy Procedia*. 2017;124:851-861. doi:[10.1016/j.egypro.2017.09.242](https://doi.org/10.1016/j.egypro.2017.09.242)
  224. Padhamnath P, Wong J, Nagarajan B, et al. Metal contact recombination in monoPoly™ solar cells with screen-printed & fire-through contacts. *Sol Energy Mater Sol Cells*. 2019;192:109-116. doi:[10.1016/j.solmat.2018.12.026](https://doi.org/10.1016/j.solmat.2018.12.026)
  225. Nandakumar N, Rodriguez J, Kluge T, et al. Approaching 23% with large-area monoPoly cells using screen-printed and fired rear passivating contacts fabricated by inline PECVD. *Prog Photovolt: Res Appl*. 2018;15(1):41. doi:[10.1002/pip.3097](https://doi.org/10.1002/pip.3097)
  226. Chaudhary A, Hoß J, Lossen J, van Swaaij R, Zeman M. Screen printed Ag contacts for n-type polysilicon passivated contacts. In: *15th International Conference on Concentrator Photovoltaic Systems (CPV-15)*. AIP Publishing; 2019:40002. AIP Conference Proceedings
  227. Feldmann F, Steinhauser B, Pernau T, et al. Industrial TOPCon solar cells realized by a PECVD tube process. In: *Proc. of the 37th European Photovoltaic Conference (EUPVSEC)*. WIP; 2020.
  228. Mack S, Lenes M, Luchies J-M, Wolf A. P-type silicon solar cells with passivating rear contact formed by LPCVD p + polysilicon and screen printed Ag metallization. *Phys Status Solidi RRL*. 2019;13(7): 1900064. doi:[10.1002/pssr.201900064](https://doi.org/10.1002/pssr.201900064)
  229. Mack S, Fellmeth T, Schube J, Feldmann F, Lenes M, Luchies J. Screen-printed metallization for p-Type poly-Si passivated contacts formed by LPCVD. In: WIP, ed. *Proc. of the 33rd Photovoltaic Solar Energy Conference (EUPVSEC)*; 2017:468-471.
  230. Mack S, Schube J, Fellmeth T, Feldmann F, Lenes M, Luchies J-M. Metallisation of boron-doped polysilicon layers by screen printed silver pastes. *Phys Status Solidi RRL*. 2017;11(12): 1700334. doi:[10.1002/pssr.201700334](https://doi.org/10.1002/pssr.201700334)
  231. Li Y, Ye F, Liu Y, et al. Research of annealing and boron doping on SiO<sub>x</sub>/p<sup>+</sup>-Poly-Si hole-selective passivated contact. *IEEE J Photovoltaics*. 2020;10(6):1552-1556. doi:[10.1109/JPHOTOV.2020.3016631](https://doi.org/10.1109/JPHOTOV.2020.3016631)
  232. Mack S, Herrmann D, Lenes M, Renes M, Wolf A. Progress in p-type tunnel oxide-passivated contact solar cells with screen-printed contacts. *Sol RRL*. 2021;2100152. doi:[10.1002/solr.202100152](https://doi.org/10.1002/solr.202100152)
  233. Romijn IG, van Aken BB, Anker J, et al. Industrial implementation of efficiency improvements in n-type solar cells and modules. In: *Proc. of the 27th Photovoltaic Solar Energy Conference (EUPVSEC)*. WIP; 2012:533-537.
  234. Kopecek R, Buck T, Libal J, et al. Large area n-type multicrystalline silicon solar cells with B-emitter: efficiencies exceeding 14%. Proc. 15th IPSEC, Shanghai. 2005:883-884.
  235. Fritz S, Engelhardt J, Ebert S, Hahn G. Contacting boron emitters on n-type silicon solar cells with aluminium-free silver screen-printing pastes. *Phys Status Solidi RRL*. 2016;10(4):305-309. doi:[10.1002/pssr.201510443](https://doi.org/10.1002/pssr.201510443)

236. Engelhardt J, Frey A, Gloger S, Hahn G, Terheiden B. Passivating boron silicate glasses for co-diffused high-efficiency n-type silicon solar cell application. *Appl Phys Lett.* 2015;107(4):42102. doi:[10.1063/1.4927667](https://doi.org/10.1063/1.4927667)
237. Engelhardt J, Frey A, Fritz S, et al. Contact formation on boron doped silicon substrates from passivating PECV-deposited dielectric doping layers with anti-reflective properties by screen-printing Ag pastes for high-efficiency n-type silicon solar cells. In: 31st EU PVSEC; 2015:351-354.
238. Engelhardt J, Fritz S, Emre E, Hahn G. Contact formation on p-doped Si by screen-printing pure Ag pastes for bifacial n-type Si solar cells. In: 32nd EU PVSEC; 2016:647-650.
239. Aoyama T, Aoki M, Sumita I, Yoshino Y, Ogura A. Effects of aluminum in metallization paste on the electrical losses in bifacial N-type crystalline silicon solar cells. *Energy Procedia.* 2016;98:106-114. doi:[10.1016/j.egypro.2016.10.086](https://doi.org/10.1016/j.egypro.2016.10.086)
240. Wöhrle N, Lohmüller E, Greulich J, Werner S, Mack S. Towards understanding the characteristics of Ag-Al spiking on boron-doped silicon for solar cells. *Solar Energy Mater Solar Cells.* 2016;146:72-79. doi:[10.1016/j.solmat.2015.11.032](https://doi.org/10.1016/j.solmat.2015.11.032)
241. Agostinelli G, Choulat P, Dekkers HFW, de Wolf S, Beaucarne G. Screen printed large area crystalline silicon solar cells on thin substrates. In: WIP, ed. *Proc. of the 20th Photovoltaic Solar Energy Conference (EUPVSEC);* 2005:647-650.
242. Liu C, Chen D, Chen Y, et al. Industrial TOPCon solar cells on n-type quasi-mono Si wafers with efficiencies above 23%. *Solar Energy Mater Solar Cells.* 2020;215:110690. doi:[10.1016/j.solmat.2020.110690](https://doi.org/10.1016/j.solmat.2020.110690)
243. Strauch T, Demant M, Lorenz A, Haunschild J, Rein S. Two image processing tools to analyse alkaline texture and finger geometry in microscope images. In: *Proc. of the 29th Photovoltaic Solar Energy Conference (EUPVSEC).* WIP; 2014.
244. Zenodo. fa-me/spotlob: v0.9.1-alpha1; 2020.
245. Pospischil M, Fellmeth T, Brand A, et al. Optimizing fine line dispensed contact grids. *Energy Procedia.* 2014;55:693-701. doi:[10.1016/j.egypro.2014.08.046](https://doi.org/10.1016/j.egypro.2014.08.046)
246. Glatthaar M, Haunschild J, Kasemann M, Giesecke J, Warta W, Rein S. Spatially resolved determination of dark saturation current and series resistance of silicon solar cells. *Phys Status Solidi RRL.* 2010;4(1-2):13-15. doi:[10.1002/pssr.200903290](https://doi.org/10.1002/pssr.200903290)
247. Haunschild J, Glatthaar M, Kasemann M, Rein S, Weber ER. Fast series resistance imaging for silicon solar cells using electroluminescence. *Phys Status Solidi RRL.* 2009;3(7-8):227-229. doi:[10.1002/pssr.200903175](https://doi.org/10.1002/pssr.200903175)
248. Trupke T, Pink E, Bardos RA, Abbott MD. Spatially resolved series resistance of silicon solar cells obtained from luminescence imaging. *Appl Phys Lett.* 2007;90(9):93506. doi:[10.1063/1.2709630](https://doi.org/10.1063/1.2709630)
249. Kampwerth H, Trupke T, Weber JW, Augarten Y. Advanced luminescence based effective series resistance imaging of silicon solar cells. *Appl Phys Lett.* 2008;93(20):202102. doi:[10.1063/1.2982588](https://doi.org/10.1063/1.2982588)
250. Berger H. Contact resistance on diffused resistors. In: *IEEE International Solid-State Circuits Conference.* IEEE; 1969:160-161.
251. Shah A. *Solar Cells and Modules.* 1sted. Berlin Heidelberg: Springer; 2020.
252. Chunduri SK, Schmela M. Market survey screen printers 2018; 2018. [taiyangnews.info/TaiyangNews\\_Market\\_Survey\\_on\\_Screen\\_Printers\\_2018\\_download\\_v1.pdf](http://taiyangnews.info/TaiyangNews_Market_Survey_on_Screen_Printers_2018_download_v1.pdf).
253. Riemer DE. Analytical engineering model of the screen printing process: part 1. *Solid State Technol.* 1988;8:107-111.
254. Riemer DE. Analytical engineering model of the screen printing process: part 2. *Solid State Technol.* 1988;9:85-90.
255. Riemer DE. The theoretical fundamentals of the screen printing process. *Microelectron Int.* 1989;6(1):8-17. doi:[10.1108/eb044350](https://doi.org/10.1108/eb044350)
256. Kossen EJ, Heurtault B, Stassen AF. Comparison of two step printing methods for front side metallisation. In: *Proc. of the 25th Photovoltaic Solar Energy Conference (EUPVSEC).* WIP; 2010:2099-2100.
257. Mouhou A, Benyahia B, Mahmoudi B, Mougas A. Selective emitters for screen printed multicrystalline silicon solar cells. *Rev Energ Ren: ICPWE.* 2003;83-86.
258. Glunz SW, Preu R, Biro D. Crystalline silicon solar cells. In: van Sark W, ed. *Comprehensive Renewable Energy.* Elsevier; 2012: 353-387.
259. Hohn O, Tucher N, Blasi B. Impact of front side pyramid size on the light trapping performance of wafer based silicon solar cells and modules. In: *Conference Records of the 44th IEEE Photovoltaic Specialist Conference (PVSC).* IEEE; 2017:352-355.
260. Aoki M, Nakamura K, Tachibana T, et al. 30 µm fine-line printing for solar cells. In: IEEE, ed. *Conference Records of 39th IEEE Photovoltaic Specialists Conference (PVSC).* IEEE; 2013:2162-2166.
261. Lorenz A, Strauch T, Demant M, et al. Impact of texture roughness on the front-side metallization of stencil-printed silicon solar cells. *IEEE J Photovoltaics.* 2015;5(4):1237-1244. doi:[10.1109/JPHOTOV.2015.2416916](https://doi.org/10.1109/JPHOTOV.2015.2416916)
262. Kafle B, Freund T, Werner S, et al. On the nature of emitter diffusion and screen-printing contact formation on nanostructured silicon surfaces. *IEEE J Photovoltaics.* 2017;7(1):136-143. doi:[10.1109/JPHOTOV.2016.2626921](https://doi.org/10.1109/JPHOTOV.2016.2626921)
263. Ney L, Tepner S, Linse M, et al. Optimization of fine line screen printing using in-depth screen mesh analysis. *AIP Conf Proc.* 2019; 20006. doi:[10.1063/1.5125871](https://doi.org/10.1063/1.5125871)
264. Hahne P. Innovative Druck- und Metallisierungsverfahren für die Solarzellentechnologie. [Dissertation]. 1st ed. Hagen; 2000.
265. Hahne P, Hirth E, Reis IE, et al. Progress i2n thick-film pad printing technique for solar cells. *Solar Energy Mater Solar Cells.* 2001;65(1): 399-407. doi:[10.1016/S0927-0248\(00\)00119-7](https://doi.org/10.1016/S0927-0248(00)00119-7)
266. Horvath E, Harsanyi G, Henap G, Torok A. Mechanical modelling and life cycle optimisation of screen printing. *J Theor Appl Mech.* 2012;50(4):1025-1036.
267. Hahne P. *Innovative Drucktechnologien: Siebdruck - Tampondruck; Photolithographie, InkJet, BubbleJet, Digitaldruck, LFP, Drop-On-Demand, Non-Impact-Verfahren, Dickfilm, Heißprägen, Offsetdruck, Flexodruck, Födel-Verfahren, Driographie.* Lübeck: Verl. Der Siebdruck; 2001.
268. Zhang Y. Knotless screen printing for crystalline silicon solar cells. 7th Workshop on Metallization & Interconnection; Konstanz, 2017.
269. Yang H, Davis CS. Silver pastes capable of narrow line, high aspect ratio and high pastes transferability for knotless high mesh screen printing. In: *2018 IEEE 7th World Conference on Photovoltaic Energy Conversion (WCPEC): (A Joint Conference of 45th IEEE PVSC, 28th PVSEC & 34th EU PVSEC): 10-15 June 2018.* Piscataway, NJ: IEEE; 2018:1079-1080.
270. Tepner S, Ney L, Linse M, Lorenz A, Pospischil M, Clement F. Studying knotless screen patterns for fine line screen printing of Si-solar cells. *IEEE J Photovoltaics.* 2020;10(2):319-325. doi:[10.1109/JPHOTOV.2019.2959939](https://doi.org/10.1109/JPHOTOV.2019.2959939)
271. Pan J, Tonkay GL, Quintero A. Screen printing process design of experiments for fine line printing of thick film ceramic substrates. *J Electron Manuf.* 1999;09(03):203-213. doi:[10.1142/S096031319900012X](https://doi.org/10.1142/S096031319900012X)
272. Ju M, Lee Y-J, Lee J, et al. Double screen printed metallization of crystalline silicon solar cells as low as 30 µm metal line width for mass production. *Solar Energy Mater Solar Cells.* 2012;100:204-208. doi:[10.1016/j.solmat.2012.01.018](https://doi.org/10.1016/j.solmat.2012.01.018)
273. Jewell E, Hamblin S, Claypole T, Gethin D. Deposition of high conductivity low silver content materials by screen printing. *Coatings.* 2015;5(2):172-185. doi:[10.3390/coatings5020172](https://doi.org/10.3390/coatings5020172)
274. Xu C, Willenbacher N. How rheological properties affect fine-line screen printing of pastes: A combined rheological and high-speed

- video imaging study. *J Coat Technol Res.* 2018;15(6):1401-1412. doi: [10.1007/s11998-018-0091-2](https://doi.org/10.1007/s11998-018-0091-2)
275. Xu C, Fies M, Willenbacher N. Impact of wall slip on screen printing of front-side silver pastes for silicon solar cells. *IEEE J Photovoltaics.* 2017;7(1):129-135. doi: [10.1109/JPHOTOV.2016.2626147](https://doi.org/10.1109/JPHOTOV.2016.2626147)
276. Tepner S, Ney L, Linse M, Lorenz A, Pospischil M. Advances in screen printed metallization for Si-solar cells—towards ultra-fine line contact fingers below 20  $\mu\text{m}$ . 29th International PV Science and Engineering Conference, Xi'an, China. 2019. doi: [10.13140/RG.2.2.33088.69126](https://doi.org/10.13140/RG.2.2.33088.69126)
277. Yüce C, Okamoto K, Karpowich L, Adrian A, Willenbacher N. Non-volatile free silver paste formulation for front-side metallization of silicon solar cells. *Solar Energy Mater Solar Cells.* 2019;200: 110040. doi: [10.1016/j.solmat.2019.110040](https://doi.org/10.1016/j.solmat.2019.110040)
278. Riemer DE. Ein Beitrag zur Untersuchung der physikalisch-technischen Grundlagen des Siebdruckverfahrens.
279. Benson AM. Thick-film screen printing. *Solid State Technol.* 1969; 12:6.
280. Messerschmitt E. Rheological considerations for screen printing inks. *Screen Printing.* 1982;10:136-139.
281. Chapman SJ, Fitt AD, Please CP. Extrusion of power-law shear-thinning fluids with small exponent. *Int J Non-Linear Mech.* 1997; 32(1):187-199. doi: [10.1016/S0020-7462\(96\)00042-X](https://doi.org/10.1016/S0020-7462(96)00042-X)
282. Hunter B. A Stokes flow analysis of the screen printing process. *Int J Microcirc Electron Packag.* 1994;17:21-26.
283. Owczarek JA, Howland FL. A study of the off-contact screen printing process. I. Model of the printing process and some results derived from experiments. *IEEE Trans Comp, Hybrids, Manufact Technol.* 1990;13(2):358-367. doi: [10.1109/33.56169](https://doi.org/10.1109/33.56169)
284. Owczarek JA, Howland FL. A study of the off-contact screen printing process. II. Analysis of the model of the printing process. *IEEE Trans Comp, Hybrids, Manufact Technol.* 1990;13(2):368-375. doi: [10.1109/33.56170](https://doi.org/10.1109/33.56170)
285. Mannan SH, Ekere NN, Ismail I, Lo EK. Squeegee deformation study in the stencil printing of solder pastes. *IEEE Trans Comp, Packag, Manufact Technol A.* 1994;17(3):470-476. doi: [10.1109/95.311758](https://doi.org/10.1109/95.311758)
286. White GS, Breward CJW, Howell PD, Young RJS. A model for the screen-printing of Newtonian fluids. *J Eng Math.* 2006;54(1):49-70. doi: [10.1007/s10665-005-9000-7](https://doi.org/10.1007/s10665-005-9000-7)
287. Taroni M, Breward CJW, Howell PD, Oliver JM, Young RJS. The screen printing of a power-law fluid. *J Eng Math.* 2012;73(1):93-119. doi: [10.1007/s10665-011-9500-6](https://doi.org/10.1007/s10665-011-9500-6)
288. Taroni M, Breward CJW, Howell PD, Oliver JM, Young RJS. Erratum to: the screen printing of a power-law fluid. *J Eng Math.* 2012;74(1): 207. doi: [10.1007/s10665-012-9548-y](https://doi.org/10.1007/s10665-012-9548-y)
289. Polfer P, Fu Z, Breinlinger T, Roosen A, Kraft T. Influence of the doctor blade shape on tape casting-comparison between analytical, numerical, and experimental results. *J Am Ceram Soc.* 2016;99(10): 3233-3240. doi: [10.1111/jace.14343](https://doi.org/10.1111/jace.14343)
290. Choi SA, Youn JT, Mok JS, Koo C. Computer simulation of ink transfer in the different printing speed and ink viscosity in the screen printing. *J Kor Printing Soc.* 2011;29(1):75-83.
291. Glinski GP, Bailey C, Pericleous KA. A non-Newtonian computational fluid dynamics study of the stencil printing process. *Proc Inst Mech Eng Part C.* 2001;215(4):437-446. doi: [10.1243/0954406011520869](https://doi.org/10.1243/0954406011520869)
292. Glinski GP, Bailey C, Pericleous K. *Simulation of the stencil printing process [solder pastes]*; 2000:364-370. doi: [10.1109/EMAP.2000.904181](https://doi.org/10.1109/EMAP.2000.904181)
293. Durairaj R, Jackson GJ, Ekere NN, Glinski G, Bailey C. Correlation of solder paste rheology with computational simulations of the stencil printing process. *Soldering Surface Mount Tech.* 2002;14(1):11-17. doi: [10.1008/09540910210416422](https://doi.org/10.1008/09540910210416422)
294. Kapur N, Abbott SJ, Dolden ED, Gaskell PH. Predicting the behavior of screen printing. *IEEE Trans Compon, Packag Manufact Technol.* 2013;3(3):508-515. doi: [10.1109/TCMT.2012.2228743](https://doi.org/10.1109/TCMT.2012.2228743)
295. Takada N, Matsumoto J, Matsumoto S. Phase-field model-based simulation of motions of a two-phase fluid on solid surface. *JCST.* 2013;7(2):322-337. doi: [10.1299/jcst.7.322](https://doi.org/10.1299/jcst.7.322)
296. Rusdi MS et al. Multiphase flow in solder paste stencil printing process using CFD approach. *J Adv Res Fluid Mech Therm Sci.* 2018;46: 147-152.
297. Kumar A, Dhiman A, Baranyi L. CFD analysis of power-law fluid flow and heat transfer around a confined semi-circular cylinder. *Int J Heat Mass Transfer.* 2015;82:159-169. doi: [10.1016/j.ijheatmasstransfer.2014.11.046](https://doi.org/10.1016/j.ijheatmasstransfer.2014.11.046)
298. Barajas LG, Egerstedt MB, Kamen EW, Goldstein A. Stencil printing process modeling and control using statistical neural networks. *IEEE Trans Electron Packag Manufact.* 2008;31(1):9-18. doi: [10.1109/TEPM.2007.914236](https://doi.org/10.1109/TEPM.2007.914236)
299. Neidert M, Zhang W, Zhang D, Kipka A. Screen-printing simulation study on solar cell front side AG paste. In: *Photovoltaic Specialists Conference, 2008, PVSC '08, 33rd IEEE: Date: 11-16 May 2008*. Piscataway, NJ: IEEE; 2008:1-4.
300. Takada N, Matsumoto J, Matsumoto S. A diffuse-interface tracking method for the numerical simulation of motions of a two-phase fluid on a solid surface. *J Comput Multiph Flows.* 2014;6(3):283-298. doi: [10.1260/1757-482X.6.3.283](https://doi.org/10.1260/1757-482X.6.3.283)
301. Powell CA, Savage MD, Guthrie JT. Computational simulation of the printing of Newtonian liquid from a trapezoidal cavity. *Int Jnl of Num Meth for HFF.* 2002;12(4):338-355. doi: [10.1108/09615530210433251](https://doi.org/10.1108/09615530210433251)
302. Ahmed DH, Sung HJ, Kim D-S. Simulation of non-Newtonian ink transfer between two separating plates for gravure-offset printing. *Int J Heat Fluid Flow.* 2011;32(1):298-307. doi: [10.1016/j.ijheatfluidflow.2010.06.011](https://doi.org/10.1016/j.ijheatfluidflow.2010.06.011)
303. Li W, Wu T, Jiao R, et al. Effects of silver nanoparticles on the firing behavior of silver paste on crystalline silicon solar cells. *Colloids Surf A Physicochem Eng Asp.* 2015;466:132-137. doi: [10.1016/j.colsurfa.2014.11.018](https://doi.org/10.1016/j.colsurfa.2014.11.018)
304. Jeon SJ, Koo SM, Am HS. Optimization of lead- and cadmium-free front contact silver paste formulation to achieve high fill factors for industrial screen-printed Si solar cells. *Solar Energy Mater Solar Cells.* 2009;93(6-7):1103-1109. doi: [10.1016/j.solmat.2009.01.003](https://doi.org/10.1016/j.solmat.2009.01.003)
305. Mette A. New concepts for front side metallization of industrial silicon solar cells. 2007; 1. Aufl. München: Verl. Dr. Hut; Ingenieurwissenschaften.
306. Hoornstra J, Weeber AW, de Moor H, Sinke WC. The importance of paste rheology in improving fine line, thick film screen printing of front side metallization. 14th European Photovoltaic Solar Energy Conference and Exhibition. 1997.
307. Hsu CP, Guo RH, Hua CC, Shih C-L, Chen W-T, Chang T-I. Effect of polymer binders in screen printing technique of silver pastes. *J Polym Res.* 2013;20(10):277. doi: [10.1007/s10965-013-0277-3](https://doi.org/10.1007/s10965-013-0277-3)
308. Thibert S, Jourdan J, Bechevet B, Chaussy D, Reverdy-Bruas N, Beneventi D. Influence of silver paste rheology and screen parameters on the front side metallization of silicon solar cell. *Mater Sci Semicond Process.* 2014;27:790-799. doi: [10.1016/j.mssp.2014.08.023](https://doi.org/10.1016/j.mssp.2014.08.023)
309. Thibert S, Chaussy D, Beneventi D, et al. Silver ink experiments for silicon solar cell metallization by flexographic process. In: *38th IEEE Photovoltaic Specialists Conference (PVSC), 2012: 3-8 June 2012, Austin Convention Center, Austin, Texas*. Piscataway, NJ: IEEE; 2012: 2266-2270.
310. Jewell EH, Claypole TC, Gethin DT. Viscosity control in the screen printing of ceramic transfers. *Surf Coat Int Part B: Coat Trans.* 2003; 86(2):155-163. doi: [10.1007/BF02699628](https://doi.org/10.1007/BF02699628)

311. Potts S-J, Phillips C, Jewell E, Clifford B, Lau YC, Claypole T. High-speed imaging the effect of snap-off distance and squeegee speed on the ink transfer mechanism of screen-printed carbon pastes. *J Coat Technol Res.* 2020;17(2):447-459. doi:[10.1007/s11998-019-00291-6](https://doi.org/10.1007/s11998-019-00291-6)
312. Pospischil M, Zengerle K, Specht J, et al. Investigations of thick-film-paste rheology for dispensing applications. *Energy Procedia.* 2011;8: 449-454. doi:[10.1016/j.egypro.2011.06.164](https://doi.org/10.1016/j.egypro.2011.06.164)
313. Pospischil M, Specht J, Konig M, et al. Paste rheology correlating with dispensed finger geometry. *IEEE J Photovoltaics.* 2014;4(1):498-503. doi:[10.1109/JPHOTOV.2013.2278657](https://doi.org/10.1109/JPHOTOV.2013.2278657)
314. Pospischil M, Specht J, Gentischer H, et al. Correlations between finger geometry and dispensing paste rheology. [4 pages/27th European Photovoltaic Solar Energy Conference and Exhibition; 1773-1776]. 2012. doi:[10.4229/27THEUPVSEC2012-2CF.5.51](https://doi.org/10.4229/27THEUPVSEC2012-2CF.5.51)
315. Pospischil M. *A Parallel Dispensing System for an improved Front Surface Metallization of Silicon Solar Cells.* Fraunhofer Verlag; 2017.
316. Yüce C, Willenbacher N. Challenges in rheological characterization of highly concentrated suspensions—a case study for screen-printing silver pastes. *J Vis Exp.* 2017;122:e55377. doi:[10.3791/55377](https://doi.org/10.3791/55377)
317. Yüce C, König M, Willenbacher N. Rheology and screen-printing performance of model silver pastes for metallization of Si-solar cells. *Coatings.* 2018;8(11):406. doi:[10.3390/coatings8110406](https://doi.org/10.3390/coatings8110406)
318. Hooke R. *Lectures de Potentia Restitutiva or of Spring—Explaining the Power of Springing Bodies.* London: John Martyn; 1678.
319. Bingham EC. *An Investigation of the Laws of Plastic Flow.* Washington: National Bureau of Standards; 1916.
320. Herschel WH, Bulkley R. Konsistenzmessungen von Gummi-Benzollösungen. *Kolloid-Zeitschrift.* 1926;39(4):291-300. doi:[10.1007/BF01432034](https://doi.org/10.1007/BF01432034)
321. Trease RE, Dietz RL. Paste rheology can improve your fine line printing. *Proceedings ISHM.* 1970.
322. Reichl H. *Hybridintegration: Technologie und Dickschichtschaltungen.* Alfred Hüthig Verlag Heidelberg; 1988.
323. Reinhardt K. *Zusammenhänge Zwischen Rheologischen Eigenschaften und der Abscheidbarkeit Keramischer Suspensionen.* Fraunhofer Verlag; 2019.
324. Barnes HA. Rheology: principles, measurements and applications. *Powder Technol.* 1996;86(3):313. doi:[10.1016/S0032-5910\(96\)90008-X](https://doi.org/10.1016/S0032-5910(96)90008-X)
325. Barnes HA. A review of the slip (wall depletion) of polymer solutions, emulsions and particle suspensions in viscometers: its cause, character, and cure. *J Non-Newtonian Fluid Mech.* 1995;56(3):221-251. doi:[10.1016/0377-0257\(94\)01282-M](https://doi.org/10.1016/0377-0257(94)01282-M)
326. Kalyon DM. Apparent slip and viscoplasticity of concentrated suspensions. *J Rheol.* 2005;49(3):621-640. doi:[10.1122/1.1879043](https://doi.org/10.1122/1.1879043)
327. Aral BK, Kalyon DM. Effects of temperature and surface roughness on time-dependent development of wall slip in steady torsional flow of concentrated suspensions. *J Rheol.* 1994;38(4):957-972. doi:[10.1122/1.550537](https://doi.org/10.1122/1.550537)
328. Kalyon DM, Dalwadi D, Erol M, Birinci E, Tsengolu C. Rheological behavior of concentrated suspensions as affected by the dynamics of the mixing process. *Rheol Acta.* 2006;45(5):641-658. doi:[10.1007/s00397-005-0022-x](https://doi.org/10.1007/s00397-005-0022-x)
329. Ahuja A, Singh A. Slip velocity of concentrated suspensions in Couette flow. *J Rheol.* 2009;53(6):1461-1485. doi:[10.1122/1.3213090](https://doi.org/10.1122/1.3213090)
330. Bertola V, Bertrand F, Tabuteau H, Bonn D, Coussot P. Wall slip and yielding in pasty materials. *J Rheol.* 2003;47(5):1211-1226. doi:[10.1122/1.1595098](https://doi.org/10.1122/1.1595098)
331. Meeker SP, Bonnecaze RT, Cloitre M. Slip and flow in pastes of soft particles: Direct observation and rheology. *J Rheol.* 2004;48(6): 1295-1320. doi:[10.1122/1.1795171](https://doi.org/10.1122/1.1795171)
332. Pawelczyk S, Kniepkamp M, Jesinghausen S, Schmid H-J. Absolute rheological measurements of model suspensions: influence and correction of wall slip prevention measures. *Materials (Basel).* 2020; 13(2):467. doi:[10.3390/ma13020467](https://doi.org/10.3390/ma13020467)
333. Gulmus SA, Yilmazer U. Effect of volume fraction and particle size on wall slip in flow of polymeric suspensions. *J Appl Polym Sci.* 2005; 98(1):439-448. doi:[10.1002/app.21928](https://doi.org/10.1002/app.21928)
334. Voronov RS, Papavassiliou DV, Lee LL. Review of fluid slip over superhydrophobic surfaces and its dependence on the contact angle. *Ind Eng Chem Res.* 2008;47(8):2455-2477. doi:[10.1021/ie0712941](https://doi.org/10.1021/ie0712941)
335. Hyvälöoma J, Harting J. Slip flow over structured surfaces with entrapped microbubbles. *Phys Rev Lett.* 2008;100(24):246001. doi: [10.1103/PhysRevLett.100.246001](https://doi.org/10.1103/PhysRevLett.100.246001)
336. Durairaj R, Man LW, Ekere NN, Mallik S. The effect of wall-slip formation on the rheological behaviour of lead-free solder pastes. *Mater Des.* 2010;31(3):1056-1062. doi:[10.1016/j.matdes.2009.09.051](https://doi.org/10.1016/j.matdes.2009.09.051)
337. Koos E, Willenbacher N. Capillary forces in suspension rheology. *Science.* 2011;331(6019):897-900. doi:[10.1126/science.1199243](https://doi.org/10.1126/science.1199243)
338. Koos E, Johannsmeier J, Schwebler L, Willenbacher N. Tuning suspension rheology using capillary forces. *Soft Matter.* 2012;8(24): 6620. doi:[10.1039/c2sm25681a](https://doi.org/10.1039/c2sm25681a)
339. Koos E, Willenbacher N. Particle configurations and gelation in capillary suspensions. *Soft Matter.* 2012;8(14):3988. doi:[10.1039/c2sm07347a](https://doi.org/10.1039/c2sm07347a)
340. Koos E, Kannowade W, Willenbacher N. Restructuring and aging in a capillary suspension. *Rheol Acta.* 2014;53(12):947-957. doi:[10.1007/s00397-014-0805-z](https://doi.org/10.1007/s00397-014-0805-z)
341. Schneider M, Koos E, Willenbacher N. Highly conductive, printable pastes from capillary suspensions. *Sci Rep.* 2016;6:31367. doi:[10.1038/srep31367](https://doi.org/10.1038/srep31367)
342. Koos E. Capillary suspensions: particle networks formed through the capillary force. *Curr Opin Colloid Interface Sci.* 2014;19(6):575-584. doi:[10.1016/j.cocis.2014.10.004](https://doi.org/10.1016/j.cocis.2014.10.004)
343. de Moor H, Hoornstra J, Weeber A, Burgers A, Sinke W. Printing high and fine metal lines using stencils. In: Proceedings of the 14th European Photovoltaic Solar Energy Conference (EPSEC); 1997: 404-407.
344. Hoornstra J, Roberts S, de Moor H, Bruton T. First experiences with double layer stencil printing for low cost production solar cells. In: Proc. of the 2nd World Conference on Photovoltaic Solar Energy Conversion (WCPEC); 1998.
345. Hannebauer H, Schimanke S, Falcon T, Altermatt PP, Dullweber T. Optimized stencil print for low Ag paste consumption and high conversion efficiencies. *Energy Procedia.* 2015;67:108-115. doi:[10.1016/j.egypro.2015.03.294](https://doi.org/10.1016/j.egypro.2015.03.294)
346. Holmes P, Loasby RG. *Handbook of Thick Film Technology.* Electrochemical Publication Ltd; 1976.
347. Hanoka JL, Danielson SE. Method for forming contacts. US5151377A.
348. Specht J, Zengerle K, Pospischil M, et al. High aspect ratio front contacts by single step dispensing of metal pastes: Conference on Photovoltaic Energy Conversion, 6-10 September 2010, Spain; 1867-1870/25th; 2010.
349. Pospischil M, Klawitter M, Kuchler M, et al. High speed dispensing with novel 6 print head. *Energy Procedia.* 2016;98:61-65. doi:[10.1016/j.egypro.2016.10.081](https://doi.org/10.1016/j.egypro.2016.10.081)
350. Pospischil M, Kuchler M, Klawitter M, et al. High speed dispensing—a high-throughput metallization technology for >21% PERC type solar cells. [4 pages/32nd European Photovoltaic Solar Energy Conference and Exhibition; 403-406]. 2016. doi:[10.4229/EUPVSEC20162016-2CO.2.2](https://doi.org/10.4229/EUPVSEC20162016-2CO.2.2)
351. Pospischil M, Riebe T, Jimenez A, et al. Applications of parallel dispensing in PV metallization. *AIP Conf Proc.* 2019;20005. doi:[10.1063/1.5125870](https://doi.org/10.1063/1.5125870)

352. Pospischil M, Kuchler M, Klawitter M, et al. Progress on industrial solar cell front side metallization by parallel dispensing technology. [3 pages/31st European Photovoltaic Solar Energy Conference and Exhibition; 369-371]. 2015. doi:[10.4229/EUPVSEC20152015-2CO.1.1](https://doi.org/10.4229/EUPVSEC20152015-2CO.1.1)
353. Pospischil M, Klawitter M, Kuchler M, et al. Development of a high-throughput fine line metallization process using CFD-simulation. In: 2013 IEEE 39th Photovoltaic Specialists Conference (PVSC): 16-21 June 2013, Tampa, Florida. Piscataway, NJ: IEEE; 2013:2250-2253.
354. Pospischil M, Klawitter M, Kuchler M, et al. Process development for a high-throughput fine line metallization approach based on dispensing technology. *Energy Procedia*. 2013;43:111-116. doi:[10.1016/j.egypro.2014.02.001](https://doi.org/10.1016/j.egypro.2014.02.001)
355. Pospischil M, Kuchler M, Klawitter M, et al. Ultrafine front side metallization on silicon solar cells by industrial dispensing technology. [3 pages/29th European Photovoltaic Solar Energy Conference and Exhibition; 1304-1306]. 2014. doi:[10.4229/EUPVSEC20142014-2CV.4.12](https://doi.org/10.4229/EUPVSEC20142014-2CV.4.12)
356. Pospischil M, Kuchler M, Klawitter M, et al. Dispensing technology on the route to an industrial metallization process. *Energy Procedia*. 2015;67:138-146. doi:[10.1016/j.egypro.2015.03.297](https://doi.org/10.1016/j.egypro.2015.03.297)
357. Gensowski K, Jimenez A, Freund T, et al. CIGS mini-modules with dispensed metallization on transparent conductive oxide layer. *Sol RRL*. 2020;4(12):2000475. doi:[10.1002/solr.202000475](https://doi.org/10.1002/solr.202000475)
358. Gensowski K, Jimenez A, Tepner S, et al. Dispensing of low-temperature silver pastes. *AIP Conf Proc*. 2020;020007. doi:[10.1063/5.0056103](https://doi.org/10.1063/5.0056103)
359. Erath D, Pospischil M, Keding R, et al. Comparison of innovative metallization approaches for silicon heterojunction solar cells. *Energy Procedia*. 2017;124:869-874. doi:[10.1016/j.egypro.2017.09.245](https://doi.org/10.1016/j.egypro.2017.09.245)
360. Kipphan H (Ed). *Handbook of Print Media*. Berlin: Springer; 2001.
361. Gallus F, Rüesch AG. Technische Daten Maschinensystem Gallus EM 280; 2015. [gallus-group.com/docs/default-source/product-documents/gallus-em-280/gallus\\_em\\_280\\_de.pdf?sfvrsn=16](http://gallus-group.com/docs/default-source/product-documents/gallus-em-280/gallus_em_280_de.pdf?sfvrsn=16). Accessed October 20, 2016.
362. Hahne P. Innovative Druck- und Metallisierungsverfahren für die Solarzellentechnologie. [PhD Thesis]. Hagen: Fernuniversität Hagen; 2000.
363. Lorenz A, Münzer A, Lehner M, et al. High-throughput front and rear side metallization of silicon solar cells using rotary screen printing. In: 7th International Conference on Crystalline Silicon Photovoltaics (SiliconPV); 2017.
364. Lorenz A, Senne A, Rohde J, et al. Evaluation of flexographic printing technology for multi-busbar solar cells. *Energy Procedia*. 2015;67: 126-137. doi:[10.1016/j.egypro.2015.03.296](https://doi.org/10.1016/j.egypro.2015.03.296)
365. Lorenz A, Kraft A, Gredy C, et al. Comprehensive comparison of different fine line printing technologies addressing the seed and plate approach with Ni-Cu-plating. In: WIP, ed. *Proc. of the 30th Photovoltaic Solar Energy Conference (EUPVSEC)*; 2015:732-736.
366. Clement F, Lorenz A, Pospischil M, et al. High throughput printing for highly efficient cost-effective Si solar cells. In: WIP, ed. *Proc. of the 33rd Photovoltaic Solar Energy Conference (EUPVSEC)*; 2017.
367. Kapur N, Hewson R, Sleigh PA, Summers JL, Thompson HM, Abbott SJ. A review of gravure coating systems. *Convertech & e-Print*. 2011;1(4):56-60. [eprints.whiterose.ac.uk/43238/](http://eprints.whiterose.ac.uk/43238/)
368. Philipp W; Tampoprint AG. Rotary tampon printing press. US 6619203 B2. April 20, 2001.
369. Hashimoto K, Ouchi M, Nakamura N, Kobayashi E, Watabe Y. Low cost module with heterojunction solar cells applied gravure offset printing and multi-wire technologies. In: WIP, ed. *Proc. of the 28th Photovoltaic Solar Energy Conference (EUPVSEC)*; 2013:1073-1076.
370. Frey M, Clement F, Dilfer S, Erath D, Biro D. Front-side metallization by means of flexographic printing. *Energy Procedia*. 2011;8:581-586.
371. Lorenz A, Kalio A, Hofmeister GT, et al. Flexographic printing—high throughput technology for fine line seed layer printing on silicon solar cells. In: WIP, ed. *Proc. of the 28th Photovoltaic Solar Energy Conference (EUPVSEC)*; 2013:1017-1023.
372. Thibert S, Jourdan J, Bechevet B, et al. Flexographic process for front side metallization of silicon solar cell. In: WIP, ed. *Proc. of the 28th Photovoltaic Solar Energy Conference (EUPVSEC)*; 2013:1013-1016.
373. Lorenz A, Gredy C, Lehner M, et al. Progress with rotational printing for the front side metallization of silicon solar cells. In: WIP, ed. *Proc. of the 32nd Photovoltaic Solar Energy Conference (EUPVSEC)*; 2016: 413-419.
374. Lorenz A, Gredy C, Beyer S, et al. Flexographic printing—towards an advanced front side metallization approach with high throughput and low silver consumption. *Solar Energy Mater Solar Cells*. 2016; 157:550-557. doi:[10.1016/j.solmat.2016.07.025](https://doi.org/10.1016/j.solmat.2016.07.025)
375. Lorenz A, Gredy C, Senne A, et al. Flexo-printed busbarless solar cells for multi-wire interconnection. *Energy Procedia*. 2016;98:46-60. doi:[10.1016/j.egypro.2016.10.080](https://doi.org/10.1016/j.egypro.2016.10.080)
376. Lorenz A, Münzer A, Lehner M, et al. High-throughput front and rear side metallization of silicon solar cells using rotary screen printing. *Energy Procedia*. 2017;124:680-690. doi:[10.1016/j.egypro.2017.09.343](https://doi.org/10.1016/j.egypro.2017.09.343)
377. Lorenz A, Röth J, Zengerle K, et al. Project “Rock-Star”—high-speed rotary printing for solar cell metallization: from vision to reality. In: WIP, ed. *Abstract submitted for 37th European Photovoltaic Conference (EUPVSEC)*; 2020.
378. Ebong A, Renshaw J, Rounsville B, et al. Ink jetted seed and plated grid solar cells with homogeneous high sheet resistance emitters. In: WIP, ed. *Proc. of the 25th Photovoltaic Solar Energy Conference (EUPVSEC)*; 2010:2390-2394.
379. Ebong A, Cooper IB, Rounsville B, et al. On the ink jetting of full front Ag gridlines for cost-effective metallization of Si solar cells. *IEEE Electron Device Lett*. 2012;33(5):637-639. doi:[10.1109/LED.2012.2186553](https://doi.org/10.1109/LED.2012.2186553)
380. Jesswein R, Fastnacht P, Weiß M, Lossen J, Meyer K, Krokszinski HJ. Process optimization of single step inkjet printed front contacts for industrially fabricated solar cells leads to an efficiency gain of 0.3 % abs with consumption of less than 60 mg silver. In: WIP, ed. *Proc. of the 28th Photovoltaic Solar Energy Conference (EUPVSEC)*; 2013:997-1003.
381. Hermans JP, Papet P, Pacheco K, et al. Advanced metallization concepts by inkjet printing. In: WIP, ed. *Proc. of the 29th Photovoltaic Solar Energy Conference (EUPVSEC)*; 2014:518-522.
382. Schube J, Weil M, Fellmeth T, Keding R, Glunz S. Intense pulsed light meets the metallization of silicon heterojunction solar cells. In: *Conference Records of the 46th IEEE Photovoltaic Specialists Conference (PVSC)*. IEEE; 2019.
383. Stüwe D, Mager D, Biro D, Korvink JG. Inkjet technology for crystalline silicon photovoltaics. *Adv Mater*. 2014;1-28. doi:[10.1002/adma.201403631](https://doi.org/10.1002/adma.201403631)
384. Lossen J, Matusovsky M, Noy A, Maier C, Bähr M. Pattern Transfer Printing (PTP) for c-Si solar cell metallization. *Energy Procedia*. 2015; 67:156-162. doi:[10.1016/j.egypro.2015.03.299](https://doi.org/10.1016/j.egypro.2015.03.299)
385. Adrian A, Rudolph D, Lossen J, Matusovsky M, Chandrasekaran V. Benefits of pattern transfer printing method for finger metallization on silicon solar cells. In: WIP, ed. *Proc. of the 35th Photovoltaic Solar Energy Conference (EUPVSEC)*; 2018:434-438.
386. Adrian A, Rudolph D, Willenbacher N, Lossen J. Finger metallization using pattern transfer printing technology for c-Si solar cell. *IEEE J Photovoltaics*. 2020;1-9. doi:[10.1109/JPHOTOV.2020.3007001](https://doi.org/10.1109/JPHOTOV.2020.3007001)
387. Hörtelis M, Bartsch J, Binder S, et al. Electrical properties of fine line printed and light-induced plated contacts on silicon solar cells. *Progr Photovoltaics: Res Applic*. 2010;18(4):n/a-n/a. doi:[10.1002/pip.938](https://doi.org/10.1002/pip.938)
388. Kluska S, Buchler A, Bartsch J, et al. Easy plating—a simple approach to suppress parasitically metallized areas in front side Ni/Cu plated

- crystalline Si solar cells. *IEEE J Photovoltaics*. 2017;7(5):1270-1277. doi:[10.1109/jphotov.2017.2720461](https://doi.org/10.1109/jphotov.2017.2720461)
389. Aguilar A, Herasimenka SY, Karas J, et al. Development of Cu plating for silicon heterojunction solar cells. In: 2016 IEEE 43rd Photovoltaic Specialists Conference (PVSC). IEEE; 2016.
390. Balucani M, Quaranta S. A breakthrough in plating for solar cell metallization. *Meet Abstr*. 2018;MA2018-02(22):818. doi:[10.1149/MA2018-02/22/818](https://doi.org/10.1149/MA2018-02/22/818)
391. Dabirian A, Lachowicz A, Schüttauf J-W, et al. Metallization of Si heterojunction solar cells by nanosecond laser ablation and Ni-Cu plating. *Sol Energy Mater Sol Cells*. 2017;159:243-250. doi:[10.1016/j.solmat.2016.09.021](https://doi.org/10.1016/j.solmat.2016.09.021)

**How to cite this article:** Tepner S, Lorenz A. Printing technologies for silicon solar cell metallization: A comprehensive review. *Prog Photovolt Res Appl*. 2023;31(6): 557-590. doi:[10.1002/pip.3674](https://doi.org/10.1002/pip.3674)